



저작자표시-비영리-변경금지 2.0 대한민국

이용자는 아래의 조건을 따르는 경우에 한하여 자유롭게

- 이 저작물을 복제, 배포, 전송, 전시, 공연 및 방송할 수 있습니다.

다음과 같은 조건을 따라야 합니다:



저작자표시. 귀하는 원저작자를 표시하여야 합니다.



비영리. 귀하는 이 저작물을 영리 목적으로 이용할 수 없습니다.



변경금지. 귀하는 이 저작물을 개작, 변형 또는 가공할 수 없습니다.

- 귀하는, 이 저작물의 재이용이나 배포의 경우, 이 저작물에 적용된 이용허락조건을 명확하게 나타내어야 합니다.
- 저작권자로부터 별도의 허가를 받으면 이러한 조건들은 적용되지 않습니다.

저작권법에 따른 이용자의 권리는 위의 내용에 의하여 영향을 받지 않습니다.

이것은 [이용허락규약\(Legal Code\)](#)을 이해하기 쉽게 요약한 것입니다.

[Disclaimer](#)

Numerical Study on Energy Harvesting Efficiency of Multi-stage Overtopping Wave Energy Converters

Sirirat Jungrungruentaworn

**A Dissertation Submitted in Partial Fulfillment of Requirements
For the Degree of Doctor of Philosophy**

February 2018

**Department of Naval Architecture and Ocean Systems Engineering
Graduate School
Korea Maritime and Ocean University**

Supervisor Beom-Soo Hyun

본 논문을 Sirirat Jungrungruentaworn 의
공학박사 학위논문으로 인준함

위원장 : 이승재

위원 : 현범수

위원 : 이성욱

위원 : 박선호

위원 : 홍기용



2017 년 12 월 22 일

한국해양대학교 일반대학원

Numerical Study on Energy Harvesting Efficiency of Multi-stage Overtopping Wave Energy Converters

Approved as to style and content by:

Seung-Jae Lee, Ph.D.



(Chairman)

Beom-Soo Hyun, Ph.D.



(Supervisor)

Sung-Wook Lee, Ph.D.



Sun-Ho Park, Ph.D.



Keyyong Hong, Ph.D.



December 22, 2017

Graduate school

Korea Maritime and Ocean University

Contents

| | |
|------------------------------|------|
| List of Tables | iv |
| List of Figures | v |
| Nomenclature | ix |
| Abstract | xiii |

1. Introduction

| | |
|----------------------|---|
| 1.1 Background | 1 |
|----------------------|---|

2. Wave energy resource

| | |
|--|----|
| 2.1 Ocean energy | 6 |
| 2.2 Wave energy resource | 8 |
| 2.2.1 Wave energy resource in world | 8 |
| 2.2.2 Wave energy resource focus on Southeast Asia | 10 |
| 2.2.3 Southeast Asia perspective | 13 |

3. Wave energy utilization

| | |
|---|----|
| 3.1 Ocean wave energy | 18 |
| 3.2 Classification of wave energy converter | 20 |
| 3.2.1 Location | 20 |

| | |
|--|----|
| 3.2.2 Orientation in wave | 21 |
| 3.2.3 Operation modes | 21 |
| 3.2.4 Structure | 22 |
| 3.3 Stage of the wave energy converter research | 23 |
| 3.3.1 Concepts for designing a wave energy device | 23 |
| 3.3.2 Model testing in a laboratory | 23 |
| 3.3.3 Testing of a wave energy converter device in sea | 24 |
| 3.4 Overtopping wave energy converter | 26 |
| 3.4.1 Wave overtopping energy | 27 |
| 3.4.2 Wave reflection analysis | 28 |
| 3.4.3 Overtopping wave energy converter configurations | 29 |
| 4. Numerical simulation of OWEC device | |
| 4.1 Numerical wave simulation | 33 |
| 4.1.1 Validation of volume of fluid model | 36 |
| 4.1.2 Outlet boundary condition testing | 38 |
| 4.1.3 Sensitivity analysis | 42 |
| 4.1.4 Validation of wave profile | 46 |
| 4.1.5 Validation of overtopping flow rate of multi-stage device | 50 |
| 4.2 Effect of slot width on the performance of multi-stage of OWECs | 51 |
| 4.2.1 Results of effect of slot width on the performance of multi-stage of OWECs | 55 |
| 4.2.2 Conclusions of effect of slot width on the performance of multi-stage of OWECs | 65 |
| 4.3 Effect of adaptive slot width on the performance of multi-stage of OWECs · | 66 |
| 4.4 Effect of overlap ramp of non-adaptive and adaptive devices | 73 |

| | |
|--|-----|
| 4.4.1 Combination of overlap ramp and adaptive slot width | 75 |
| 4.5 Effect of submerged depth on the performance of multi-stage of OWECs ... | 80 |
| 4.5.1 Multi-stage OWEC installed on breakwater | 80 |
| 4.6 Effect of span on the performance of multi-stage of OWECs | 84 |
| 4.7 Scenario of overtopping wave energy converter in Thailand | 92 |
| 5. Conclusions and perspectives | |
| References | 100 |
| Acknowledgement | 109 |



List of Tables

| | |
|--|----|
| Table 2.1 Ocean power in OES countries | 9 |
| Table 3.1 Example of OWEC device configurations | 30 |
| Table 4.1 Outlet boundary conditions | 38 |
| Table 4.2 Mesh sensitivity of wave generation | 42 |
| Table 4.3 Mesh and time sensitivity | 44 |
| Table 4.4 General parameters conditions | 53 |
| Table 4.5 Parameter conditions | 66 |
| Table 4.6 Adaptive slot width parameters | 68 |
| Table 4.7 Parameters of adaptive slot width | 75 |
| Table 4.8 Parameter condition of overlap ramp | 75 |
| Table 4.9 Parameter of submerged depth study | 80 |
| Table 4.10 Wave elevation of three-dimensional simulation of multi-stage OWEC | 91 |

List of Figures

| | |
|---|----|
| Fig. 1.1 Wave Dragon | 2 |
| Fig. 1.2 Spiral-reef overtopping device (single-stage OWEC type) | 3 |
| Fig. 1.3 Graphics of SSG wave energy converter (multi-stage OWEC type) | 4 |
| Fig. 2.1 Ocean energy form | 6 |
| Fig. 2.2 Global status of ocean renewable energy | 7 |
| Fig. 2.3 Global wave power resource by Gunn and Stock-Williams | 8 |
| Fig. 2.4 Map of country in Southeast Asia | 10 |
| Fig. 2.5 Annual mean wave energy of Southeast Asia | 12 |
| Fig. 2.6 Example of simulation result of wave energy potential in Thailand | 13 |
| Fig. 2.7 Testing the WEC device in the sea of Thailand | 14 |
| Fig. 2.8 Basic principle of Drakoo operation | 15 |
| Fig. 2.9 Drakoo model testing in a laboratory | 16 |
| Fig. 2.10 Example of Drakoo-III prototype testing in the sea | 17 |
| Fig. 2.11 Results of the experiment and calculates the energy obtained from the Drakoo wave energy absorber | 17 |
| Fig. 3.1 Characteristics of a regular wave | 18 |
| Fig. 3.2 Stage of research | 23 |
| Fig. 3.3 DEXAWAVE model, 1:10 scale, in the water wave basin | 24 |
| Fig. 3.4 Example of wave energy converter operation in the sea | 25 |
| Fig. 3.5 Basic principle concept of OWEC | 26 |

| | |
|--|----|
| Fig. 4.1 Two-dimensional numerical wave tank used to simulate wave overtopping behavior. The locations of wave probes are indicated by P1, P2, P3, P4, and P5 | 34 |
| Fig. 4.2 Contour of water and air phases of a dam break over a dry bed | 36 |
| Fig. 4.3 Time history of the position of the leading edge of water | 37 |
| Fig. 4.4 Domain of outlet boundary condition testing | 39 |
| Fig. 4.5 Surface elevation at $x = 1\lambda$ from the wave generate | 40 |
| Fig. 4.6 Grid near a free surface | 42 |
| Fig. 4.7 Mesh sensitivity of linear wave..... | 43 |
| Fig. 4.8 Time step size testing | 44 |
| Fig. 4.9 Mesh sensitivity of single-stage device | 45 |
| Fig. 4.10 Example of creating a domain grid by dividing the grid resolution into 3 ranges | 46 |
| Fig. 4.11 Coefficients of viscous resistance relative to distance | 47 |
| Fig. 4.12 Wave surface elevation of two-dimensional numerical wave tank at $t = 10T$ | 48 |
| Fig. 4.13 Numerical wave tank validation. The generated wave profile is compared with linear wave theory | 49 |
| Fig. 4.14 Comparison of the calculated overtopping rates using Eq. 4.11 with comparable numerical results of multi-stage device | 50 |
| Fig. 4.15 Layouts of the single- and multi-stage devices. The incident wave direction is from left to right | 52 |
| Fig. 4.16 Meshing structure grid on the single stage device | 54 |
| Fig. 4.17 Overall hydraulic efficiency, reflection, transmission and loss rates | 56 |
| Fig. 4.18 Effect of slot width on efficiency and loss rate | 58 |
| Fig. 4.19 Wave run-up process of single- and multi-stage devices | 59 |
| Fig. 4.20 Run-up and fall-down processes | 60 |

| | |
|---|----|
| Fig. 4.21 Partial hydraulic efficiencies of each reservoir as functions of relative slot width | 61 |
| Fig. 4.22 Hydraulic efficiencies of multi-stage device for different wave periods..... | 62 |
| Fig. 4.23 Hydraulic efficiencies of multi-stage device for different wave heights..... | 64 |
| Fig. 4.24 Example of non-adaptive and adaptive devices layout | 67 |
| Fig. 4.25 Example of hydraulic efficiency of each extra slot of device | 69 |
| Fig. 4.26 Contour of hydraulic efficiency η , reflection rate K_r^2 , transmission rate K_t^2 and loss rate L of multi-stage device on the $(\bar{w}, \Delta w/\bar{w})$ parametric space | 70 |
| Fig. 4.27 Run-up process of non- and adaptive devices based on $\bar{w} = 0.5$ m..... | 71 |
| Fig. 4.28 Fall-down process of non- and adaptive devices based on $\bar{w} = 0.5$ m..... | 72 |
| Fig. 4.29 Layouts of non-overlap ramp multi-stage devices base on the relative slot width of 0.2 | 74 |
| Fig. 4.30 Example of overlap ramp layout of non-adaptive device | 74 |
| Fig. 4.31 Effect of overlap ramp applied to multi-stage devices on overall hydraulic efficiency as function of relative extended ramp. The non-overlap ramp is represented by the relative extended ramp $y/\bar{w} = 0$ | 76 |
| Fig. 4.32 Comparison of overall hydraulic efficiency, reflection, transmission and loss rates of overlap ramp non-adaptive and adaptive device base on $y/\bar{w} = 0.125$ | 77 |
| Fig. 4.33 Partial hydraulic efficiencies of each reservoir versus the relative extended ramp | 78 |
| Fig. 4.34 Water flow run-up processes of overlap ramp multi-stage device based on $y/\bar{w} = 0.25$ at different time | 79 |
| Fig. 4.35 Water flow fall-down processes of overlap ramp multi-stage device based on $y/\bar{w} = 0.25$ at different time | 79 |

| | |
|--|----|
| Fig. 4.36 Schematic of multi-stage device to study the effect of submerged depth on performance | 80 |
| Fig. 4.37 Overall hydraulic efficiencies of single- and multi-stage device as function of relative submerged depth | 81 |
| Fig. 4.38 Effect of submerged depth on overall hydraulic efficiencies of OWEC devices | 82 |
| Fig. 4.39 Water flow into reservoirs of multi-stage device with and without breakwater | 83 |
| Fig. 4.40 Schematic of three-dimensional domain to study the effect of span on the performance of multi-stage device | 84 |
| Fig. 4.41 Mesh of three-dimensional domain | 85 |
| Fig. 4.42 Surface mesh of multi-stage OWEC device | 86 |
| Fig. 4.43 Numerical wave tank validation in three-dimensional domain. The generated wave profile is compared with linear wave theory. (Surface elevation at $x = 1\lambda$) | 88 |
| Fig. 4.44 Overall hydraulic efficiency of multi-stage OWEC in three-dimensional simulation compare with the results of two-dimensional simulation | 89 |
| Fig. 4.45 Partial hydraulic efficiencies of each reservoir of multi-stage devices as function of relative breakwater length. The two-dimensional result is represented by the relative breakwater length $L_B/\lambda = \infty$ | 90 |
| Fig. 4.46 Wave surface elevation in three-dimensional domain | 90 |
| Fig. 4.47 Energy Sources of Thailand in 2012 | 92 |
| Fig. 4.48 Ten year alternative energy development plan of Thailand | 93 |
| Fig. 4.49 Significant wave height with wave direction around Thailand | 95 |
| Fig. 4.50 Southern of Thailand map | 96 |
| Fig. 4.51 Beaches and coastlines in Nakhon Si Thammarat, Thailand | 97 |

Nomenclature

| | |
|-------------|--|
| a_i | : Incident wave amplitude [m] |
| a_r | : Reflected wave amplitude [m] |
| a_t | : Transmitted wave amplitude [m] |
| a_w | : Volume fraction of water |
| A | : Wave amplitude [m] |
| A_n | : Measured amplitude of the n^{th} probe [m] |
| c | : Phase velocity [m/s] |
| C_w | : Wave speed [m/s] |
| C_2 | : Inertial resistance factor [1/m] |
| E | : Energy of ocean wave or wave energy density [Joules/m ²] |
| E_k | : Kinetic energy [Joules/m ²] |
| E_p | : Potential energy [Joules/m ²] |
| g | : Gravitational acceleration [m/s ²] |
| h | : Water depth [m] |
| H | : Wave height [m] |
| H/λ | : Wave steepness [-] |
| H/h | : Relative wave height [-] |
| k | : Wave number $k = \frac{2\pi}{\lambda}$ [rad/m] |
| K_r | : Reflection coefficient $K_r = a_r/a_i$ [-] |
| K_r^2 | : Reflection rate $K_r^2 = P_r/P_{wave}$ [-] |
| K_t | : Transmission coefficient $K_t = a_t/a_i$ [-] |
| K_t^2 | : Transmission rate $K_t^2 = P_t/P_{wave}$ [-] |
| L | : Length of the ramp [m] |

| | |
|---------------|--|
| L_B | : Span length of breakwater [m] |
| L_B/λ | : Relative of span length of breakwater [-] |
| L_l | : Loss rate $L_l = P_L/P_{wave}$ [-] |
| n | : Factor [-] |
| P_L | : Dissipated wave power or loss [Watt/m] |
| P_{crest} | : Potential power in the overtopping water [Watt/m] |
| P_r | : Reflected wave power [Watt/m] |
| P_t | : Transmitted wave power [Watt/m] |
| P_{wave} | : Wave energy flux or power in the incident wave [Watt/m] |
| Q_i | : Average overtopping flow rate per unit length of the i^{th} reservoir [m ³ /s/m] |
| R | : Ramp height [m] |
| R_c | : Freeboard or crest height [m] |
| $R_{c,i}$ | : Crest height of the i^{th} reservoir [m] |
| R_{c1} | : Crest height of the first reservoir [m] |
| R_{c2} | : Crest height of the second reservoir [m] |
| R_{c3} | : Crest height of the third reservoir [m] |
| R_{c4} | : Crest height of the main reservoir [m] |
| R_c/H | : Relative freeboard [-] |
| R_s | : Draught or submerged depth [m] |
| R_s/H | : Relative submerged depth [-] |
| S | : Sloping ratio of device, $S = R/L$ [-] |
| S_i | : Additional source term for the i -th (x, y or z) momentum equation [N/m ³] |
| t | : Time [s] |
| T | : Wave period [s] |

| | |
|---------------------|---|
| w | : Slot width [m] |
| w_i | : Slot width of the i^{th} reservoir [m] |
| w_1 | : First slot width [m] |
| w_2 | : Second slot width [m] |
| w_3 | : Third slot width [m] |
| \bar{w} | : Average slot width [m] |
| w/R_{c4} | : Relative slot width [-] |
| \bar{w}/R_{c4} | : Relative average slot width [-] |
| w_i/\bar{w} | : Relative slot width of the i^{th} reservoir [-] |
| $\Delta w/\bar{w}$ | : Relative of difference in size of the slots [-] |
| x | : Any position in x-axis [m] |
| x_0 | : Maximum displacement of the wavemaker [m] |
| x_{ab} | : Beginning point of absorber zone in x direction [m] |
| y | : Overlap distance [m] |
| y/\bar{w} | : Relative extended ramp [-] |
| Δ | : Dimensionless distance between two probes [-] |
| Δw | : Difference in size of the slots [m] |
| $1/\alpha$ | : Viscous resistance coefficient [$1/m^2$] |
| $(1/\alpha)_{\max}$ | : Maximum viscous resistance coefficient [$1/m^2$] |
| η | : Hydraulic efficiency [-] |
| η_w | : Wave surface elevation [m] |
| λ | : Wavelength [m] |
| δ | : Measured phase angle of second probe relative to that of the first probe and is obtained by fast Fourier transform (FFT) algorithm |
| ω | : Angular frequency $\omega = \frac{2\pi}{T}$ [rad/s] |
| θ | : $\theta = kx - \omega t$ [rad] |

ρ : Sea water density $\rho = 1,025 \text{ kg/m}^3$
 μ : Viscosity of the fluid $\mu = 0.0012 \text{ kg/s}\cdot\text{m}$



Numerical Study on Energy Harvesting Efficiency of Multi-stage Overtopping Wave Energy Converters

Sirirat Jungrungruentaworn

Department of Naval Architecture and Ocean Systems Engineering

Graduate School of Korea Maritime and Ocean University



Abstract

A viscous solver based on RANS simulations is used to numerically investigate flow physics as well as performance of wave energy devices used to harvest ocean wave power based on overtopping principle. Several validations have been done for VOF model and overtopping rates in comparison with laboratory experimental data, analytical solutions and a comparable study. The regular linear wave is utilized in the present study as an incident wave using dynamic mesh in which the generated wave profile is in satisfactory agreement with the linear wave theory.

The baseline model is stationary buoyant overtopping wave energy converter in which several geometrical design strategies have been applied in order to study their effects on the wave energy harvesting mechanism and performance. The partial hydraulic efficiency based on captured crest energy is used as the main performance indicator in the present study. A design strategy in order to maximize the efficiency is applied by the mean of multi-stage reservoirs and their opening called slot at different crest heights. The hydraulic efficiency of different device layouts is compared with that of single-stage device to determine the effect of the geometrical design. Based on two-

dimensional simulation, The results show optimal trends giving a significant increase in overtopping energy. The optimal efficiency is obtained at relative slot width of 0.15 and 0.2 for variable slope and fixed slope devices respectively. Moreover, the use of adaptive slot width is studied. It has been concluded that the effect of adaptive slot on performance is unnoticeable.

Results of two-dimensional simulations show that the design of overlap ramp has a slight effect on overall hydraulic efficiency whether the slot layout is adaptive or non-adaptive. However, the partial efficiency is noticeably effected. Particularly, the larger overlap distance gives the greater hydraulic efficiency of the main reservoir and subsequently the smaller hydraulic efficiency of the lower ones. This seemingly influence on control strategy of power take-off unit. Additionally, the influence of submerged depth of multi-stage device installed on breakwater has been studied. The land-based device has greater efficiency in energy capture since the transmission wave is eliminated and is partly converted into overtopping energy. The deeper submerged depth results in the greater efficiency and finally tends to converge to a certain value.

Three-dimensional simulations have also been performed and compared to the two-dimensional results. The wider span or aspect ratio gives the greater capture crest energy. The result implies that further increasing the span, the efficiency tends to closely converge to that of two-dimensional device.

KEY WORDS: Wave energy converter 파력발전장치; Overtopping 월파형; Multi-stage device 다단식; CFD 전산유체역학

Chapter 1 Introduction

1.1 Background

The available energy resources in the world can be categorized into two kinds: Non-renewable energy, i.e., oil or fossil fuels, and Renewable energy, i.e., solar, wind or wave energy. Over the past decades, renewable energy becomes one of the most interesting research topics. Marine renewable energy is huge and available in the forms of tidal, current, offshore wind, ocean thermal, and sea wave.

Extracting energy from wave has advantage over other kinds of renewable energy because sea waves offer the greatest energy density compared to other renewable energy sources (Clément et al., 2002). Moreover, harvesting wave energy has little environmental impact. It has been estimated that the potential worldwide wave energy is approximately 2 TW (Thorpe, 1999). In 2014, it is reported that there is 3,730 kW installed capacity of wave energy utilization in UK, 700 kW in Portugal, 296 kW in Spain, 180 kW in Sweden, 200 kW in Norway, 350 kW in China, 500 kW in Korea, 16 kW in Singapore (Villate, 2014).

As a result of this, a large variation of concepts for wave energy conversion has been introduced worldwide (Drew et al., 2009), for example, overtopping device. Developers of Wave Energy Converters (WECs) have been focusing on maximizing the performance of the device by optimizing geometric design. The Overtopping Wave Energy Converter (OWEC) has an inclined wall, called ramp, to lift waves overtop and flow into a reservoir in order to raise the water head higher than the surrounding sea level. Then it simultaneously releases the stored water back to sea through power take-off unit, which generally is a low-head turbine. A well-known example of this device is the Wave Dragon as shown in Fig. 1.1 (Kofoed et al., 2006, Tedd and Kofoed, 2009).



Fig. 1. 1 Wave Dragon (Tedd and Kofoed, 2009)

The performance of OWEC has been investigated by the means of experiments and numerical simulations (Liu et al., 2008b, Liu et al., 2009, Jin et al., 2012, Nam et al., 2008, Victor et al., 2011). Researchers have focused on the influence of geometry on the discharge, more precisely the volume flow rate into the reservoir, which directly determines the performance of an OWEC and consequently the generation rate of useful electrical energy. Fig. 1.2 shows the example of single-stage OWEC type which had been studied by Nam et al. (2008).

Liu et al. (2008b) numerically studied the influence of sloping wall of the ramp and incident wave conditions, i.e., wave height and period, on the flow rate into the reservoir. It has been shown that the larger wave period results in larger discharge. The results also showed that, for the wave height smaller than the hydro head, the discharge is null within the parameter range considered. The slope also plays an important role in the volume discharge in which the smaller slope ratio gives greater discharge. This is later questioned by Liu et al. (2009b) who repeatedly conducted simulations to study the effect of wave conditions and slope ratio in more detail. The more recent study showed that the less slope gives smaller discharge than that of the steep one.

The two-dimensional numerical simulation of different shape of sloping arm of OWEC has been presented by Liu et al. (2009a). Several incident wave conditions in combination with three types of sloping arm have been simulated. The convex type gives the best performance on the discharge whilst the concave type gives the lowest performance compared to the others.

The number of guide vane installed on the ramp has been also investigated by Jin et al. (2012) in a three-dimensional numerical wave tank. The results showed that the larger number of guide vane will increase the overtopping discharge resulting in an increase in performance of the device. Moreover, the effects of draft height, i.e., the underwater height of the ramp, were studied. The deeper draft can capture more wave volume, hence discharge enhancement (Jin et al., 2012). The disadvantage of deeper draft is that more wave load is acting on the structure and may cause an unpredictable damage.

Victor et al. (2011) studied the effects of adaptive geometry control on the overall hydraulic efficiency and the overall hydraulic power of OWEC. The research focused on the effects of variable slope angle and crest freeboard on the performance of OWEC, base on wave characteristics collected from three nearshore locations: Ostend (Belgian Continental Shelf), MPN (Dutch Continental Shelf) and Fjaltring (Danish Continental Shelf). The effects of five difference geometry control scenarios have been simulated. The results showed that the effect of adaptive crest freeboard and adaptive slope angle are applied for each sea state in comparison with a fixed crest freeboard and fixed slope. It was shown that the effect of an adaptive slope angle is relative small whereas that of crest freeboard is significant.



Fig. 1. 2 Spiral-reef overtopping device (single-stage OWEC type) (Nam et al., 2008).

In order to enhance the performance of OWEC, the use of multi-stage reservoirs, as seen in the Sea Slot-cone Generator (SSG), has been suggested and studied (Kofoed, 2005, Vicinanza and Frigaard, 2008, Margheritini et al., 2009, Tanaka et al., 2015) as shown in Fig. 1.3.

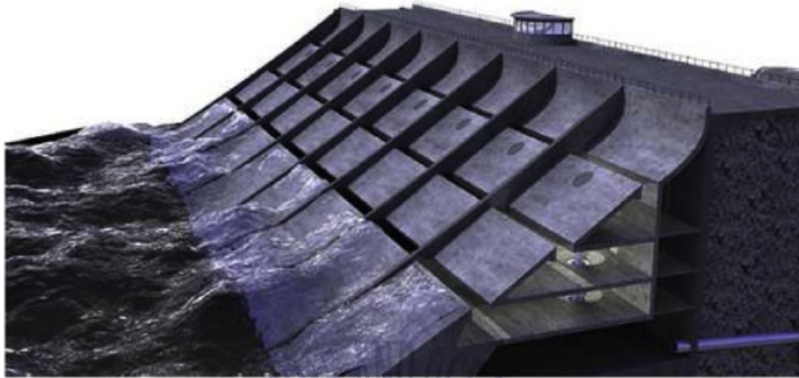


Fig. 1. 3 Graphics of SSG wave energy converter (multi-stage OWEC type)
(Vicinanza and Frigaard, 2008)

The relation between the wave energy and overtopping volume discharge has been presented by Tanaka et al. (2015) through experiments in wave tank. In these experiments, two types of the overtopping volume storage tank, a single tank and a multistage tank with varying hydro head or lifting range, were studied. The slope of the inclined wall and water depth were fixed constantly at 20° and 0.7 m respectively. The volume discharge is increasing linearly with increasing wave energy such that $q = \alpha E$, where q is the discharge, E is the wave energy and α is the linear coefficient. The coefficient or constant in the linear equation of the single tank is slightly more than the multistage tank. In addition, the discharge is a function of lifting range, more in particular, the discharge is decreasing with increasing lifting range.

In the experiments and numerical simulations of Minami and Tanaka (2015), equations used to predict the discharge of single-type and multi-type OWEC are proposed, in which the discharge can be calculated from four dimensionless variables. It has been shown that the predicted discharges of both single-type and multi-types are approximately 92 - 96 %

of the experimental results. The two-dimensional numerical results showed that the turbulent flow model with high reproducibility is Prandtl's-model.

Generally, the overall hydraulic efficiency of wave energy converters, based on the overtopping principle, can be 20 - 35 % when a single reservoir is used, and surprisingly up to 45 - 50 % for structure with reservoirs at 4 levels (Kofoed, 2002). The multi-stage OWEC employs several reservoirs for which the overtopping discharge of incoming waves is stored in different levels depending on the wave potential and run-up height. Generally, the potential energy of water in the reservoirs is extracted by the Multi-Stage Turbine (MST). This wave energy device can be floating or land-based.

However, the unsteady mechanism of overtopping flow is unclear, especially for the multi-stage devices. Several studies (Kofoed, 2006, Minami and Tanaka, 2015, Van der Meer and Janssen, 1995), proposed equations used to predict the amount of water captured in the reservoirs of single-stage and multi-stage OWECs, in which the discharge can be calculated from dimensionless variables. It has been shown that the predicted discharges of both types are approximately equivalent to the measured overtopping rates from comparable experiments. However, these analytical solutions do not explain flow physics and overtopping mechanism in detail. Also due to the complicated geometry of the multi-stage device, there are many other variables, affecting the energy harvesting efficiency of the device, that have not been studied yet.

In this thesis, numerical investigations have been performed using two- and three-dimensional RANS simulations in order to study flow physics and performance of wave energy devices used to harvest ocean wave power based on overtopping principle. Several geometrical design strategies have been utilized in order to study their effects on the performance of both stationary buoyant as well as land-based overtopping wave energy converter. Additionally, the reflection and transmission coefficients are used to determine the energy transportation. The goals of this study are to find a geometry giving optimal efficiency and to gain a better understanding of unsteady water flow mechanisms.

Chapter 2 Wave energy resource

2.1 Ocean energy

Ocean energy or marine renewable energy is huge and available in the forms of tidal, current, ocean wave, salinity gradients and ocean thermal energy as shown in Fig 2.1 (OES, 2012). Tidal energy is available in form of elevation rise and fall (potential energy) and current (kinetic energy) which can normally be extracted by the mean of turbines. Temperature gradients thermal energy due to the temperature gradient between the sea surface and deepwater can be utilized using different Ocean Thermal Energy Conversion (OTEC) processes. At the mouth of rivers where fresh water mixes with salt water, energy associated with the salinity gradient can be harnessed using pressure-retarded reverse osmosis process and associated conversion technologies. Waves kinetic and potential energy associated with ocean waves can be harvested using a device called Wave Energy Converter (WEC). Fig 2.2 shows the potential of marine renewable energy resource (SoerensenHC, 2008, IEA-OES, 2009, OpenEI, 2014), and indicates that the global availability of wave energy is approximately 80,000 TWh annually.

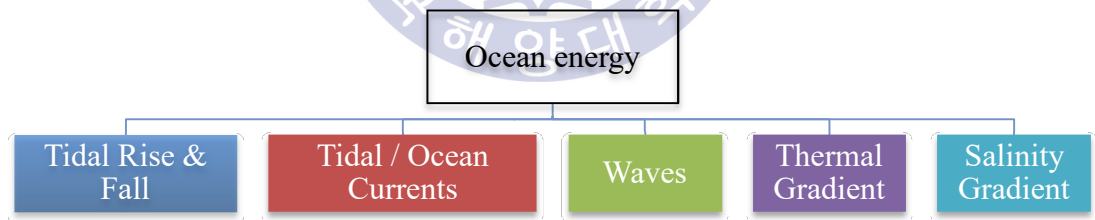
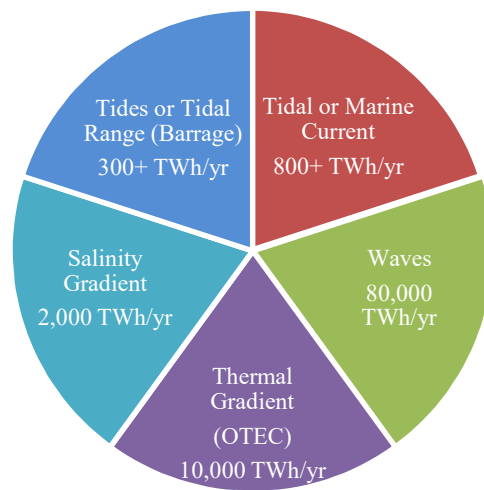
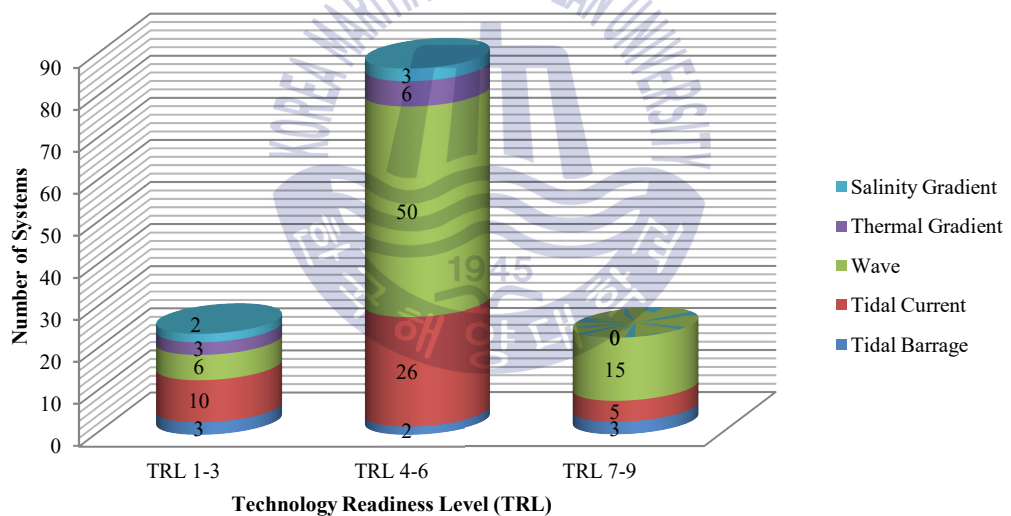


Fig. 2. 1 Ocean energy form



(a) Global Electricity Production in 2004 (IEA Statistics): 17,400 TWh/h



10+ years ↑

TRL 7-9: Field operational tests / commercial deployment
 TRL 4-6: Validation tests in simulated environment
 TRL 1-3: Proof of principle / Proof of concept

(b) Technology Readiness Level

Fig. 2. 2 Global status of ocean renewable energy

2.2 Wave energy resource

2.2.1 Wave energy resource in world

Extracting energy from wave has advantage over other kinds of renewable energy because sea waves offer the greatest energy density compared to other renewable energy sources (Clément et al., 2002). Moreover, harvesting wave energy has little environmental impact. It has been estimated that the potential worldwide wave energy is approximately 2 TW (Thorpe, 1999) which is analogous to a study by Gunn and Stock-Williams (2012). The more recent study estimated the global wave power resource as show in Fig. 2.3, that is, the total wave power incident on the ocean-facing coastlines of the world (neglecting certain islands and the poles), to be 2 TW.

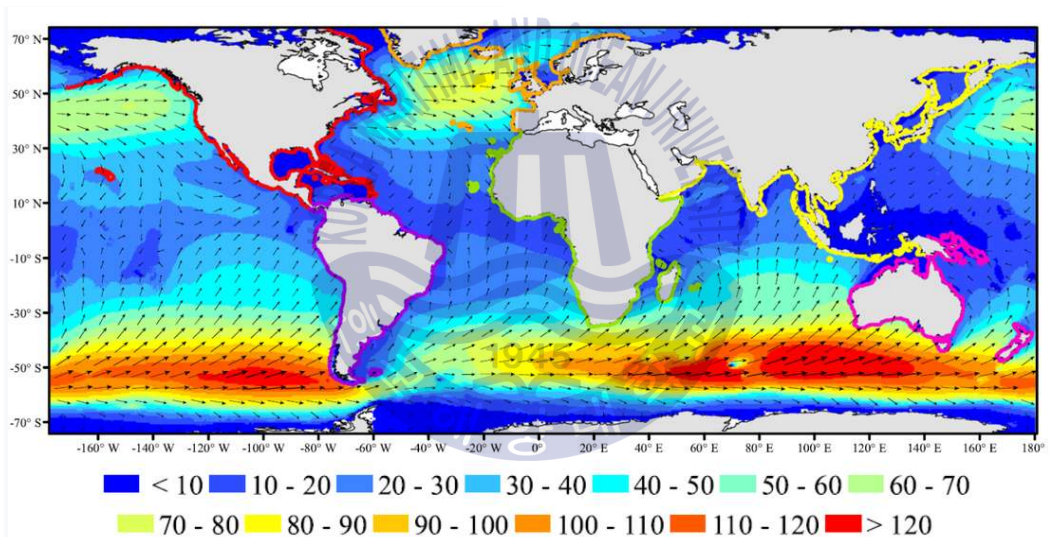


Fig. 2.3 Global wave power resource by Gunn and Stock-Williams (2012)

In 2014, it is reported that there is 3,730 kW installed capacity of wave energy utilization in UK, 700 kW in Portugal, 296 kW in Spain, 180 kW in Sweden, 200 kW in Norway, 350 kW in China, 500 kW in Korea, 16 kW in Singapore (Villate, 2014). Moreover, wave energy and the activity of wave energy utilization had been observed by Ocean Energy System (OES) that focused on the country of member in OES. Ocean Energy System (OES) summarized the ocean power of the countries member in OES which had been reported by the map of ocean power as show in Table 2.1.

Table 2. 1 Ocean power in OES countries (OES website)

| | Resource | Capacity (kW) | |
|---------------|----------|---------------|-----------|
| | | Installed | Consented |
| Europe | Waves | 2,056 | 45,149 |
| | Currents | 3,408 | 96,000 |
| | Salinity | 50 | 100,000 |
| North America | Waves | 20,000 | 1,350 |
| | Currents | 0 | 20,490 |
| | Waves | 9 | 1,545 |
| Oceania | Waves | 0 | 201,000 |
| | Currents | 0 | 22,040 |
| Asia | Tidal | 258,105 | 254,200 |
| | Currents | 1,170 | 5,850 |
| | Waves | 966 | 3,260 |
| | Thermal | 220 | 220 |

2.2.2 Wave energy resource focus on Southeast Asia

Southeast Asia is a sub region of Asia, as show in Fig. 2.4, which consists of eleven countries, Vietnam, Laos, Cambodia, Thailand, Myanmar, Malaysia, Indonesia, Singapore, Philippines, East Timor and Brunei. The only country that is not located near the sea is Laos.

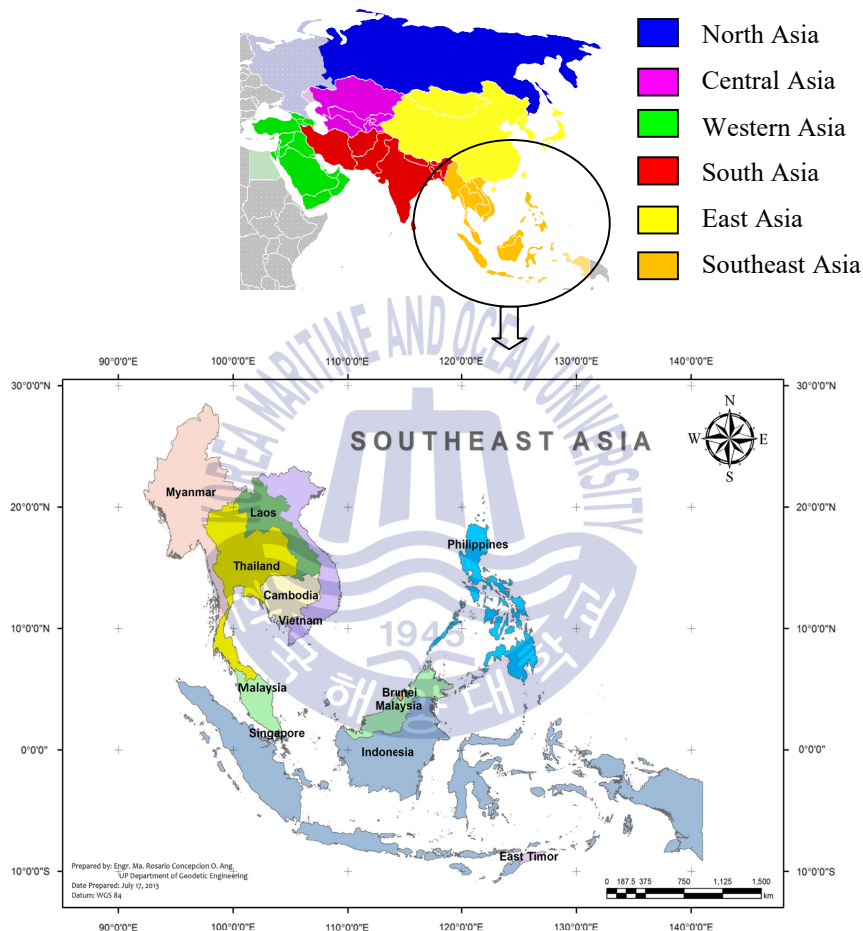


Fig. 2. 4 Map of country in Southeast Asia

Source: Top (United Nations Statistics Division, 2016)
and Bottom (Quirapas et al., 2015)

In this section, the wave energy resource or potential in Southeast Asia is presented. The overview of ocean renewable energy potential or resource data in Southeast Asia had been presented by Quirapas et al. (2015). A study of Malik (2011) indicated that Brunei Darussalam has potential for wave energy. However it may be economically infeasible since the country is seen to still rely on fossil fuels for the next decades.

Although Cambodia seems to have potential for tidal energy, it is not commercially suitable for tidal energy harvesting. Moreover, there is no data available for wave energy potential for the country.

Indonesian Ocean Energy Association (INOCEAN) theoretically conforms that there is a resource of 57 GW, 160 GW and 510 GW for OTEC, tidal current and ocean wave energy respectively. However there is only 1.2 GW for wave energy in practice. A study of Yaakob et al. (2006) concluded that Malaysia has less potential for ocean renewable energy in comparison to other locations. The average wave height in Malaysia is about 1 m. However, a study of Mirzaei et al. (2014) pointed out that the wave energy potential along the east coast of Peninsular Malaysia is significant. The northern part of the coast has wave potential of 2.6 - 4.6 kW/m while that of southern part is 0.5 - 1.5 kW/m.

Myanmar has about 11.5 - 23 GW wave energy potential estimated from 5 - 10 kW/m along the coastline of about 2,300 km. Other source of ocean energy in Myanmar are suitable for economic utilization, for example 5 - 7 m range of semi-diurnal tides or 20 - 22 °C temperature difference between sea surface and depth of 1 km. Total ocean energy potential in Philippines is approximately 170 GW. The range of wave potential is 33 - 35 kW/m depending on location.

Since the average wave height in Singapore is 1 m, several studies focus on extraction of tidal power which has about 3 TWh annually. Wave energy in Thailand has been estimated to be about 0.5 ktoe (500 tonnes of oil equivalent). Andaman sea has higher wave potential than gulf of Thailand due to geography conditions. There are several potential sites for wave energy in Vietnam. Offshore wave energy flux is considered as potential energy source which is about 40 - 411 kW/m.

Moreover, wave energy resource in Southeast Asia has been estimated by Ly et al. (2014). The result of research presented the maps of annual mean wave energy of Southeast Asia which shows in Fig. 2.5.

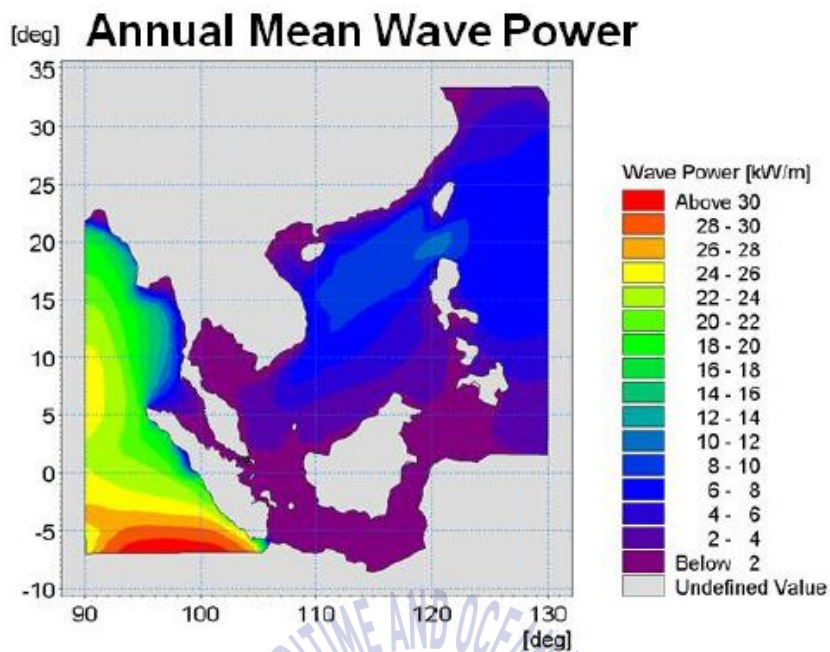
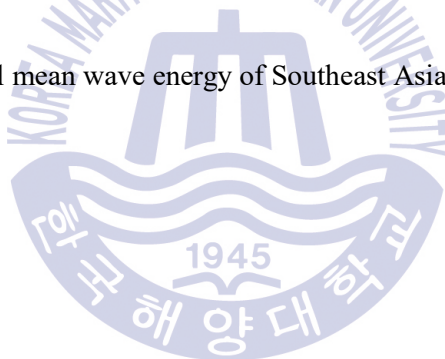


Fig. 2. 5 Annual mean wave energy of Southeast Asia (Ly et al., 2014)



2.2.3 Southeast Asia perspective

In this section, the examples of WEC researches in Southeast Asia are shown. Utilization of wave energy in Thailand has been research topic in local/national universities. Equipment called drifter has been developed to be used as ocean wave measuring system in order to study wave potential (Sanitwong na Ayutthaya and Iamraksa, 2016). It was found that wave energy potential in most part of gulf of Thailand is low, however, the potential in Andaman sea is applicative. Moreover, a study funded by the Thai ministry of energy, reports that harvesting energy from wave is possible in both gulf of Thailand and Andaman sea despite low-to-medium potential of wave power, see Fig. 2.6.

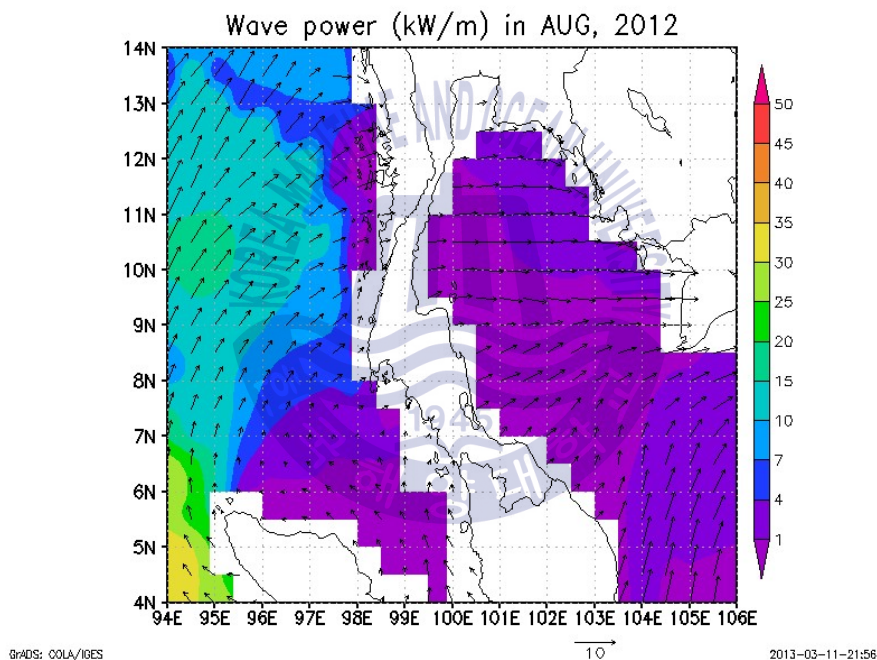


Fig. 2. 6 Example of simulation result of wave energy potential in Thailand
(Report of KUWave device, 2013)

Since Thailand is one of the most well-known and popular countries for beautiful beaches, hence shoreline or nearshore devices might have significant negative visual impact. An offshore device has therefore been said to be suitable for the country.

Scientists and researchers in Thailand have been studying a possibility to harvest energy from wave. Numerical studies (Thaweewat et al. 2013, Thaweewat, 2017) focus on an oscillating wedge buoy as a wave energy converter. A wave flume has been constructed in order to be used in designing and testing a prototype of the WEC.



(a) Preparing WEC for moving to test



(b) Checking the structure of WEC

Fig. 2. 7 Testing the WEC device in the sea of Thailand (Report of KUWave device, 2013)

Although the mentioned studies concern about WEC in laboratory scale or by the mean of numerical simulations, Thai researchers in Kasetsart university have designed and constructed a 10 kW wave energy converter, namely KUWave working as a terminator and pitching buoy, which has been installed and tested near Laem Chabang, Chonburi, see Fig. 2.7. The device is expected not only for electrical power generation but also for coastal erosion control since it is a main problem for Thailand on both Gulf of Thailand and Andaman Sea coasts which approximately have a total length of about 1,900 km.

Last example of research, Singapore's researchers had been developed the wave energy converter that is called *Drakoo* (Dragon King of Ocean). Researchers show the basic idea and conception design of *Drakoo*, as shown in Fig. 2.8, is a twin-chamber oscillating water column system (Drakoo WEC). Collect water from the wave into the trap system. The water flow is continuously transferred to the turbine to generate electricity. First, the waves move into the trapdoor. The water in the trap room will be higher. The second stage, the water level is reduced by the flow control valve. And the water flows through the turbine to the generator. Drakoo's work ethic was developed and built in several versions. There are experiments in various ratios in the laboratory and tested in the sea.

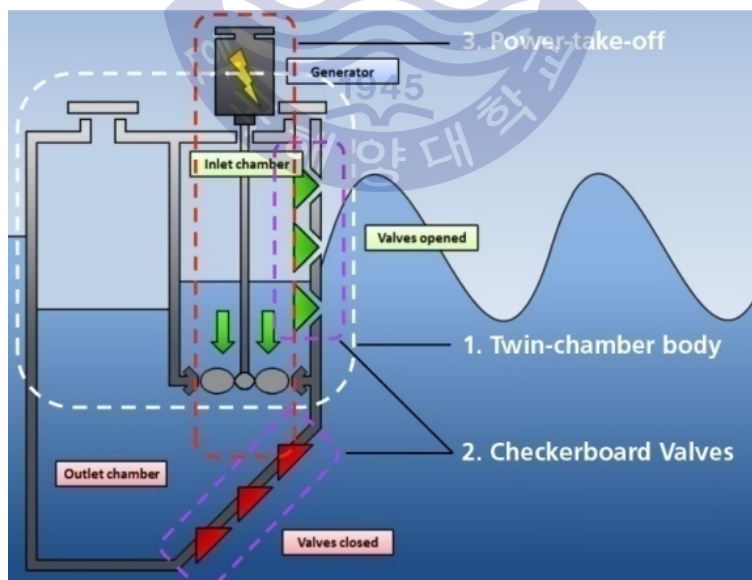


Fig. 2. 8 Basic principle of Drakoo operation (Drakoo WEC)

In the step of model testing, research and development of Drakoo Wave Power Equipment introduces the concept of working device to miniaturized model. For laboratory testing, the equipment in the laboratory as shown in Fig. 2.9, and in September 2010, the R & D team tested the 1:5 model of the Drakoo-II device at Nanyang Technological University (NTU). The test results achieved a CWR of 66 %. After that the device was developed to be ready for testing in the sea. Device development continues to be patented in 2008.

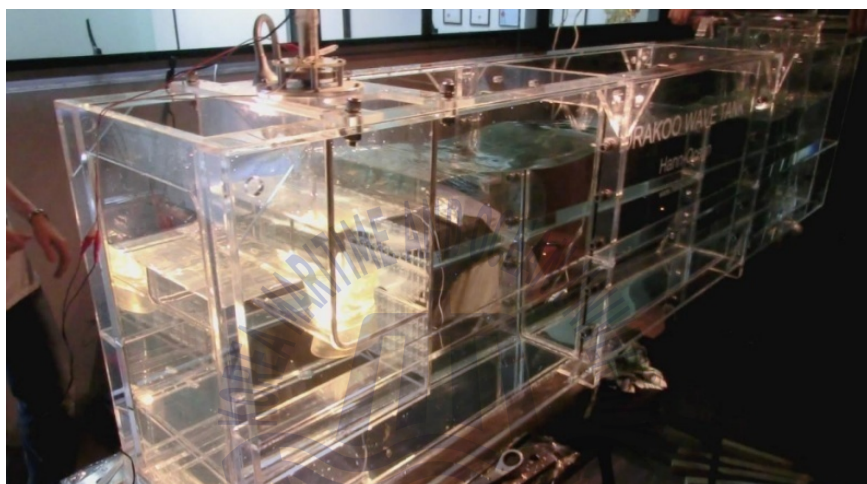


Fig. 2. 9 Drakoo model testing in a laboratory (Drakoo)

The prototype of Drakoo was tested in the sea began in May 2011, a model test 1:2 scale of Drakoo-III device with other systems were tested in Singapore and July In the same year, the performance of the Drakoo WEC device was tested by the UK's National Renewable Energy Center (Narec) for its powerful Capture Width Ratio (CWR) to convert wave energy to maximum water flow to 90 % and an average CWR efficiency of 50 % for regular waves. Fig. 2.10 shows the device was tested in the sea (Drakoo WEC). Moreover, Drakoo-B0004 commercial wave energy converter is commercially available. This is the first commercial Drakoo wave energy converter device.



Fig. 2. 10 Example of Drakoo-III prototype testing in the sea (Drakoo device)

Fig. 2.11 shows the results of the experiment and calculates the energy obtained from the Drakoo wave energy absorber at the height and wavelength. It will be seen that the device is highly effective when the wave size is appropriate for the size of the device according to the design conditions.

| Wave Height Hs (m) | Wave Period, Tp (sec) | | | | | | | | | |
|-----------------------|-----------------------|------|------|------|------|------|------|------|------|------|
| | 3 | 4 | 5 | 6 | 7 | 8 | 9 | 10 | 11 | 12 |
| 0.2 | 0.04 | 0.10 | 0.15 | 0.17 | 0.16 | 0.14 | 0.11 | 0.09 | 0.07 | 0.01 |
| 0.3 | 0.08 | 0.25 | 0.37 | 0.43 | 0.41 | 0.35 | 0.28 | 0.20 | 0.15 | 0.03 |
| 0.4 | 0.15 | 0.45 | 0.68 | 0.78 | 0.75 | 0.64 | 0.50 | 0.40 | 0.29 | 0.04 |
| 0.5 | 0.26 | 0.72 | 1.10 | 1.30 | 1.22 | 1.03 | 0.81 | 0.63 | 0.46 | 0.07 |
| 0.6 | 0.37 | 1.07 | 1.64 | 1.87 | 1.80 | 1.54 | 1.20 | 0.93 | 0.68 | 0.10 |
| 0.7 | 0.52 | 1.52 | 2.24 | 2.55 | 2.45 | 2.10 | 1.68 | 1.33 | 0.95 | 0.14 |
| 0.8 | 0.68 | 1.98 | 2.92 | 3.33 | 3.21 | 2.74 | 2.19 | 1.74 | 1.30 | 0.18 |
| 0.9 | 0.88 | 2.51 | 3.69 | 4.00 | 4.00 | 3.47 | 2.77 | 2.21 | 1.65 | 0.25 |
| 1 | 0.88 | 2.51 | 3.69 | 4.00 | 4.00 | 3.47 | 2.77 | 2.21 | 1.65 | 0.25 |
| 1.1 | 0.88 | 2.51 | 3.69 | 4.00 | 4.00 | 3.47 | 2.77 | 2.21 | 1.65 | 0.25 |
| 1.2 | 0.88 | 2.51 | 3.69 | 4.00 | 4.00 | 3.47 | 2.77 | 2.21 | 1.65 | 0.25 |
| 1.3 | 0.88 | 2.51 | 3.69 | 4.00 | 4.00 | 3.47 | 2.77 | 2.21 | 1.65 | 0.25 |

Fig. 2. 11 Results of the experiment and calculates the energy obtained from the Drakoo wave energy absorber (Drakoo)

Chapter 3 Wave energy utilization

3.1 Ocean wave energy

Ocean wave is generated by wind passing over the surface of the sea. As long as the waves propagate slower than the wind speed just nearly above the waves, there is an energy transfer from the wind to the waves. The energy in the ocean waves is a form of both kinetic and potential energy which are theoretically proportional to wave height and wave period. The size of the wave height significantly depends on the wind speed.

The basic principle of wave theory is the linear wave theory which is useful to explain the behavior of ocean wave, particularly regular wave despite the model simplicity. The most elementary wave theory is the small-amplitude or linear wave theory. This theory, developed by Airy (1845), is easy to apply, and gives a reasonable approximation of wave characteristics for a wide range of wave parameters. Although there are limitations to its applicability, linear theory can still be useful since the assumptions made in developing this simple theory are not grossly violated. Fig. 3.1 shows the characteristics and definition of the Airy wave.

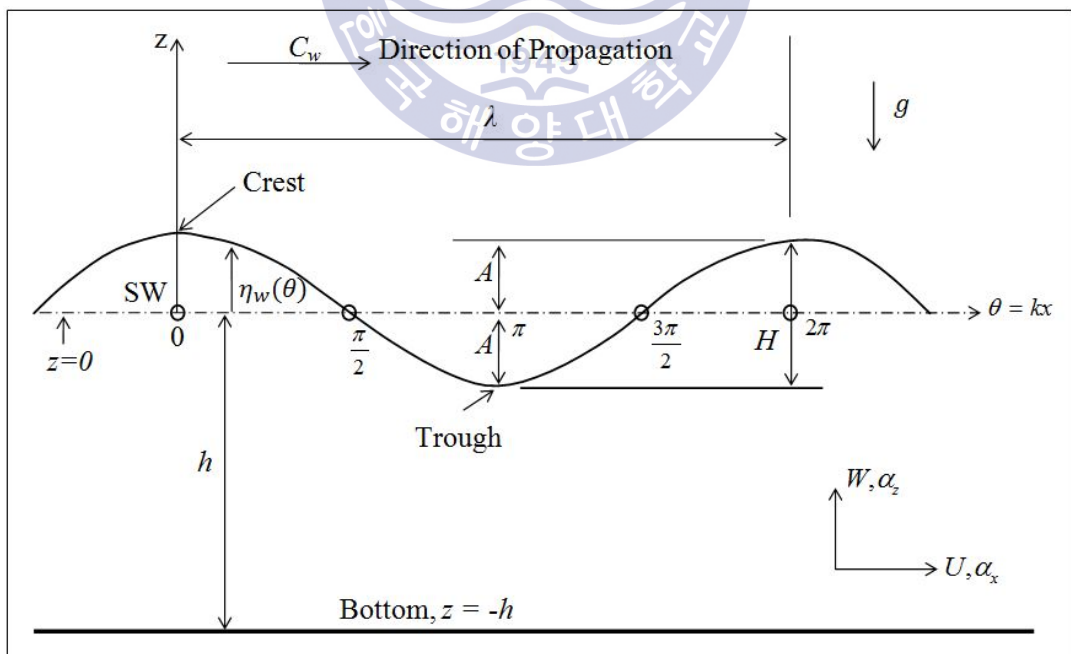


Fig. 3. 1 Characteristics of a regular wave

The wave surface elevation η_w is function of horizontal position x and time t which can be defined by:

$$\eta_w = A \cos(\theta) = \frac{H}{2} \cos(kx - \omega t) = \frac{H}{2} \cos\left(\frac{2\pi x}{\lambda} - \frac{2\pi t}{T}\right) \quad (3.1)$$

here η_w is wave surface elevation, λ is wavelength, A is amplitude, H is wave height, ω is angular frequency, k is wave number, T is wave period, C_w is wave speed and g is gravitational acceleration.

Energy of ocean wave or wave energy density E consists of two parts of energy form: potential energy E_p and kinetic energy E_k which can be defined by:

$$E = E_p + E_k \quad (3.2)$$

The average potential energy E_p is obtained as the integral over one wavelength and the total kinetic energy E_k is given as the sum of $1/2mv^2$ over all fluid particles. The equation 3.2 can be written by:

$$E = \frac{1}{\lambda} \int_0^\lambda \int_{-h}^{\eta_w} \rho g z dz dx + \frac{1}{\lambda} \int_0^\lambda \int_{-h}^{\eta_w} \frac{1}{2} \rho (u^2 + w^2) dz dx \quad (3.3)$$

$$E = \frac{1}{16} \rho g H^2 + \frac{1}{16} \rho g H^2 \quad (3.4)$$

Total wave energy is:

$$E = \frac{1}{8} \rho g H^2 \quad (3.5)$$

here u and w is horizontal and vertical orbital velocity respectively. Moreover, the units of total wave energy E is joules/m².

The wave energy flux P_{wave} explained the transport of energy across vertical sections of water that is equal to the energy density carried along by the moving waves:

$$P_{wave} = \frac{1}{T} \int_0^T \int_{-h}^{\eta_w} [\Delta p(x, z, t)] u dz dt \quad (3.6)$$

$$P_{wave} = \frac{1}{8} \rho g H^2 c \frac{1}{2} \left[1 + \frac{2kh}{\sinh(2kh)} \right] = Ecn \quad (3.7)$$

The wave energy flux or wave power shown in the Eq. 3.7 consists of three terms: wave energy density E , phase velocity c and factor n . The factor n is relates to the region of water depth, for deep water, $n = 1/2$ and for shallow water, $n = 1$. Moreover, the unit of wave power P_{wave} is watts/m.

3.2 Classification of wave energy converter

Wave energy converter (WEC) is a machine or device which is able to harvest or extract energy from ocean wave and then store or convert it into a useful form. Generally, a wave energy converter (WEC) consists of two systems or devices: wave capture device and power take-off system (PTO). The former directly interacts with incident wave and subsequently extracts energy from it. Then the latter simultaneously take-off energy from wave capture device and accumulate in an energy storage, i.e., battery or hydraulic accumulator. There is a large variation of concepts for wave energy conversion. However the wave energy converters (WECs) can be categorized by location, orientation, operation modes and structure (Drew et al., 2009).

3.2.1 Location

The advantage of Shoreline devices is being close to the utility network resulting in the ease of maintenance. On the other hand, devices installed on shoreline have less energy harvesting potential as wave travelling into shallow water and therefore lower power itself. Nearshore devices are located in relatively shallow or intermediate water. The devices are normally attached to the seabed. Similar to the shoreline devices, the disadvantage of nearshore devices is that wave energy is reduced due to decreased depth of water. Offshore devices are generally installed in deep water which has greater wave power density. The

disadvantages of these devices are difficulties in construction and maintenance as well as risk of operation in extreme conditions. Moreover, the grid connection is considerably difficult and expensive.

3.2.2 Orientation in wave

Point Absorber is a small size of WEC device relative to the incident wavelength. It is normally a floating structure in which the pressure differential cause the device can be heave up and down on the surface of the water. An example of a point absorber WEC is Ocean Power Technology's Powerbuoy. Attenuator is a WEC device that its orientation lie perpendicular to the wave front (parallel to the predominate wave direction) and ride the wave. One example of an attenuator-type WEC is the Pelamis, developed by Ocean Power Delivery Ltd. Wave energy converter devices that are arranged in a direction obstruct waves and perpendicular to the predominant wave direction (parallel to the wavefront) is called Terminator devices. Salter's Duck is an example of this type of WEC.

3.2.3 Operation modes

Oscillating Devices are using the concept of mechanical vibration to capture wave energy. The system consists of a wave capture device and PTO. The former is generally an oscillating buoy representing an inertia in the equation of motion. The latter can be hydraulic device or electrical generator which represents damping coefficient in the equation of motion. In order to obtain optimal performance, the system requires approximate resonant motion with the incident wave which is acting as exciting force (Falnes, 1997, 2007, Mei, 2012). Not only does the kinematics play an important role in wave capture mechanism but also the shape of the buoy. With the optimum phase condition, only 50% of wave energy can be theoretically absorbed by a symmetrical body oscillating in only one mode of motion (Evans, 1976). However, Falnes (1997) stated the possibility to capture wave energy beyond that limit. It is suggested to employ a symmetrical body with two modes of oscillation or an efficient asymmetric body with one mode of oscillation.

A wave capture device of Oscillating Water Column (OWC) is water chamber, whilst a PTO is turbine. The oscillatory water level in the chamber depends on surrounding wave condition and wave capture capability of the device. Then the water interacts with the air

within the chamber. Both positive and negative pressures are applied to the air which is forced to flow in and out the chamber through turbine. Therefore, the turbine used in this type of WEC must be able to rotate irrespectively of airflow direction, i.e., self-rectifying air turbine.

An Overtopping Wave Energy Converter (OWEC) has an inclined wall, called ramp, to lift waves overtop and flow into a reservoir which has greater head than the surrounding sea level. Then it simultaneously releases the stored water back to sea through PTO which is generally low-head turbines. Some of overtopping devices are installed with parabolic reflectors to increase wave power concentration toward the ramp. An example of this device is the Wave Dragon.

Another type of WEC is the Cycloidal Wave Energy Converter (CycWEC) which consists of one or more blades oriented parallel to a main shaft similar to a vertical axis wind turbine (VAWT). To harvest energy from waves into useful electrical energy, the CycWEC must synchronize with incident waves, efficiently extracts the wave energy to drive a shaft on a generator working as PTO. An example of this device is the Atargis CycWEC studied by Siegel et al. (2011, 2012), Siegel (2014).

3.2.4 Structure

Anchored structure is a device that floats on the water surface and has the mooring system. A device which fixed or installed on the sea floor is called Seabed structure. A device with Land-based structure is installed on shoreline or any other fixed structure, such as breakwater.

3.3 Stage of the wave energy converter research

Generally, the research and development stages of devices used to capture wave energy can be divided into 3 steps: step 1: conceptual design of wave energy converter device, step 2: a model testing in laboratory and last step is a prototype of a wave energy converter device testing in sea. The three steps are all important.



Fig. 3. 2 Stage of research

3.3.1 Concepts for designing a wave energy device

The first step of research in engineering field is a conceptual design. In this step, a researcher can give and suggest some ideas but the idea have to base on the scientific and engineering theories. The design of a wave energy converter may be derived from a similar concept but finally the shape of device does not need to be the same, it depends on many factors, i.e., wave condition, location. In general, the design concept has limits and conditions to consider, such as cost, production, maintenance and environmental impact.

3.3.2 Model testing in a laboratory

Based on the idea of designing a wave energy device in section 3.3.1, the next step of research and development is model testing. This step is a testing of model device system, such as a mooring system, a power take off system and a response system of a device. An example device in the wave basin shows in Fig. 3.3. Generally, a researcher should make a model of device for testing in the laboratory after the design concept is completed. Because the concept design of device is needed to prove by the model testing. Moreover, the results of laboratory testing will give some data which can use to improve and develop the device. In this stage, if a researcher does not have the laboratory for test a model that some researcher use only a numerical simulation method to simulate then they will find some

experiment results to compare that. In the world, there are many laboratory-tested of wave energy converter devices such as SEAREV, Salter's Duck WEC, OPT Powerbouy, Wavebob WEC, Pelamis WEC, DEXAWAVE and Wave Dragon.

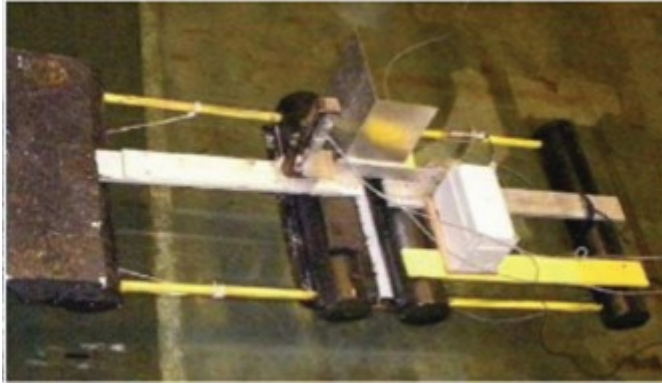


Fig. 3. 3 DEXAWAVE model, 1:10 scale, in the water wave basin (Ruol et al., 2011)

3.3.3 Testing of a wave energy converter device in sea

Normally, when testing a model of device in a laboratory that can control variables and give a good result, then the testing equipment required to test in the sea. In this step, a prototype can make in the real or scale size that depends on the researcher. The advantage of sea trial is the device locates in the real situation and researcher will get the data collection from the real behavior of device. There are many devices that have been tested in the laboratory and were created in scale or real size. For example, OPT Powerbouy, Wavebob WEC, Pelamis WEC, DEXAWAVE, Wave Dragon, Drakoo Wave, Wave Star, Poseidon and SSG-breakwater. Fig. 3.4 shows the example of wave energy converters which are operated in the sea.



(a) DEXAWAVE



(b) Pelamis WEC



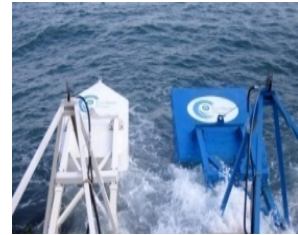
(c) Archimedes Wave Swing



(d) Wave Star
(Marquis et al., 2010)



(e) Drakoo



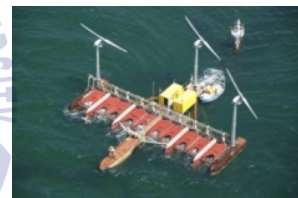
(f) Wave Clapper



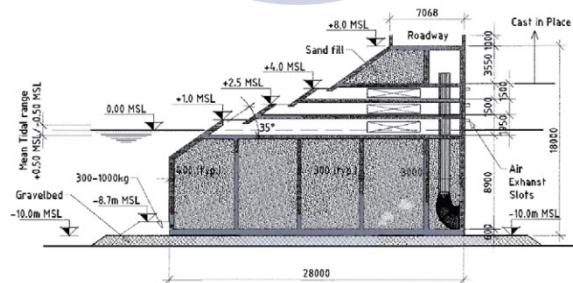
(g) Wave Dragon



(h) Oyster WEC
(Whittaker et al., 2007)



(i) Poseidon



(j) SSG-breakwater caisson (Vicinanza et al., 2012)

Fig. 3. 4 Example of wave energy converter operation in the sea

3.4 Overtopping wave energy converter

In this research, an overtopping wave energy converter (OWEC) type is focused to study. Generally, an overtopping wave energy converter has incline wall to lift water wave overtop flow into the reservoir. Then it releases water back to sea through power take-off. The basic principle concept of OWEC shows in Fig 3.5.

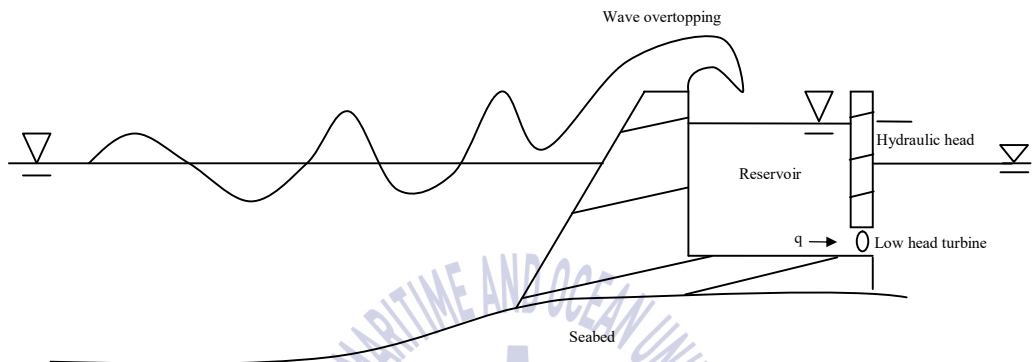


Fig. 3. 5 Basic principle concept of OWEC

The performance of OWEC has been investigated by the means of experiments and numerical simulations. Scientists and researchers have focused on the influence of geometry on the discharge, volume flow rate into the reservoir, which directly determines the performance of an OWEC and consequently the generation rate of useful electrical energy.

3.4.1 Wave overtopping energy

Generally, the overall efficiency of OWEC device consists of four partial efficiencies, i.e., hydraulic efficiency, reservoir efficiency, turbines efficiency and generator efficiency. In the present study, the numerical results are represented by the hydraulic efficiency η calculated based on crest levels $R_{c,i}$ and averaged discharge Q_i . The hydraulic efficiency η is defined as the ratio between the potential power P_{crest} in the overtopping water and the power in the incident wave P_{wave} which is also used by Margheritini et al. (2009) and Tanaka et al. (2015) as:

$$\eta = \frac{P_{crest}}{P_{wave}} \quad (3.8)$$

where

$$P_{crest} = \sum_{i=1}^n Q_i \rho g R_{c,i} \quad (3.9)$$

here ρ is the sea water density, g is the gravitational acceleration, Q_i is the average overtopping flow rate per unit length of the i^{th} reservoir, $R_{c,i}$ is the crest height of the i^{th} reservoir.

The average overtopping flow rate is calculated from the range where the data is periodically repeated. The simulations are monitored for at least 15 wave periods to obtain solutions. In case of aperiodic solution, the simulation is further monitored until a periodic solution is obtained.

The incident, reflected and transmitted wave power can be calculated using Eq. 3.7, when the height or amplitude of these waves is known. The transportation of energy conservation of the overtopping phenomenon can be explained by:

$$P_{wave} = P_{crest} + P_r + P_t + P_L \quad (3.10)$$

here P_r is the reflected wave power, P_t is the transmitted wave power and P_L is the dissipated wave power or loss.

Since the wave power is proportional to H^2 or a^2 then the dimensionless wave energy in reflection wave is proportional to K_r^2 where K_r is the reflection coefficient which is ratio between the reflected and incident wave amplitudes: $K_r = a_r/a_i$. In addition, Eq. 3.10 can be expressed in dimensionless form by:

$$1 = \eta + K_r^2 + K_t^2 + L_l \quad (3.11)$$

where K_r^2 is the reflection rate, K_t^2 is the transmission rate and L_l is the loss rate which is defined as ratio between the dissipated wave power P_L to the incident wave power: $L_l = P_L/P_{wave}$. This equation is similar to transportation of energy conservation used by Tanaka et al. (2015).

3.4.2 Wave reflection analysis

It is possible to determine the reflection coefficient from wave profiles recorded using numerical wave probes, since the free surface elevation is assumed to be the superposition of sinusoidal incident and reflected wave trains. Several publications proposed different experimental techniques to calculate wave reflection. A summary of these publications explaining methods for obtaining the incident wave height H and reflection coefficient K_r is presented by Isaacson (1991). In the present study, the method of two fixed probes is used to calculate the reflection coefficient since it is cited as the most accurate method. The incident and reflected wave amplitudes can be represented respectively by:

$$a_i = \frac{1}{2|\sin \Delta|} \sqrt{A_1^2 + A_2^2 - 2A_1A_2 \cos(\Delta + \delta)} \quad (3.12)$$

$$a_r = \frac{1}{2|\sin \Delta|} \sqrt{A_1^2 + A_2^2 - 2A_1A_2 \cos(\Delta - \delta)} \quad (3.13)$$

where A_n is the measured amplitude of the n^{th} probe, Δ is the dimensionless distance between two probes, and δ is the measured phase angle of second probe relative to that of the first probe and is obtained by fast Fourier transform (FFT) algorithm. The ratio between the reflected and incident wave amplitudes: $K_r = a_r/a_i$ is defined as reflection

coefficient. Similarly, the transmission coefficient is expressed as the ratio between the transmitted and incident wave amplitudes: $K_t = a_t/a_i$.

3.4.3 Overtopping wave energy converter configurations

In this section, the overtopping wave energy converter configurations are presented. There are many concepts of OWEC shape in the world. From the literature review for research of OWEC devices, as summarized in Table 3.1, the device can be divided into two categories, fixed structure and floating structure. The most of structure type was designed and used is a fixed structure type. The main reason is that the fixed structure devices have a less complex mechanism than floating structures.

The fixed structure does not take into account the mechanism of the mooring system. While the floating device must consider the mooring system and dimension of the structure corresponding to the behavior of the wave, such as the length of the wave affecting the length of the floating structure. If the wavelength is greater than the length of the device, the device will have a very high pitch and heave response, which directly affects the performance of the device. This type of device possesses the most difficulty to simulate since the fluid-structure interactions and hence its motion must be taken into the equations.

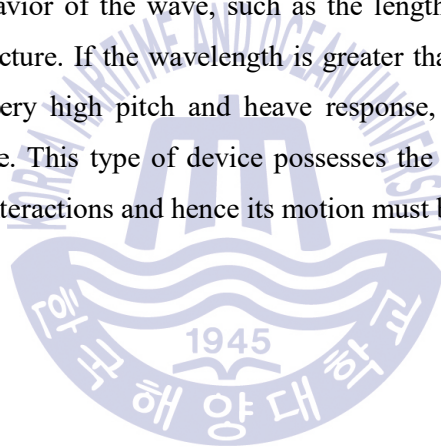
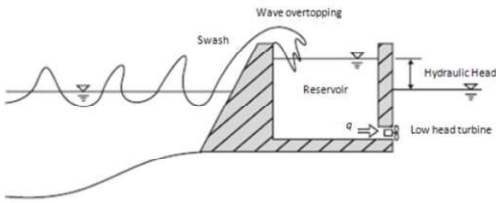
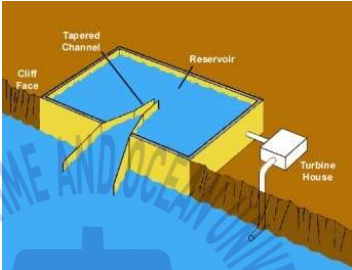
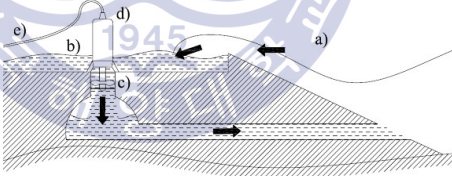

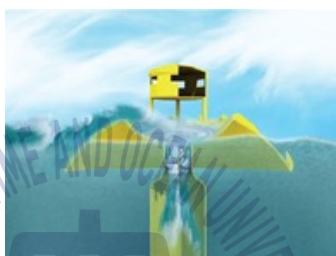


Table 3. 1 Example of OWEC device configurations

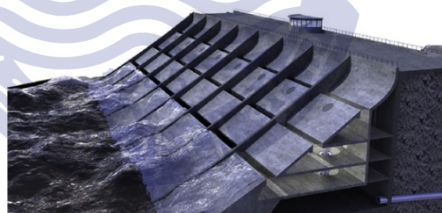
| Type | Item |
|-----------------|---|
| Fixed structure |  <p>General configuration of OWEC (Shin and Hong, 2005)</p> |
| |  <p>A shoreline WEC of the overtopping type, TAPCHAN (Clément et al., 2002)</p> |
| |  <p>Overtopping Device (on-shore) (Energy Industry Challenges (Renewable Uk), The European Marine Energy Centre LTD)</p> |
| |  <p>OWEC model without guide vane was tested by Liu et al. (2011)</p> |



Model testing in the wave tank OWEC model with guide vanes
(Park et al., 2011, Jin-Seok 2009)



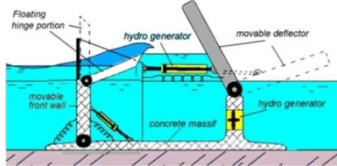


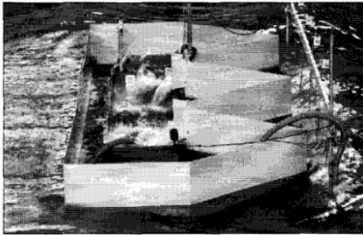
Spiral-reef overtopping device (single-stage OWEC type) (Nam et al., 2008)



Muti level overtopping Vicinanza and Frigaard (2008)



The multi-stage reservoir of OWEC model test in Japan
(Minami and Tanaka, 2015)

| | |
|--------------------|--|
| | <p>Final result : Converter with the movable front wall working like «Oyster» system</p>  <p>The Overtopping and Oyster wave energy converter mixed system (Gentova A.A. and Kovalenko S.V)</p> |
| |  <p>Wave Dragon had been installed in the sea (Tedd and Kofoed, 2009)</p> |
| Floating structure |  <p>WaveCat model test in the wave tank which has four reservoirs for storing overtopping water. (Fernandez et al., 2012)</p> |
| |  <p>The experiment of the wave overtopping control structure (Shin and Hong, 2006)</p> |

Chapter 4 Numerical simulation of OWEC device

4.1 Numerical wave simulation

In the present study, a commercial CFD solver ANSYS FLUENT V.17 is used to simulate wave overtopping behavior and characteristics for single- and multi-stage OWEC devices. The governing equations used in the present investigation are the continuity and the Reynolds Averaged Navier-Stokes (RANS) equations for viscous, incompressible, two-dimensional flow, in combination with two-phase volume of fluid (VOF) method proposed by Hirt and Nichols (1981) in order to track and locate the free surface. The standard $k-\varepsilon$ turbulence model is applied for turbulence closure.

$$\frac{\partial u_i}{\partial x_i} = 0 \quad (4.1)$$

$$\frac{\partial u_i}{\partial t} + u_j \frac{\partial u_i}{\partial x_j} = -\frac{1}{\rho} \frac{\partial p}{\partial x_i} + f_i + \frac{\partial}{\partial x_j} \left(\nu \frac{\partial u_i}{\partial x_j} - \overline{u'_i u'_j} \right) \quad (4.2)$$

where ν , ρ , p and f_i are the kinematic viscosity coefficient, the fluid density, the fluid pressure and the body force, respectively. u_i , x_i represent the coordinate directions and corresponding velocity components. The component $\overline{u'_i u'_j}$ requires the Reynolds Stress induces a new turbulence model to enclose the equations.

The volume fractions of air and water in the computational cell sum to unity. If the volume fraction of water is defined as a_w , then the following three different conditions of volume fraction of water are possible: 1) $a_w = 0$, the cell is empty of water; 2) $a_w = 1$, the cell is full of water; 3) $0 < a_w < 1$, the cell contains the interface. The volume fraction a_w is calculated as:

$$\frac{\partial a_w}{\partial t} + \frac{\partial (a_w u_i)}{\partial x_i} = 0 \quad (4.3)$$

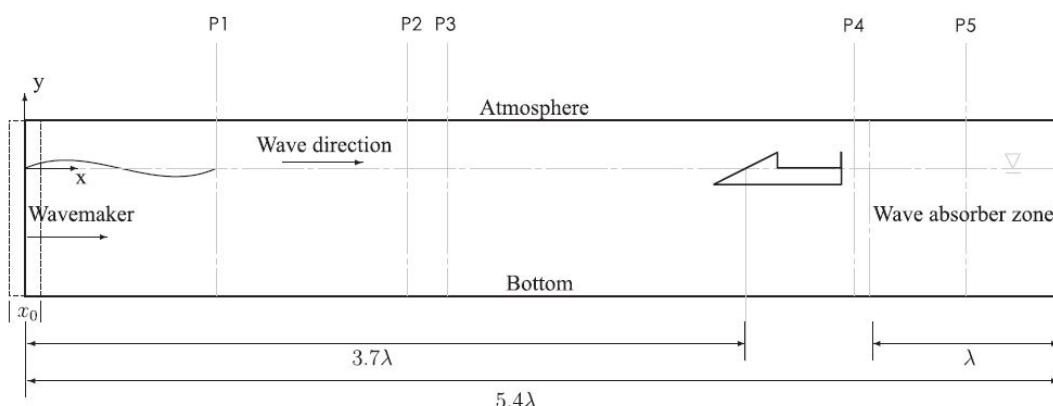


Fig. 4. 1 Two-dimensional numerical wave tank used to simulate wave overtopping behavior. The locations of wave probes are indicated by P1, P2, P3, P4, and P5

The wave overtopping behavior is simulated in a two-dimensional numerical wave tank as shown in Fig. 4.1, which has water depth of 20 m and the tank length is 300 m. Numerical wave probes are employed in order to monitor surface elevation. The pressure outlet and open channel flow condition combined with porous media zone is applied on the right boundary acting as a wave absorber such as used by Du and Leung (2011) and Hu and Liu (2014), while the wall condition combined with dynamic mesh model is utilized on the left boundary acting as a wavemaker.

The airy wave is generated as an incident wave in the present study. The kinematics of the piston type wavemaker $x(t)$ is defined by:

$$x(t) = \frac{x_0}{2} \left(1 - e^{\frac{-5t}{2T}} \right) \sin \omega t \quad (4.4)$$

where x_0 is the maximum displacement of the wavemaker and ω is the angular frequency.

For numerical wave tank, a numerical beach is necessary, as a wave absorber or dissipation zone in order to avoid the occurrence of wave reflection. In the present study, the porous media condition is applied to form an artificial wave absorber zone which is located on the right boundary of domain.

Behind the device is the wave absorber zone which has the length of a wavelength (1λ) measured from the right boundary. The shorter of the absorber zone could give the higher wave reflection rate, while increasing length of the absorber results in the more computational expense. In this zone, the pressure outlet and open channel flow condition combined with porous media zone is applied on the right boundary acting as a wave absorber such as used by Du and Leung (2011) and Hu and Liu (2014). The porous media condition is defined by an additional momentum source term which is added to the Navier-Stokes equations as:

$$\rho \left(\frac{\partial u}{\partial t} + u \cdot \nabla u \right) = (-\nabla p + \mu \nabla^2 u + f) + S_i \quad (4.5)$$

and

$$S_i = - \left(\frac{\mu}{\alpha} u_i + C_2 \frac{1}{2} \rho |u_i| u_i \right) \quad (4.6)$$

where S_i is the additional source term for the i -th (x, y or z) momentum equation, $|u_i|$ is the velocity magnitude, μ is the viscosity of the fluid, C_2 is the inertial resistance factor, and $1/\alpha$ is the viscous resistance coefficient.

This momentum source term is composed of two parts: a viscous loss term (the first term on the right-hand side of Eq. 4.6), and an inertial loss term (the second term on the right-hand side of Eq. 4.6) which is added in the Navier-Stokes equations. In this work, the coefficient $1/\alpha$ is the main parameter in order to define the rate of absorption. As described in Du and Leung (2011), only $1/\alpha$ can be considered. If $1/\alpha$ is too small, the wave energy cannot be effectively absorbed. If $1/\alpha$ is too large, the porous media will act as a solid wall and the wave will reflect at the entrance of porous zone. The viscous resistance coefficient is defined as a function of the position, which is described by a UDF code.

4.1.1 Validation of volume of fluid model

In this present study, the VOF model used in ANSYS Fluent is validated by the laboratory experimental data of a dam break over a dry bed conducted by Martin and Moyce (1952) which is a very useful benchmark. The contour and position of the leading edge of water is plotted against non-dimensional time, see Fig. 4.2 - 4.3. The numerical result of the present study is in satisfactory agreement with the experiment and a comparable study (Hirt and Nichols, 1981).

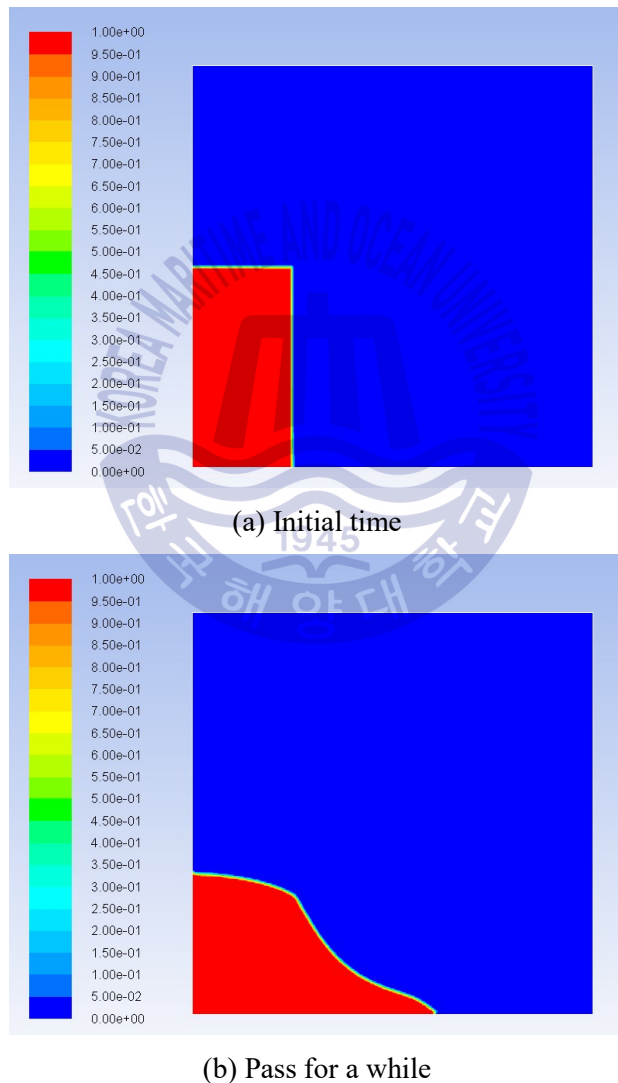


Fig. 4. 2 Contour of water and air phases of a dam break over a dry bed

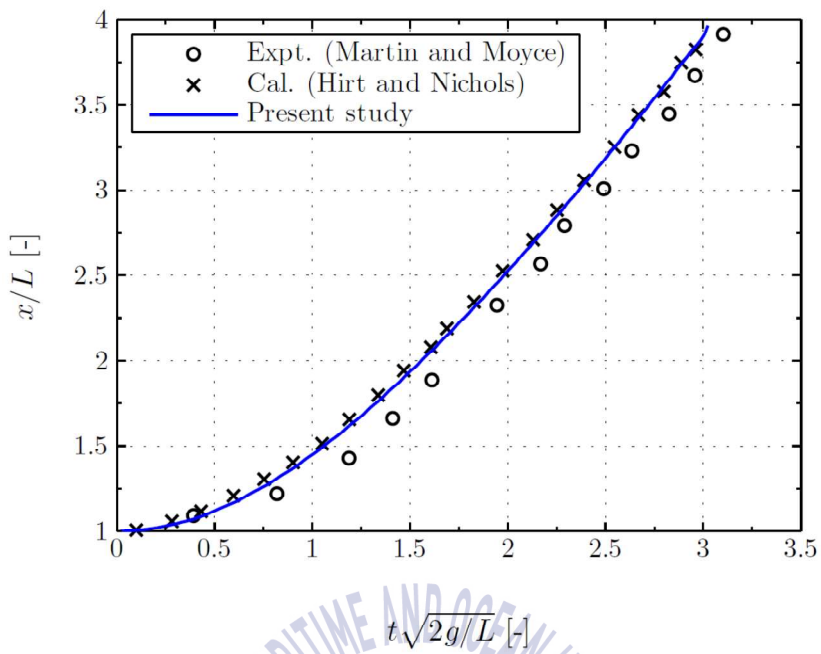
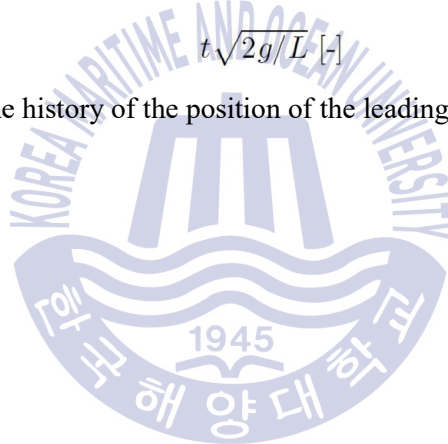


Fig. 4. 3 Time history of the position of the leading edge of water



4.1.2 Outlet boundary condition testing

The outlet boundary condition is studied in this section in order to find the suitable condition for the numerical wave flume. There are four cases of outlet boundary condition tested in this section as shown in Table 4.1. For all cases, the generated wave profile is monitored at $x = 1\lambda$ from wavemaker for 15 wave periods. The incident wave period is $T = 6$ s, wave height is $H = 1$ m and the domain length of 3λ .

Table 4. 1 Outlet boundary conditions

| Case | Outlet boundary condition | |
|------|--------------------------------|----------------------------------|
| | Pressure outlet + Open channel | Porous media $(1/\alpha)_{\max}$ |
| 1 | / | - |
| 2 | / | 1×10^5 |
| 3 | / | 1×10^7 |
| 4 | / | 1×10^9 |

Three values of the absorption coefficient $1/\alpha$ are investigated. If $1/\alpha$ is too small, the wave energy cannot be effectively absorbed. If $1/\alpha$ is too large, the porous media will act as a solid wall and the wave will reflect at the entrance of porous zone. The viscous resistance coefficient is defined as a function of the position, which is described by a UDF code as:

If

$$x < x_{ab}, \quad \frac{1}{\alpha} = 0 \quad (4.7)$$

$$x > x_{ab}, \quad \frac{1}{\alpha} = \left(\frac{1}{\alpha}\right)_{\max} \left(-\cos\left(\left(\frac{x-x_{ab}}{2\lambda}\right)\pi\right) + 1\right) \quad (4.8)$$

where x is any position in x-axis and x_{ab} is the beginning point of absorber zone in x direction.

Two-dimensional domain for simulation of outlet boundary condition is shown in Fig. 4.4 while Fig. 4.5 presents the results of difference outlet boundary condition. It can be seen that case 3, the coefficient $1/\alpha$ of 1×10^7 gives a good and suitable result for wave absorber zone.

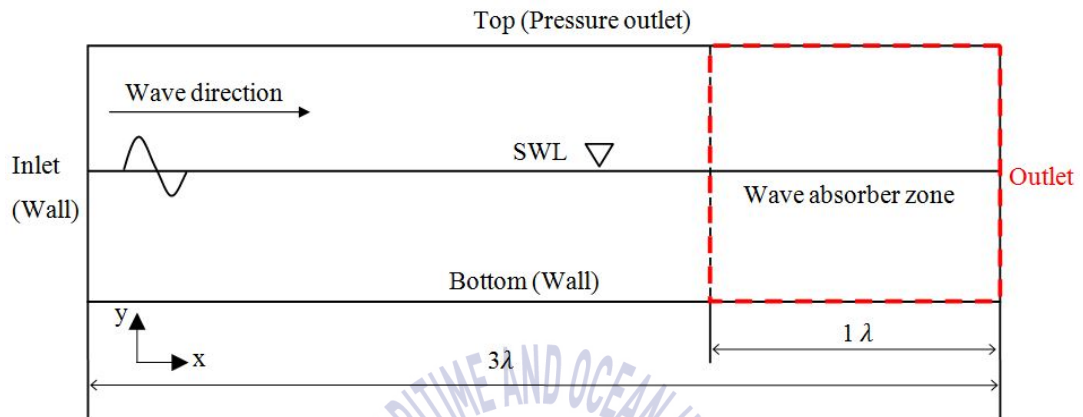
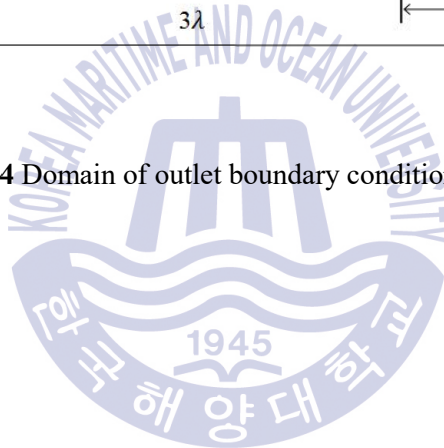
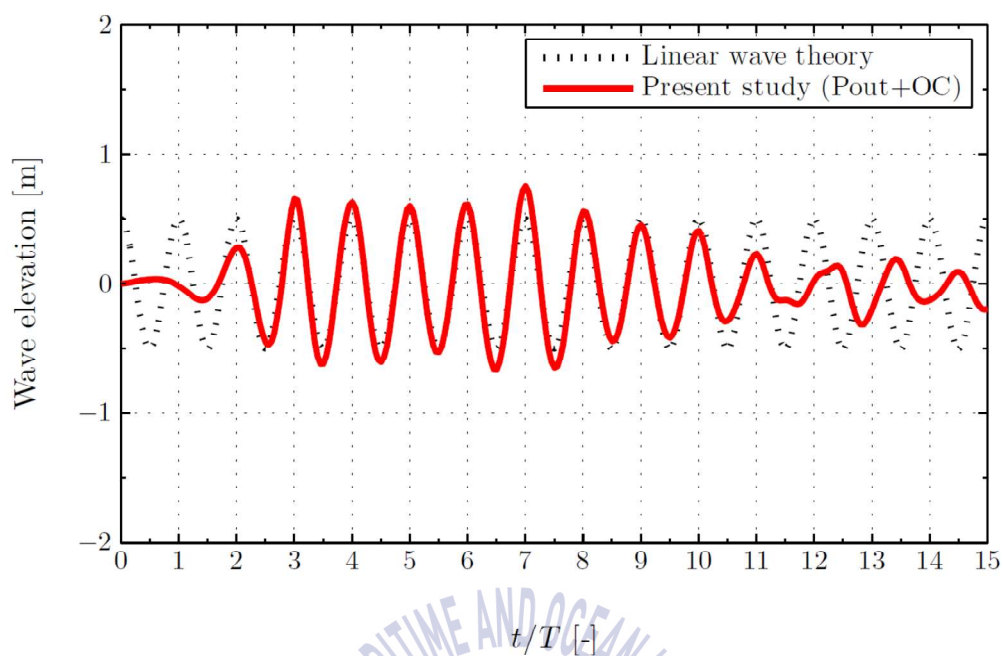
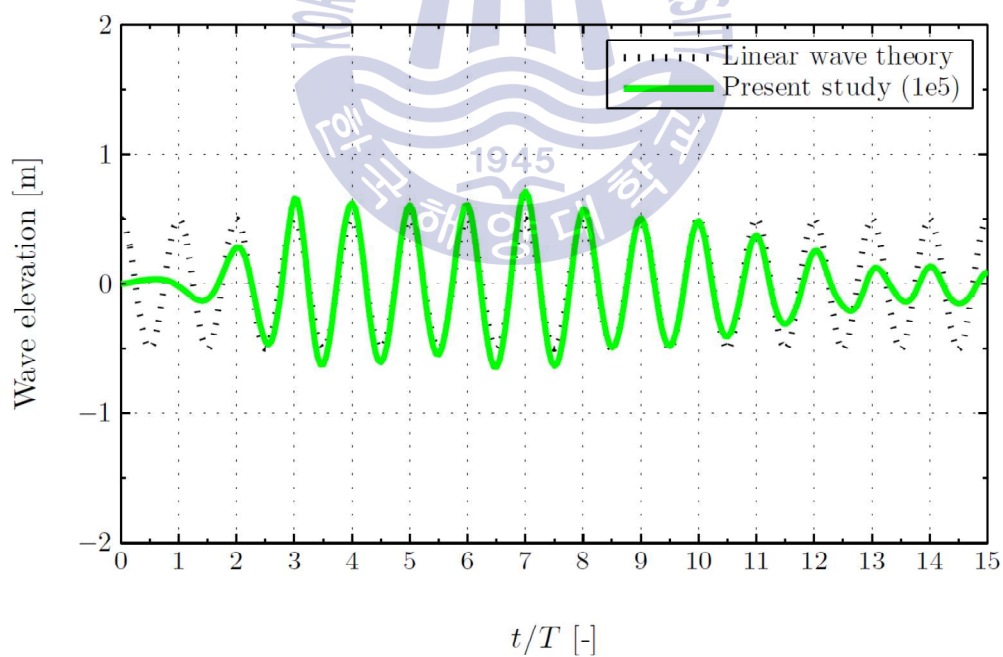


Fig. 4. 4 Domain of outlet boundary condition testing





(a) Case 1



(b) Case 2

Fig. 4. 5 Surface elevation at $x = 1\lambda$ from the wave generate

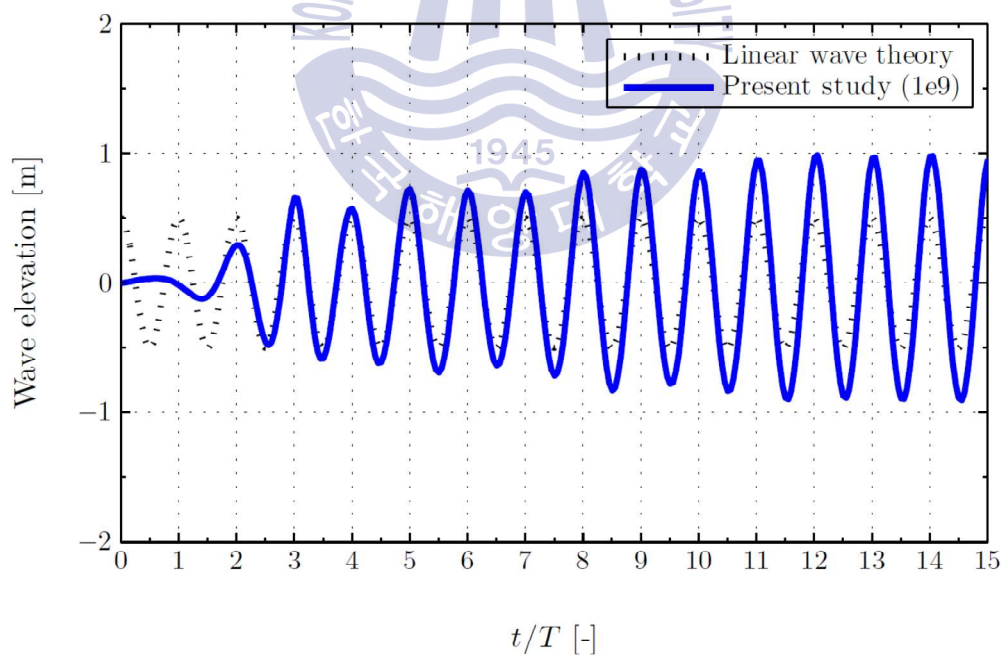
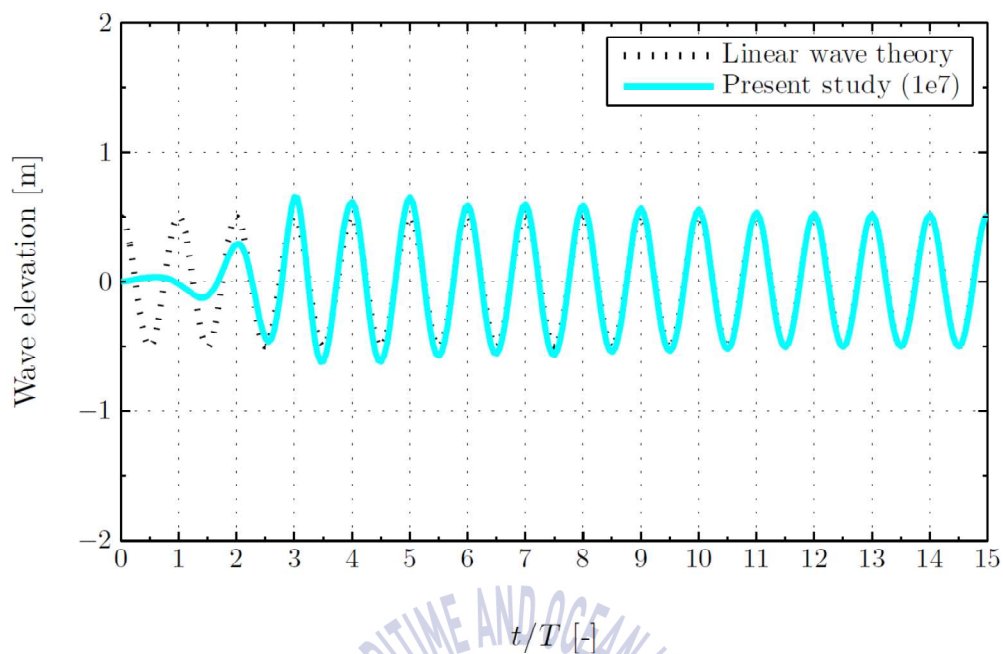


Fig. 4. 5 Surface elevation at $x = 1\lambda$ from the wave generate (continue)

4.1.3 Sensitivity analysis

A refined mesh is generated near the free surface in order to qualitatively monitor the surface elevation. Fig. 4.6 shows a grid system near the area of free surface elevation. Mesh sensitivity of wave generation is investigated in which the mesh size is a function of the wave height and length.

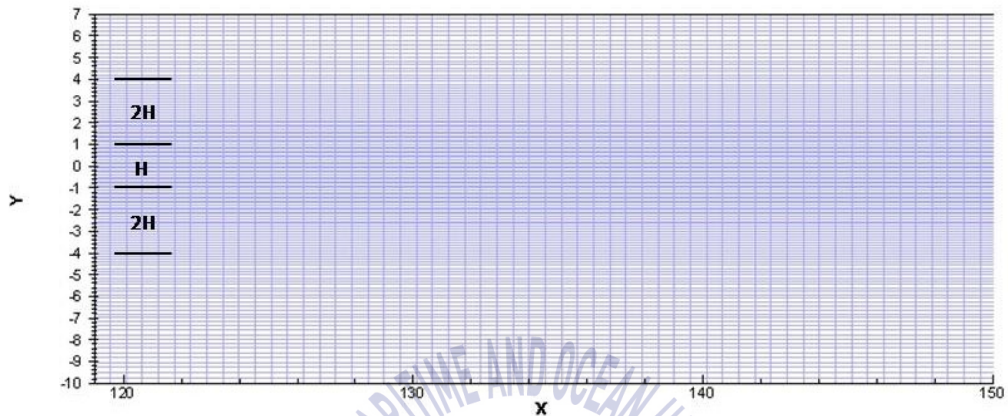


Fig. 4. 6 Grid near a free surface

The number of cells per wavelength is varied as 50, 100 and 200 cells while that of cells per wave height is kept constant as presented in Table 4.2. The generated wave profile is monitored at $x = 1\lambda$ from wavemaker for 15 wave periods. The incident wave period is $T = 6$ s, wave height is $H = 2$ m and the time step size is $dt = T/6000$ comparable to Liu et al. (2008b).

Table 4. 2 Mesh sensitivity of wave generation

| | Mesh sensitivity |
|--------|---------------------|
| Coarse | $H/20, \lambda/50$ |
| Middle | $H/20, \lambda/100$ |
| Fine | $H/20, \lambda/200$ |

The results of mesh sensitivity investigation are shown in Fig. 4.7. It can be seen that the result corresponding to the finer mesh $\lambda/200$ nearly coincides with that of $\lambda/100$ and agrees well with linear wave theory, while that of $\lambda/50$ noticeably deviates from the others. This means the mesh density of $\lambda/100$ is considered sufficiently to monitor the free surface and capture the flow physics.

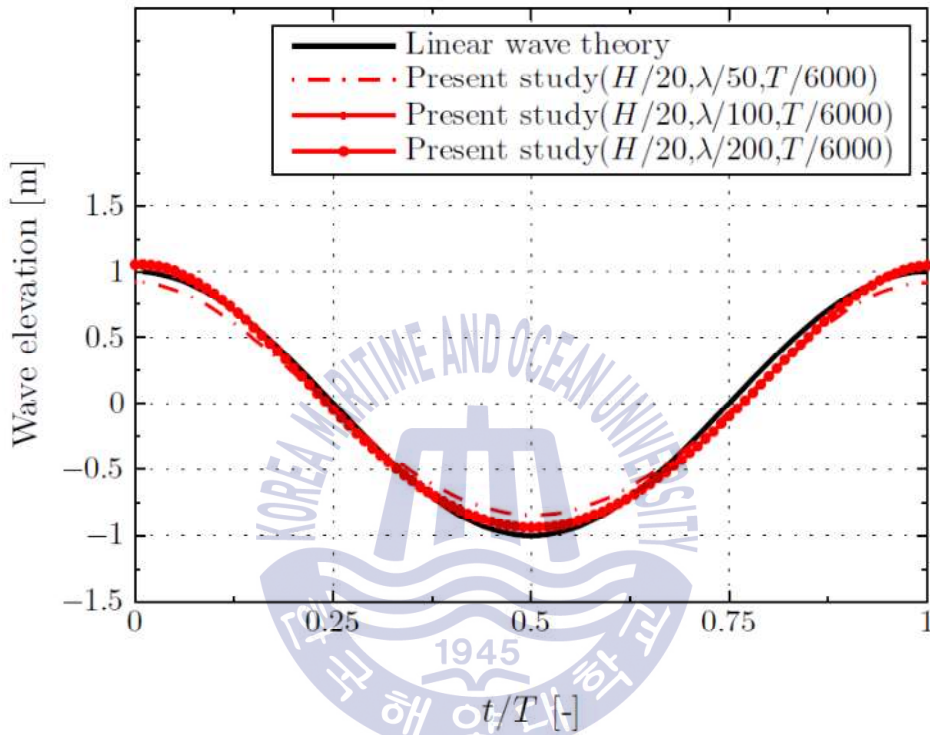


Fig. 4. 7 Mesh sensitivity of linear wave

The mesh and time step sensitivities are further investigated in more detailed as presented by Table 4.3. Firstly the time step size is varied as $T/3000$, $T/6000$ and $T/9000$. Fig 4.8 presents the hydraulic efficiency of single stage device simulated using the mentioned time step sizes. The results show that the time step of $T/6000$ is adequate since the results using this time step agree well with that of a finer time step. Moreover, the results also consistently ensure that the mesh system of $\lambda/100$ is dense enough. The mesh sensitivity in wave height direction is also investigated using $H/10$, $H/20$ and $H/30$. As presented in Fig. 4.9, the grid system used in the present study is $\lambda/100$ in combination with $H/20$.

Table 4. 3 Mesh and time sensitivity

| Mesh sensitivity (number of cells per H and λ) | | Computing time (reference: 90 s or 15T) | | |
|--|-----------|--|---------------|---------------|
| H | λ | $T/3000$ | $T/6000$ | $T/9000$ |
| 10 | 100 | | 17 hrs 30 min | |
| 20 | 50 | 10 hrs | 20 hrs | 30 hrs |
| | 100 | 11hrs 15 min | 27 hrs 30 min | 40 hrs |
| | 200 | 12 hrs 30 min | 32 hrs 30 min | 47 hrs 30 min |
| 30 | 100 | | 37 hrs 30 min | |

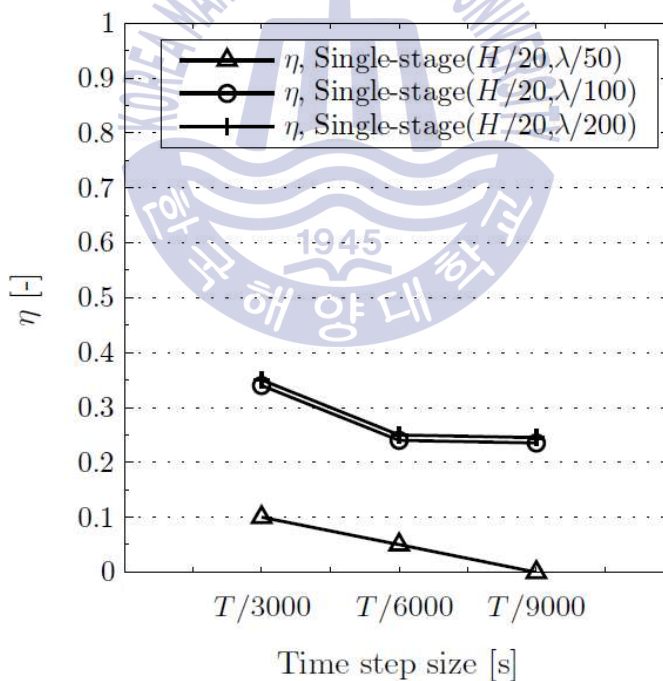
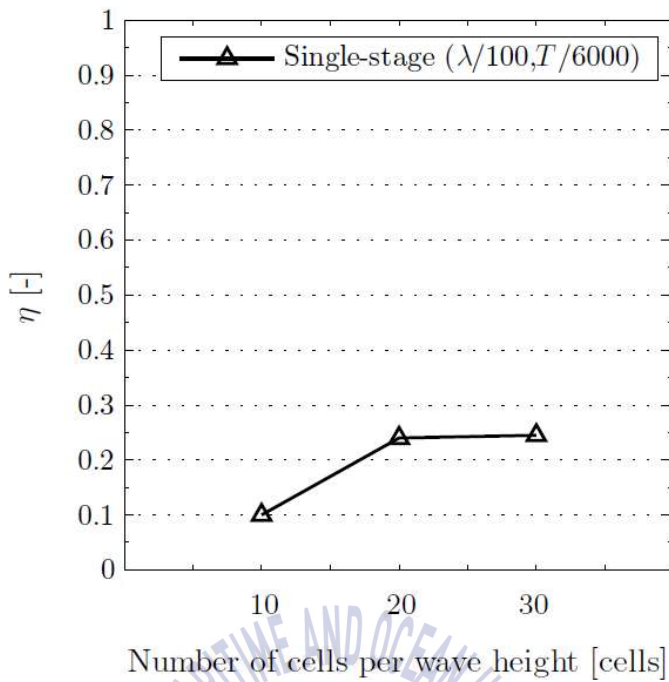
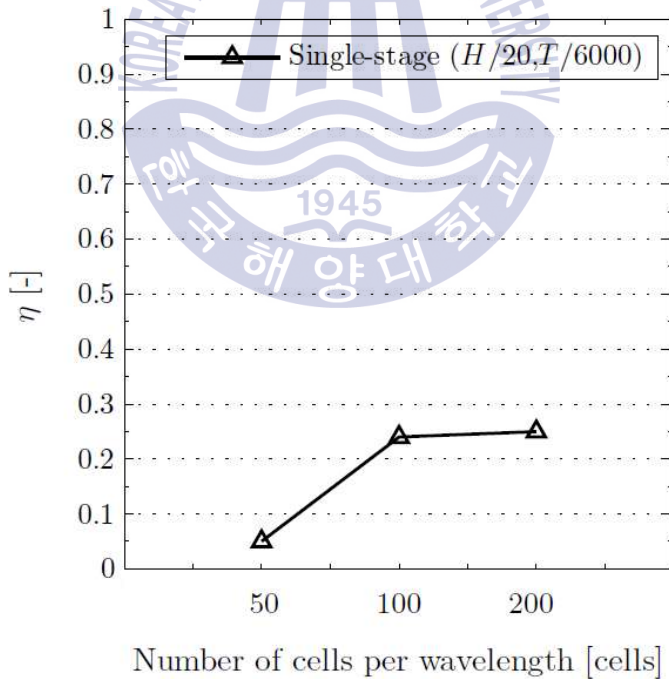


Fig. 4. 8 Time step size testing



(a) Different number of cells per wave height



(b) Different number of cells per wavelength

Fig. 4. 9 Mesh sensitivity of single-stage device

4.1.4 Validation of wave profile

For this research, wave condition was selected and considered based on data of research from Hong et al. (2005). His research studies the intensity of the wave energy around Jeju Island by using the SWAN (Simulating Waves Nearshore) program. The research indicates that the wave height is in the range of 0.4 to 2.0 m whilst the wave period is in the range of 4.0 to 6.6 s. In addition, research involving overtopping devices (Nam et al., 2008, Liu et al., 2008a, Liu et al., 2008b) utilized a regular wave, with a wave height of 2 m and a wave period of 6 s, which is corresponding to a wave condition in the southern sea of Korea.

The generated wave profile is monitored at $x = 1\lambda$ for 10 wave periods and at $t = 12T$ in a range of 4λ from wavemaker. The incident wave period is $T = 6$ s, wave height is $H = 2$ m and the time step size is $dt = T/6000$ comparable to Liu et al. (2008b).

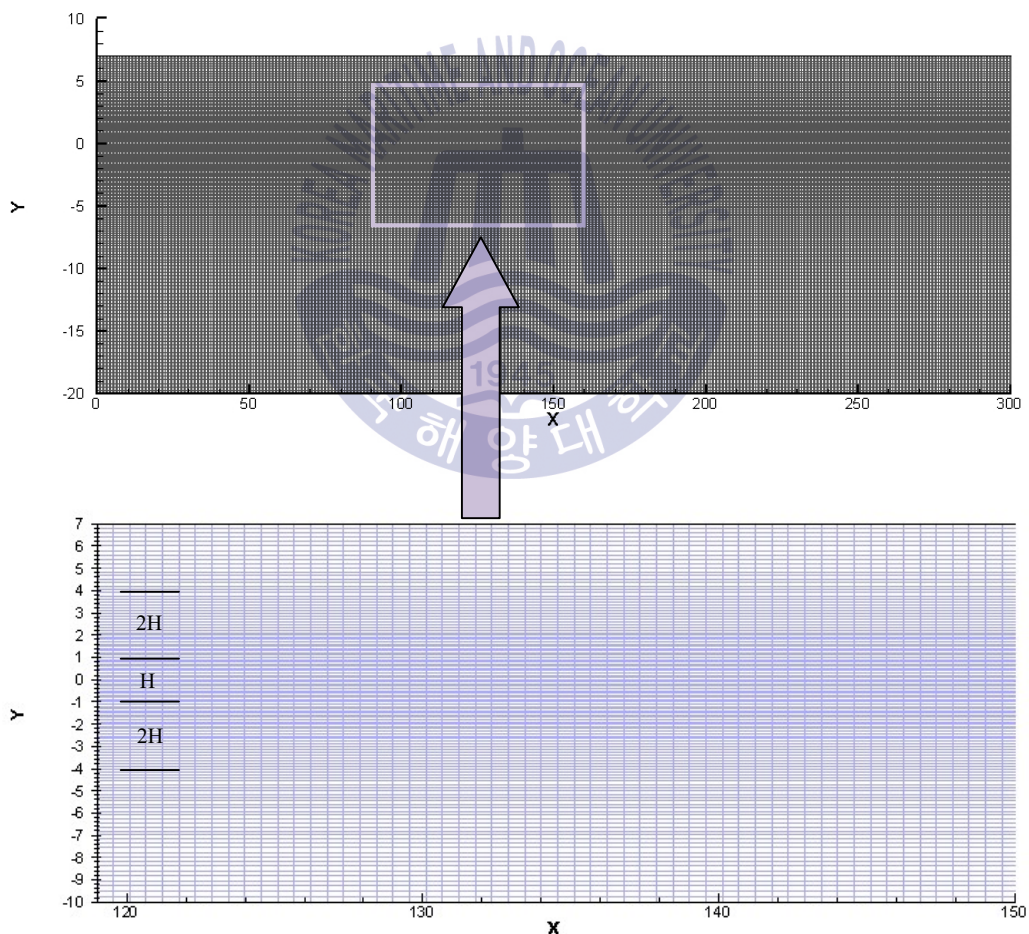


Fig. 4. 10 Example of creating a domain grid by dividing the grid resolution into 3 ranges

Grid system of computational domain has been generated with adaptive refinement as show in Fig. 4.10. A dense or more refined mesh is generated in regions of interest which are the vicinity of free surface and device. The mesh size is dependent on the wave height and length. In the present study, the number of cells per wave height is 20 cells and 100 cells per wavelength is utilized which is finer than the suggestion from Connell and Cashman (2016) since the simulation of OWEC possesses strong fluid-structure interactions, wave breaking and overtopping behavior.

From section 4.1.2, the maximum coefficient $1/\alpha$ in porous media function is defined of 1×10^7 . The UDF code of porous media model is written as:

If

$$x < 244.4, \frac{1}{\alpha} = 0 \quad (4.9)$$

$$x > 244.4, \frac{1}{\alpha} = 1 \times 10^7 \left(-\cos \left(\left(\frac{(x-244.4)}{2\lambda} \right) \pi \right) + 1 \right) \quad (4.10)$$

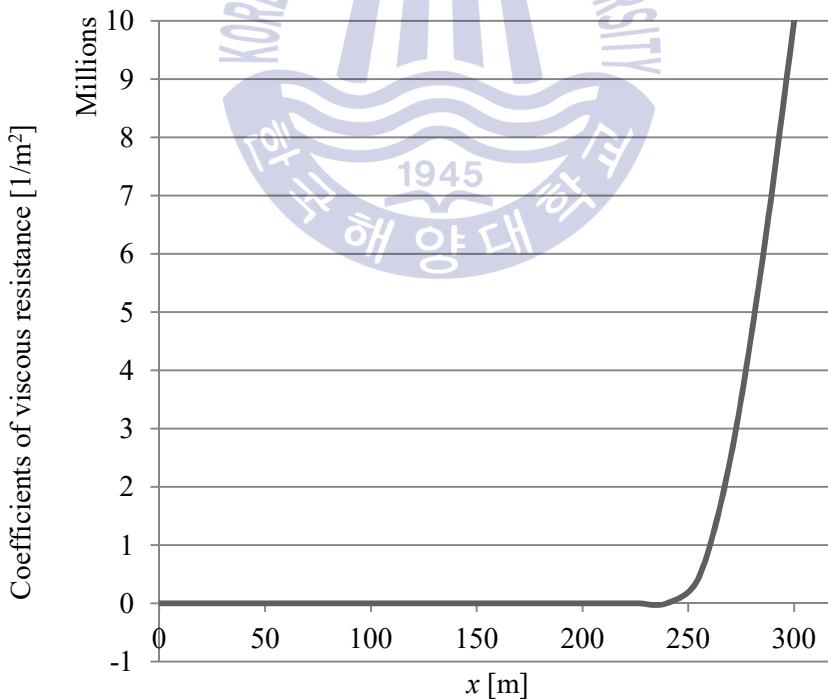


Fig. 4. 11 Coefficients of viscous resistance relative to distance

Fig. 4.11 shows the coefficient of viscous resistance as a function of distance. The total length of this absorber zone is equivalent to 1λ . The graphic of wave surface elevation of two-dimensional simulation wave tank is shown in Fig. 4.12. Note that the water phase is represented by red color while blue is air.

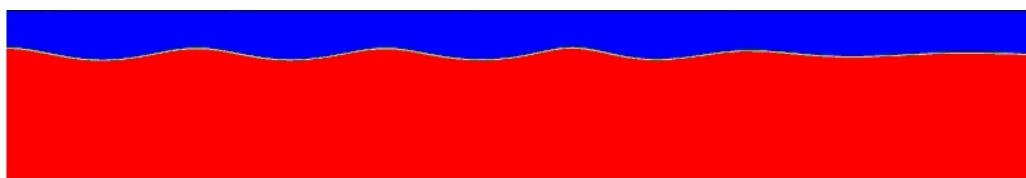
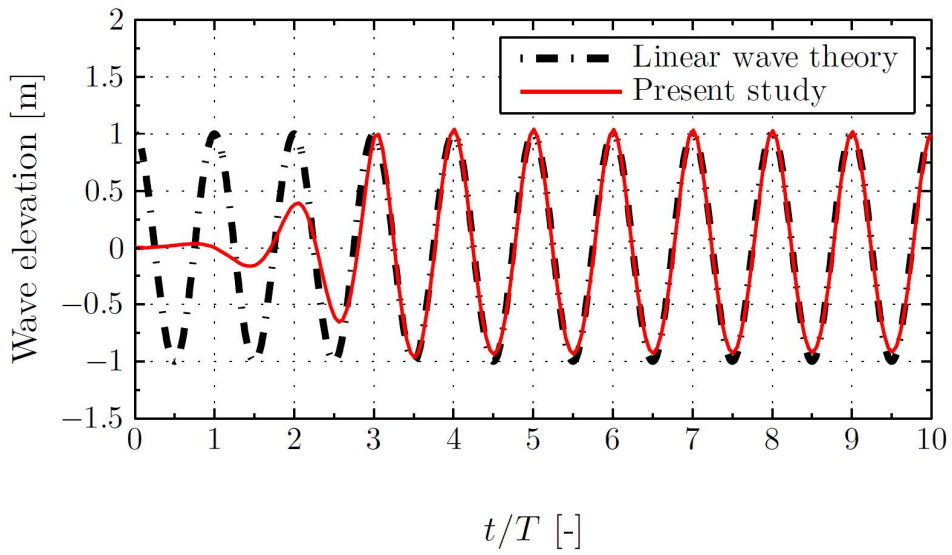


Fig. 4. 12 Wave surface elevation of two-dimensional numerical wave tank at $t = 10T$

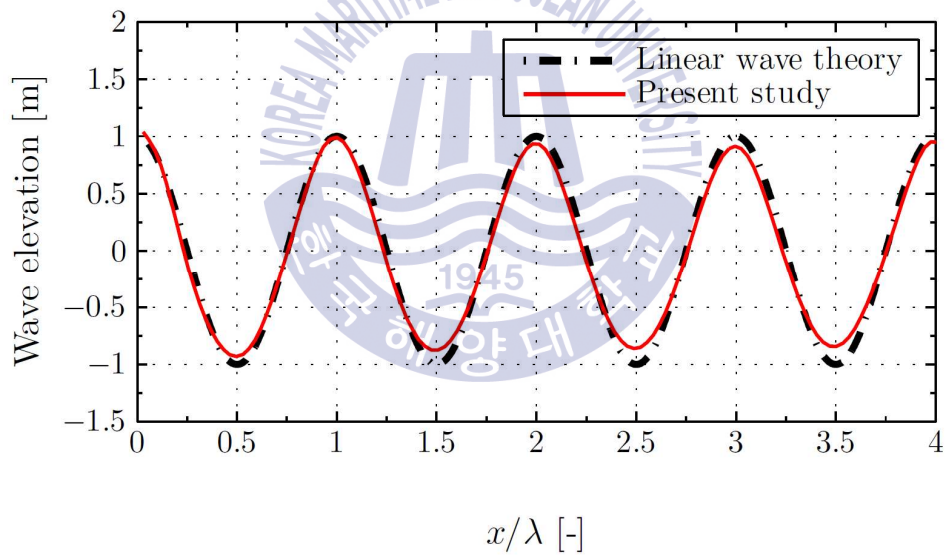
The generated wave profile is shown in Fig. 4.13 in dimensionless time and spatial domains along with calculated wave using linear wave theory. It can be seen that the generated wave using dynamic mesh agrees well with the calculated linear wave.

At $x/\lambda = 2$, the measured wave amplitude is slightly decreasing, approximately 3 - 4 % lower than that of the initial position where the wave maker is installed, which is considered acceptable. Therefore, the wave height at the location where the device is installed and simulated is reasonable.

In the case of devices installed in the domain, surface wave elevation is measured by numerical wave probes in front of the device, which is the same location as the domain without device. These recorded surface wave profiles are used to calculate the actual incident wave according to Eq. 3.12 and subsequently the P_{wave} . The actual incident wave of the domain with the device is found to be consistent and close to the actual incident wave of the domain without device.



(a) Surface elevation at $x = 12\lambda$.



(b) Wave surface elevation at $t = 12T$

Fig. 4. 13 Numerical wave tank validation. The generated wave profile is compared with linear wave theory

4.1.5 Validation of overtopping flow rate of multi-stage device

In addition, the overtopping flow rate of multi-stage device is validated. Fig. 4.14 shows the numerical result of multi-stage device in comparison with the overtopping flow rate calculated using Eq. 4.11 which is proposed by Kofoed (2006). The equation is useful for validation as seen in several studies such as Nam et al. (2008), Vicinanza and Frigaard (2008) and Margheritini et al. (2009).

$$q_n(z_1, z_2) = \sqrt{gH_s^3} \frac{A}{B} e^{C \frac{R_{c,1}}{H_s}} \left[e^{B \frac{z_2}{H_s}} - e^{B \frac{z_1}{H_s}} \right] \quad (4.11)$$

where q_n is the average overtopping flow rate of each reservoirs, H_s is significant wave height, $R_{c,1}$ is the crest freeboard of the lowest reservoir, z_1 is the crest freeboard of the current reservoir as the lower limit, z_2 is the crest freeboard of the reservoir above as the upper limit. The coefficients A , B and C are defined by experiment data.

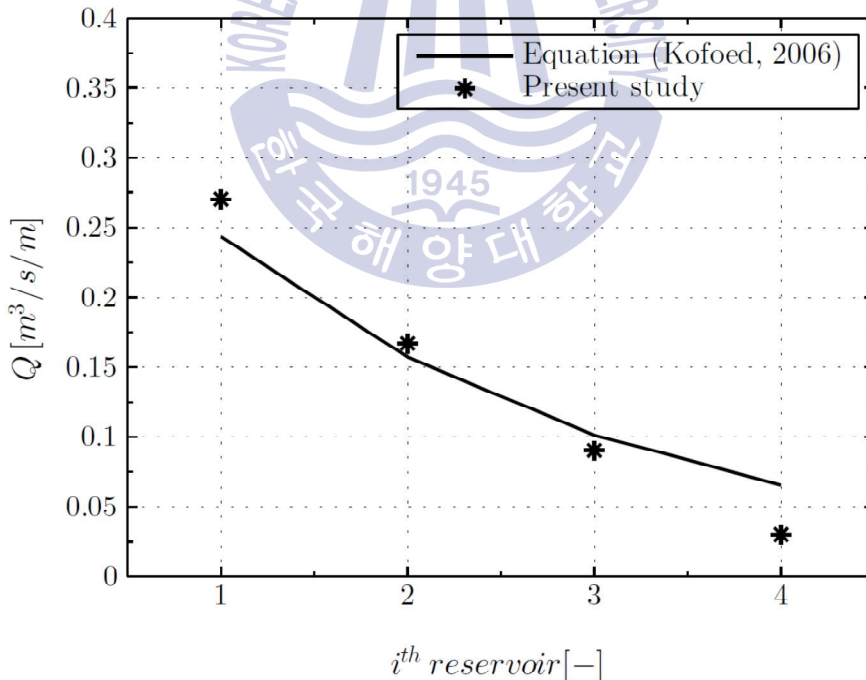
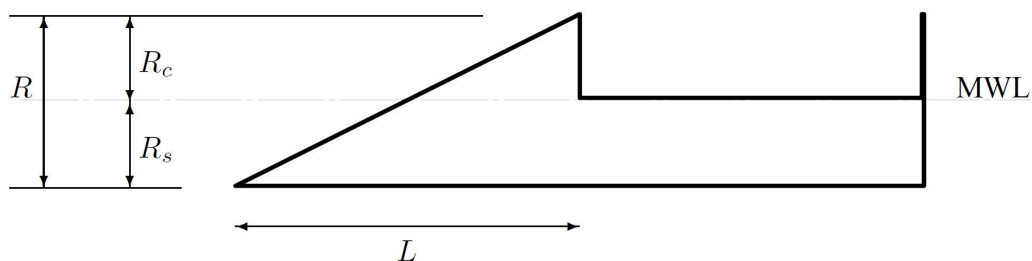


Fig. 4. 14 Comparison of the calculated overtopping rates using Eq. 4.11 with comparable numerical results of multi-stage device

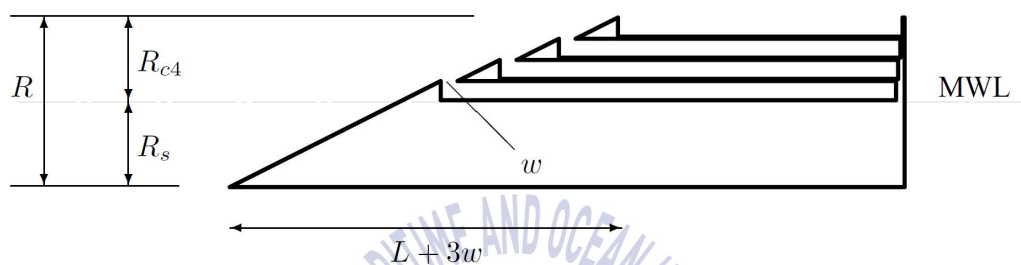
4.2 Effect of slot width on the performance of multi-stage of OWECs

The dimension of domain for simulation was shown in Fig. 4.1. The baseline layout is based on single-stage OWEC, such as used by Liu et al. (2008b), and is schematically illustrated in Fig. 4.15a. The sloping ratio S is defined as the ratio between the height R and length L of the ramp, $S = R/L$. The freeboard or crest height R_c and draught or submerged depth R_s are fixed as 2 m relative to the mean water level (MWL), while length of the ramp is $L = 8$ m, giving the slope ratio S of 1/2 for both freeboard and draught parts. The multi-stage devices employed in this study have 2 different layouts; fixed discrete slope with extended overall length and variable discrete slope with fixed overall length. The illustrations of the multi-stage layout are given in Fig. 4.15b and c respectively. Both layout models have 3 extra slots compared to the single-stage device. The width of these slots is w measured horizontally. The crest height of the slots are $R_{c1} = 0.5$ m, $R_{c2} = 1.0$ m and $R_{c3} = 1.5$ m. The crest height of the main reservoir R_{c4} and the submerged depth R_s are fixed equivalent to that of single-stage device.

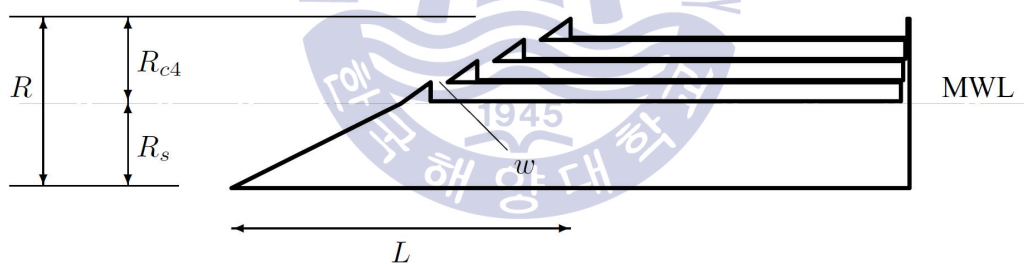
For the layout of fixed discrete slope with extended overall length, the slope ratio of both freeboard and draught ramps are fixed as 1/2 equivalent to that of single-stage device. This results in the $3w$ extended length of the ramp. For the layout of variable discrete slope with fixed overall length, the slope ratio of draught part is equivalent to that of single-stage device ($S = 1/2$), whereas the discrete ramps of freeboard part have more steep slope ratio as: $S = R_{c4}/(L/2 - 3w)$.



(a) Single-stage device



(b) Fixed discrete slope with extended overall length



(c) Variable discrete slope with fixed overall length.

Fig. 4. 15 Layouts of the single- and multi-stage devices. The incident wave direction is from left to right

To study the influence of the slot width on the performance of the devices, the parameter is varied within the range of $0.1 \text{ m} \leq w \leq 0.6 \text{ m}$ with a 0.1 m increment, corresponding to the relative slot of $0.05 \leq w/R_{cd} \leq 0.30$. In the present study, the generated incident wave height H of 2 m and the wave period T of 6 s is utilized following Liu et al. (2008b). The wave and other testing conditions are summarized in Table 4.4.

Liu et al. (2008b) reported that when using a wave height of 1 m together with wave period of 4 and 6 s , the wave cannot flow across the reservoir of a single-stage device of $1:1$, $2:3$ and $1:2$ slope ratios. However, when the wave height is 2 m , the wave can noticeably flow into the device. In addition, the case of 2 m wave height in combination with wave period of 6 s with the device of a slope of $1:2$ results in the most abundant overtopping discharge. Therefore, this research uses the wave conditions and the size of this device as the basis for the simulations of both single and multi-stage devices.

Table 4. 4 General parameters conditions

| Parameters | |
|-------------------------------------|------------------------------------|
| Wave height, H [m] | 2.0 |
| Wave period, T [s] | 6.0 |
| Water depth, h [m] | 20.0 |
| Wave steepness, H/λ [-] | 0.036 |
| Relative slot width, w/R_{cd} [-] | 0.05, 0.10, 0.15, 0.20, 0.25, 0.30 |
| Relative freeboard, R_c/H [-] | 1.0 |
| Relative wave height, H/h [-] | 0.1 |

The structure grid is meshed on the device as show in Fig. 4.16.

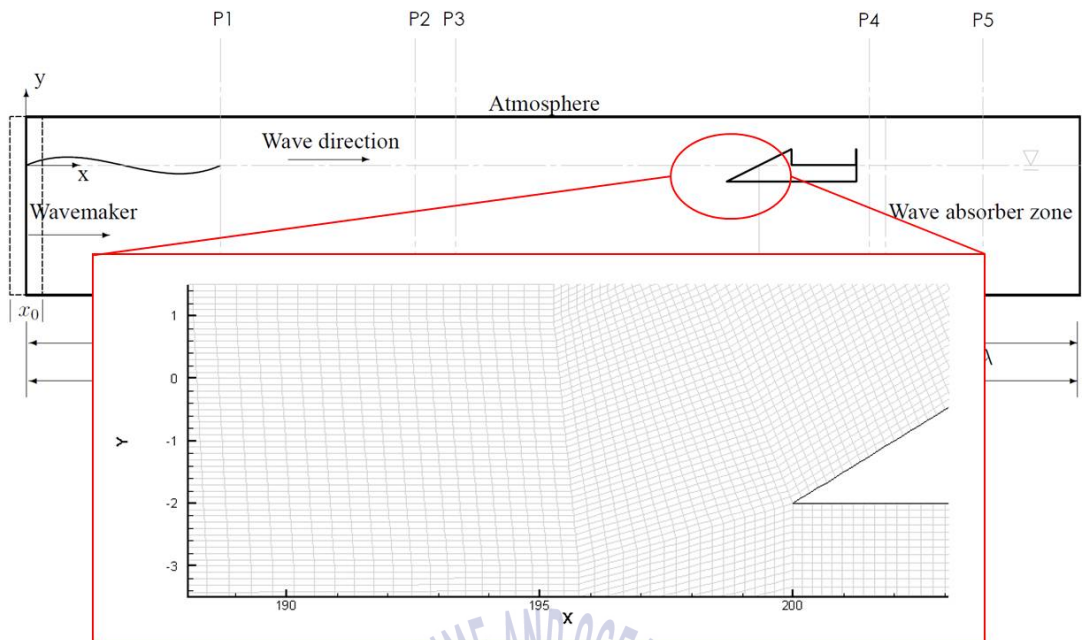


Fig. 4. 16 Meshing structure grid on the single-stage device

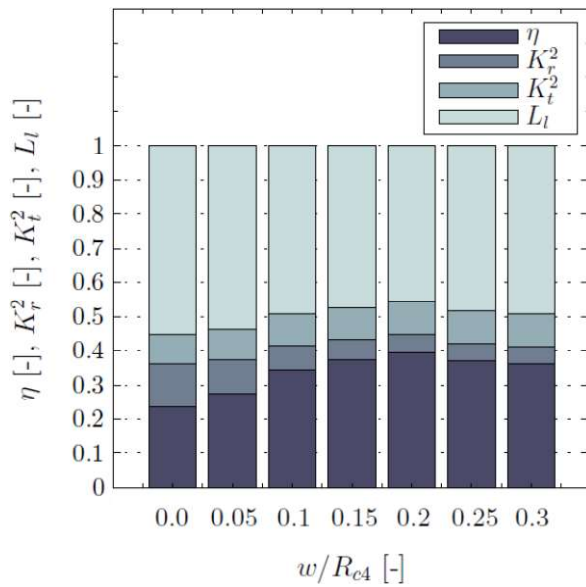


4.2.1 Results of effect of slot width on the performance of multi-stage of OWECS

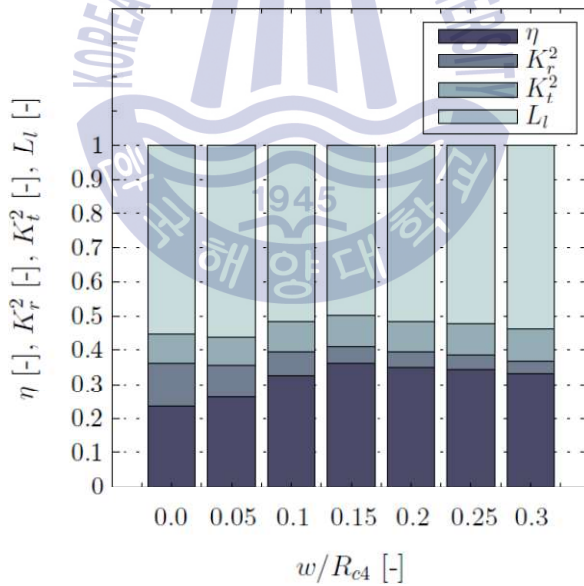
In the present study, the overtopping flow rate into the reservoir and the energy captured are the main performance indicators of the devices. The simulations are monitored for at least 15 wave periods to obtain solutions. In case of aperiodic solution, the simulation is further monitored until a periodic solution is obtained.

The transportation of energy is given in Fig. 4.17 and 4.18, in which the overall hydraulic efficiency, reflection, transmission and loss rates are shown in functions of relative slot width. Note that the relative slot width $w/R_{c4} = 0$ represents the single-stage device. It can be seen that the multi-stage devices capture wave energy effectively compared to single-stage device. Performance of both layouts of multi-stage devices have a similar trend. The efficiencies of both multi-stage layouts are approximately on par for the pre-peak regime. However, the fixed slope device performs better for large slot width, i.e., peak and post-peak regimes. This is because the variable slope device has more steep slope compared to the fixed slope layout. The steep slope ratio results in less discharge according to Liu et al. (2008b).

Moreover, the numerical results of the present study show that the optimal hydraulic efficiency of the multi-stage device is nearly on par with hydraulic efficiency proposed by Margheritini et al. (2009) which states that the hydraulic efficiency is within a range of 30 - 40 %.



(a) Fixed slope with extended overall length. This graph is corresponding to Fig. 4.15b and 4.21a



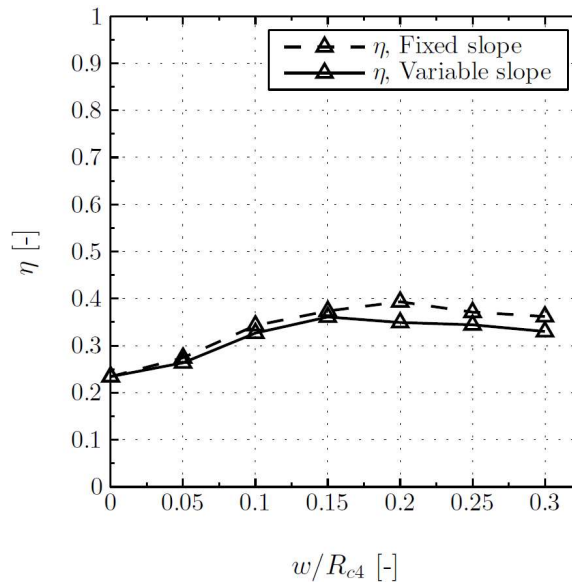
(b) Variable slope with fixed overall length. This graph is corresponding to Fig. 4.15c and 4.21b

Fig. 4. 17 Overall hydraulic efficiency, reflection, transmission and loss rates

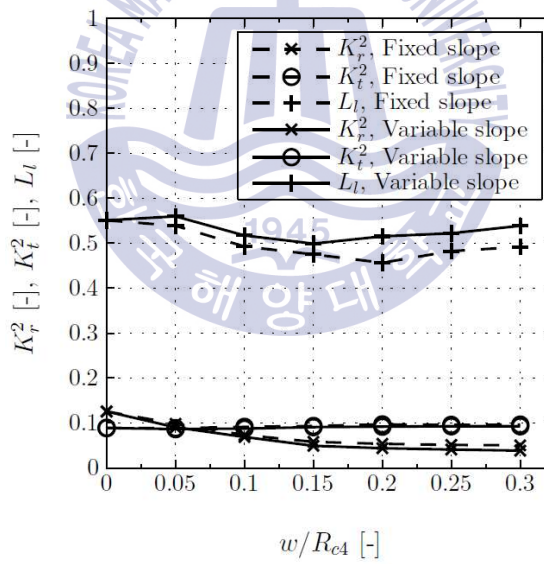
In addition, the reflected wave energy is decreasing with increasing slot width since the amount of water being stored by the reservoir is increasing. However, the transmitted wave energy is about to remain constantly, as shown in Fig. 4.18b. This can be concluded that the influence of slot width on underpass wave is insignificant.

Eq. 3.9 shows that the potential power in the overtopping water depends on two main variables: average overtopping flow rate Q_i and crest height $R_{c,i}$. Considering the slot width of multi-stage device was designed to be small, it is found that most of the water can flow into the main reservoir while relatively small portion of the water volume flows into the lower reservoirs. This means that the main reservoir could effectively harvest wave energy from maximizing both variables, i.e., large amount of overtopping water and highest crest height. However, the enhancement in overall hydraulic efficiency is not significant since of the amount of overtopping water in lower reservoirs is decreasing. That is the extracted energy stored by the main reservoir is not enough to compensate the decrease in energy captured by the lower reservoirs. In case of the slot width of the device was designed to be large, it was found that most of the water was captured by the lower reservoirs which caused the device to lose its potential energy from the main reservoir.

For smaller slot width, i.e., pre-peak regime, increasing the parameter gives an increase in overall hydraulic efficiency, hence a performance gain. The optimal performance is obtained at an intermediate value of the relative slot width: $w/R_{c4} = 0.2$ for fixed slope device and $w/R_{c4} = 0.15$ for variable slope device with in the parametric range considered in the present study. Further increasing the slot width gives reduction in efficiency.



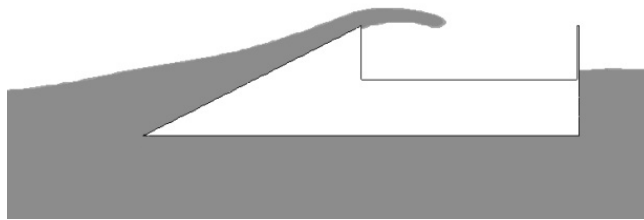
(a) Overall hydraulic efficiency



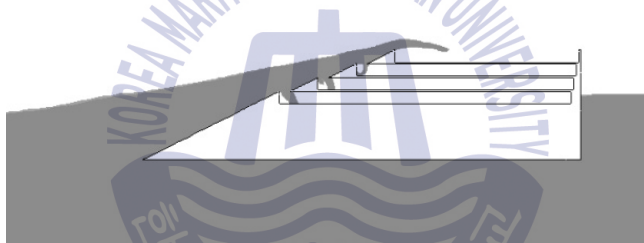
(b) Reflection, transmission and loss rates

Fig. 4. 18 Effect of slot width on efficiency and loss rates

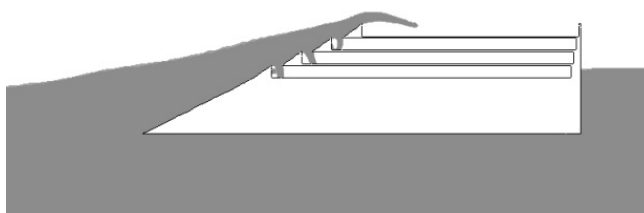
Water wave flows into the reservoir of single- and multistage devices are shown in Fig. 4.19. For the multi-stage device, the extra slots at lower levels capture water during both, run-up and fall-down processes, see Fig. 4.20. On the other hand, the single stage device has only one main reservoir, therefore the whole water volume run-up to the main reservoir. As a result of this overtopping mechanism, the overall hydraulic efficiency of the multi-stage device is higher than the single stage device.



(a) Single-stage device

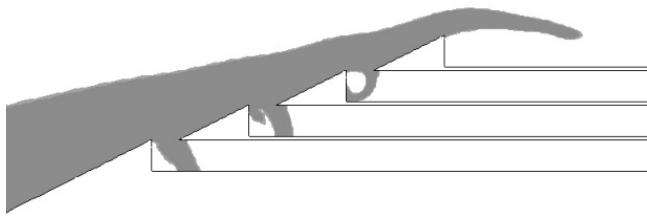


(b) Fixed slope multi-stage device, $w/R_{c4} = 0.2$

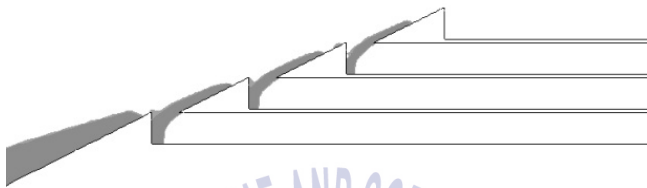


(c) Variable slope multi-stage device, $w/R_{c4} = 0.2$

Fig. 4. 19 Wave run-up process of single- and multi-stage devices



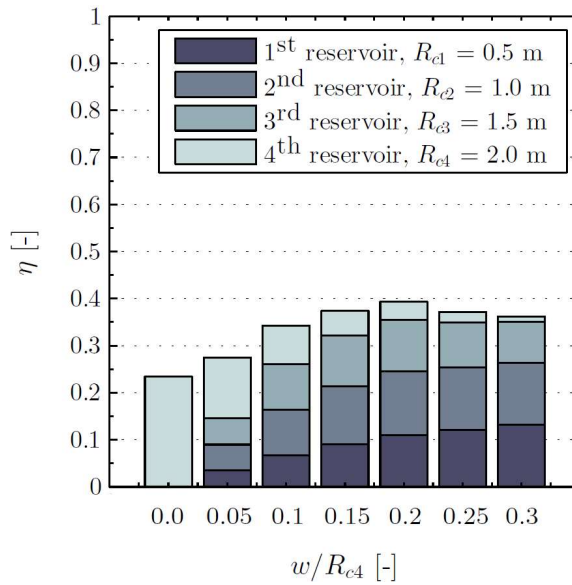
(a) Run-up process



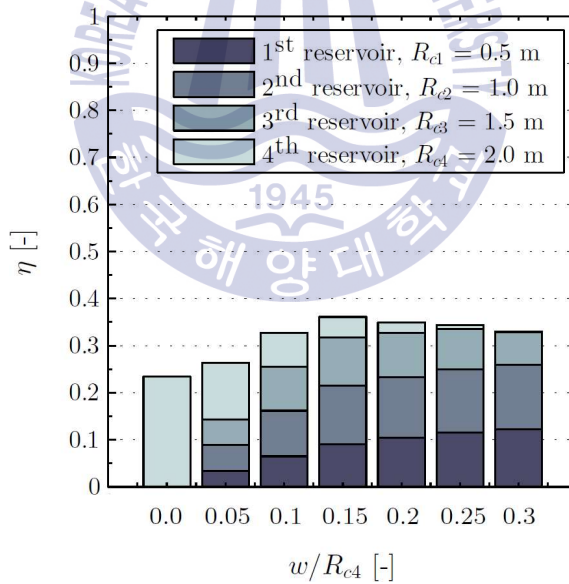
(b) Fall-down process

Fig. 4. 20 Run-up and fall-down processes

The performance enhancement is obtained via increasing the overtopping flow rate and energy captured by extra reservoirs at lower crest heights, see Fig. 4.21. As a result of this, the overtopping flow rate and energy captured by the main reservoir are reduced. This explains why the overall hydraulic efficiency is decreasing with large slot width. The water and therefore wave energy are mainly captured and stored by the lower reservoirs, then the remaining water with small amount of energy will run-up to the upper reservoir, being stored at a higher level. For wider slots, the larger amount of water is stored at the lower level with the lower potential energy, whilst the higher ones have less water being stored.



(a) Fixed slope with extended overall length. This graph is corresponding to Fig. 4.15b and 4.17a



(b) Variable slope with fixed overall length. This graph is corresponding to Fig. 4.15c and 4.17b

Fig. 4. 21 Partial hydraulic efficiencies of each reservoir as functions of relative slot width

In addition, the fixed slope multi-stage device based on relative slot width of 0.2 was tested with different wave periods. Fig. 4.22 shows the hydraulic efficiencies of multi-stage device for different wave periods, e.g., 5 s, 6 s and 7 s. As a result, the wave period of 5 s and 6 s gives consistent results and is relatively constant. In this research, the choice to study the wave period of 6 s is considered to be in the appropriate range.

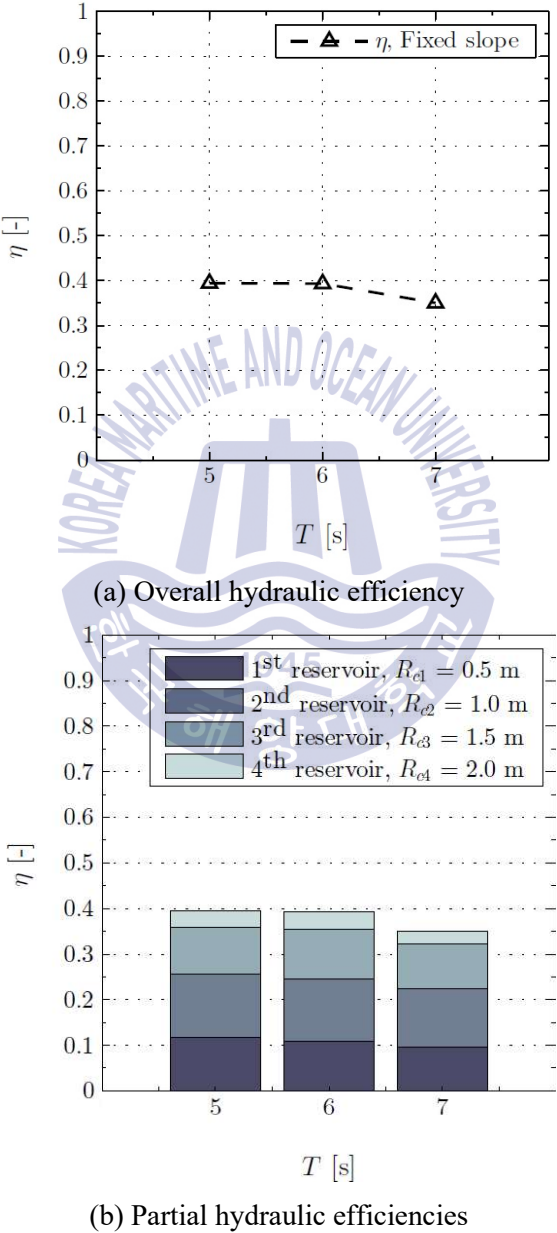
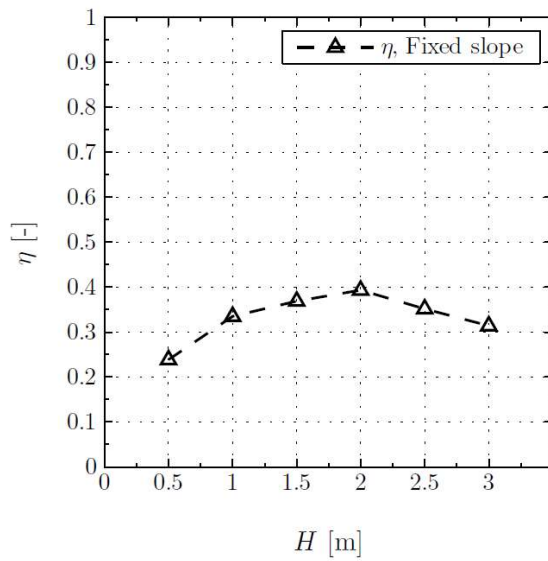


Fig. 4. 22 Hydraulic efficiencies of multi-stage device for different wave periods

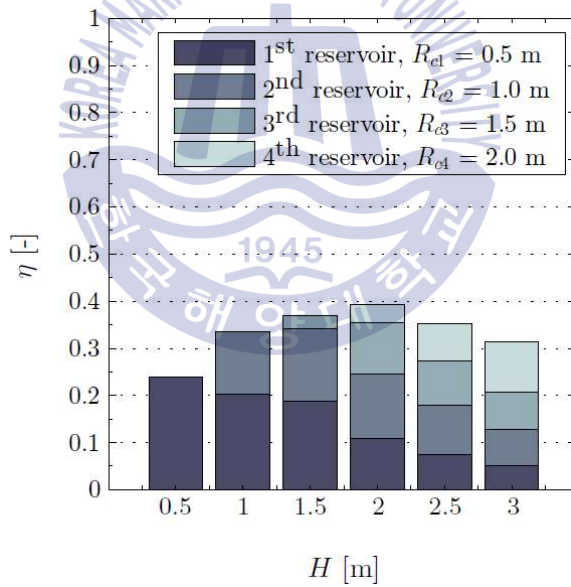
In this part, the multi-stage device operating in various wave height conditions is investigated. The device layout is the fixed slope based on relative slot width of 0.2. Fig. 4.23a and b show the overall and partial hydraulic efficiencies of device for different wave heights, the parameter is varied within the range of $0.5 \text{ m} \leq H \leq 3.0 \text{ m}$ with a 0.5 m increment. For wave height of 0.5 m, the wave can run-up and then overtop into the first reservoir only. An increase in wave height results in the higher level that the water can climb-up and overtop. For wave height of 2.0 m or greater, the wave can reach the main reservoir.

The partial efficiency of the first reservoir is decreasing with increasing wave height. This is because, within the almost entire range of parametric space investigated, the amount of water captured by this lowest reservoir seems to remain unchanged regardless the wave height, while the incident wave energy available due to the higher wave amplitude is increasing. This means that the first reservoir could capture the wave effectively within this range of wave conditions. The second reservoir can be reached for wave height of 1.0 m or greater. For $1.0 \text{ m} \leq H \leq 1.5$, the change in water captured by this reservoir is more significant than the increase in available wave energy, resulting the enhancement in the partial efficiency. Further increase wave height reduces the partial efficiency in the similar manner as that of the first reservoir. Similarly, the third and the main reservoirs follow this trend.

The device performs effectively for wave height of 2.0 m or greater. However, the wave height greater than 2.0 m gives a reduction in the overall efficiency since the incident wave energy available due to the higher wave amplitude increases more noticeably than the increase of total overtopping energy captured by the reservoirs.



(a) Overall hydraulic efficiency



(b) Partial hydraulic efficiencies

Fig. 4. 23 Hydraulic efficiencies of multi-stage device for different wave heights

4.2.2 Conclusions of effect of slot width on the performance of multi-stage of OWECs

A numerical model for two-dimensional flow was used to investigate the effect of slot width of multi-stage overtopping wave energy devices on energy captured. The numerical wave tank has been validated. The generated wave agrees well with the linear wave theory. The multi-stage OWECs have 2 different layouts; fixed slope and variable slope device. The hydraulic efficiency of the multi-stage devices is compared with that of baseline single-stage device. Moreover, the fixed slope device is studied more in detail via application of adaptive slot width. Optimal performance based on hydraulic efficiency of multi-stage device exists at an intermediate value of slot width giving a huge increase in energy captured and efficiency. The enhancement is obtained by increasing the overtopping flow rate into extra slots with lower crest heights, in both wave run-up and fall-down processes. This results in a decrease in overtopping flow rate of the main reservoir. This can be avoided by using a controllable gate or valve which manages to close the extra slots during wave run-up process and automatically open during wave fall-down process.

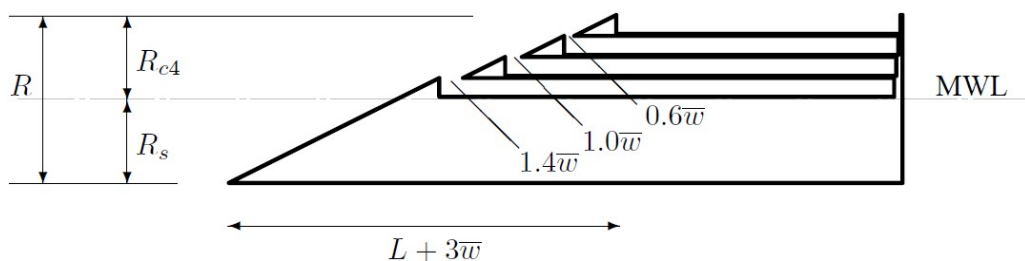
Since the computational costs are high and the parameters cannot be varied continuously, we were not able to complete an efficiency chart for the suggested control strategy. However, we believe the present study is beneficial for understanding and validating the comparable experiment. A better understanding of overtopping flow mechanism explained in the present study could therefore provide a guideline in the field of OWEC design. Further investigations are recommended in order to study the effects of the suggested control strategy and the influence of adaptive slot within the wider range of parametric space. The study of three dimensional phenomena of overtopping flow is also recommended.

4.3 Effect of adaptive slot width on the performance of multi-stage of OWECs

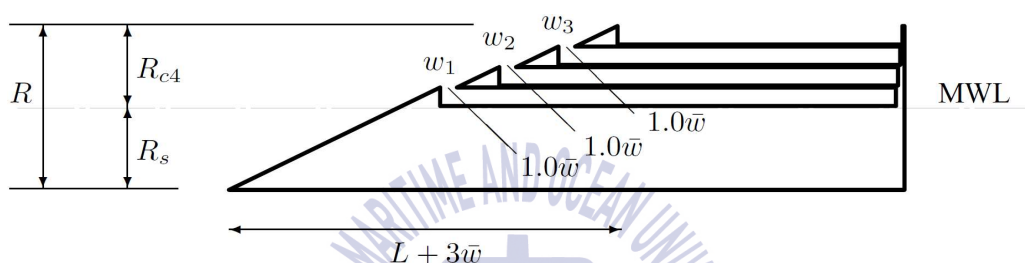
In this section, the non-adaptive device is the baseline model which is schematically illustrated in Fig. 4.24b. The multi-stage device has the inclined wall, called ramp, in order to lift wave overtop and flow into the extra reservoirs. The ramp height R consists of two parts, the submerged depth R_s and freeboard height R_{c4} . These two parameters are fixed as 2 m. The slope S of each ramp is defined as the ratio between the ramp height R and horizontal ramp length L which is kept constant as $S = 1/2$ for both freeboard and draught parts. This consequently results in the $3\bar{w}$ extended length of the ramp. The multi-stage devices have three extra slots which are defined as w_1 (the lowest), w_2 (the middle) and w_3 (the highest). The crest height of the slots are $R_{c1} = 0.5$ m, $R_{c2} = 1.0$ m and $R_{c3} = 1.5$ m. The adaptive layout gives difference in size of the slots as $\Delta w = w_2 - w_1 = w_3 - w_2$, so that the average width of each device is $\bar{w} = w_2$. There are four base-line models which are non-adaptive layout with average slot width of $\bar{w} = 0.2, 0.3, 0.4$ and 0.5 m which show in Table 4.5. Each base-line model has four corresponding adaptive layouts as shown in Table 4.6. Moreover, the adaptive device has two layouts: reservoir width varies from large to small ($w_1 = 1.4\bar{w}$) and vice versa which are shown in Fig. 4.24a and 4.24c.

Table 4. 5 Parameters conditions

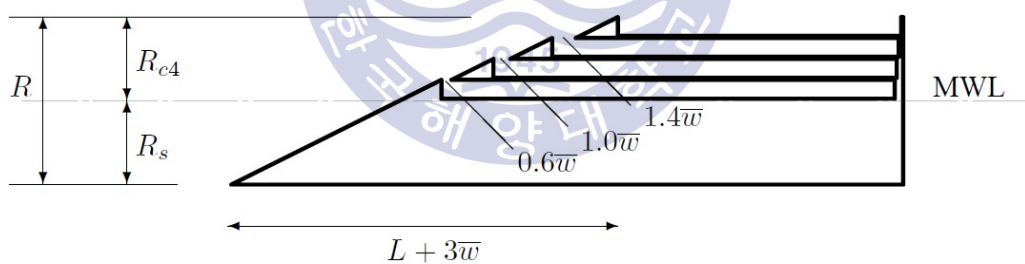
| Parameters | |
|-----------------------------------|------------------------|
| Wave height, H [m] | 2.0 |
| Wave period, T [s] | 6.0 |
| Water depth, h [m] | 20.0 |
| Average slot width, \bar{w} [m] | 0.20, 0.30, 0.40, 0.50 |
| Wave steepness, H/λ [-] | 0.036 |
| Relative freeboard, R_c/H [-] | 1.0 |
| Relative wave height, H/h [-] | 0.1 |



(a) Adaptive device ($w_1 = 1.4\bar{w}$)



(b) Non-adaptive device ($w_1 = 1.0\bar{w}$)



(c) Adaptive device ($w_1 = 0.6\bar{w}$)

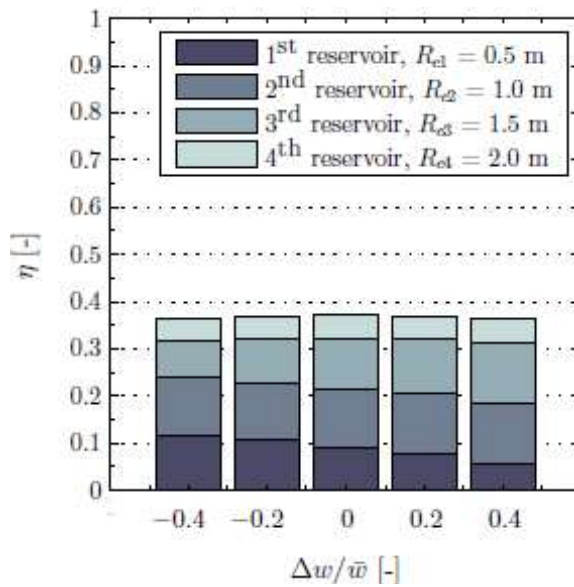
Fig. 4. 24 Example of non-adaptive and adaptive devices layout

Table 4. 6 Adaptive slot width parameters

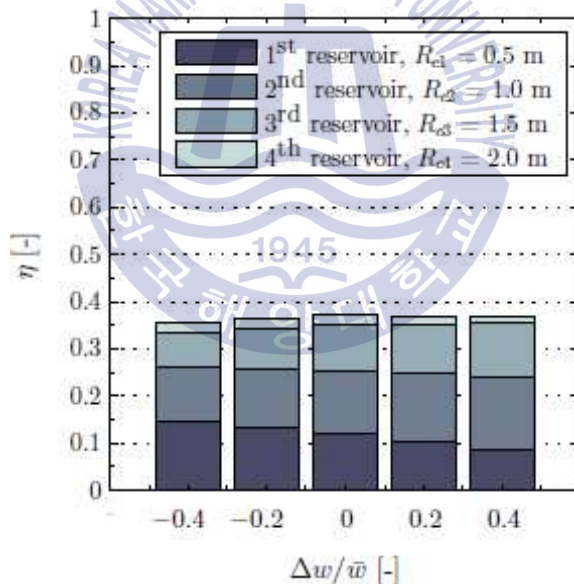
| Case | $\Delta w/\bar{w}$ | w_i/\bar{w} | | |
|------|--------------------|---------------|--------|--------|
| | | Slot 1 | Slot 2 | Slot 3 |
| 1 | -0.4 | 1.4 | 1.0 | 0.6 |
| 2 | -0.2 | 1.2 | 1.0 | 0.8 |
| 3 | 0.0 | 1.0 | 1.0 | 1.0 |
| 4 | 0.2 | 0.8 | 1.0 | 1.2 |
| 5 | 0.4 | 0.6 | 1.0 | 1.4 |

The wave overtopping energy is captured by the main and extra slots. Fig. 4.25 demonstrates the partial hydraulic efficiency of each reservoir for both adaptive and non-adaptive layouts with average slot width of 0.3 m and 0.5 m. It can be seen that the overall hydraulic efficiency of non-adaptive device ($\Delta w/\bar{w} = 0$) is slightly superior compared to that of adaptive devices. In case of adaptive device, the overall efficiency is nearly on par for both positive or negative $\Delta w/\bar{w}$. However, the discharge into each extra reservoir depends on the level and size of slot. The wider slot results in larger amount of water being captured and stored.

When the lowest slot of device is designed to be narrowest ($\Delta w/\bar{w} = 0.4$), it captures smaller portion of water and allows the water run-up to the greater level which has higher potential. On the other hand, if the lowest slot is the widest ($\Delta w/\bar{w} = -0.4$), it captures large amount of water and lets a major part of water volume run-up to the higher but narrower slot. The partial efficiency enhancement gain by wider slot compensates with the reduction in that of the narrower one. As a result of this, the adaptive layouts could not give performance improvement. However, this behavior could affect strategy of energy extraction via multi-stage turbines.



(a) The multi-stage devices based on average slot width of 0.3 m



(b) The multi-stage devices based on average slot width of 0.5 m

Fig. 4. 25 Example of hydraulic efficiency of each extra slot of device

Contours of hydraulic efficiency, reflection rate, transmission rate and loss rate plotted as a function of \bar{w} and $\Delta w/\bar{w}$ are shown in Fig. 4.26. It can be seen that the non-adaptive layout, i.e., $\Delta w/\bar{w} = 0$ in combination with $\bar{w} = 0.4$ m. gives optimal performance in the considered range of parametric space. An adaptive layout, either $\Delta w/\bar{w}$ is positive or negative, results in a slight drop in the efficiency.

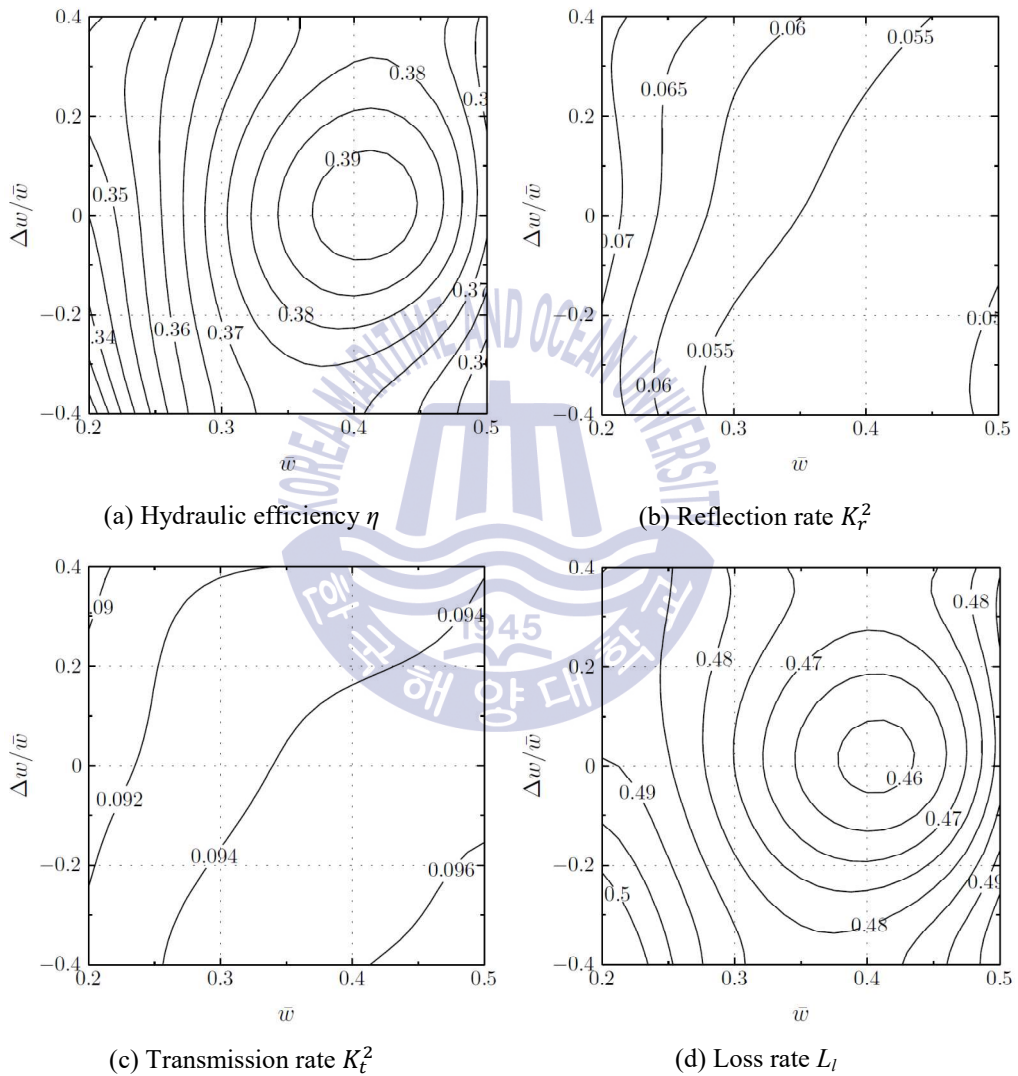


Fig. 4. 26 Contour of hydraulic efficiency η , reflection rate K_r^2 , transmission rate K_t^2 and loss rate L_l of multi-stage device on the $(\bar{w}, \Delta w/\bar{w})$ parametric space

The reflection rate K_r^2 is decreasing with increasing the slot width as seen in Fig. 4.26b while Fig. 4.26c shows that the variation of transmission rate K_t^2 is relatively small. As a result of this, the non-adaptive layout of $\bar{w} = 0.4$ m has smallest loss rate within the range of parametric space considered as shown in Fig. 4.26d.

The water flow mechanism of both run-up and fall-down processes are shown in Fig. 4.27 - 28. It can be seen that the amount of water can be captured by the extra slots in both run-up and fall-down processes.

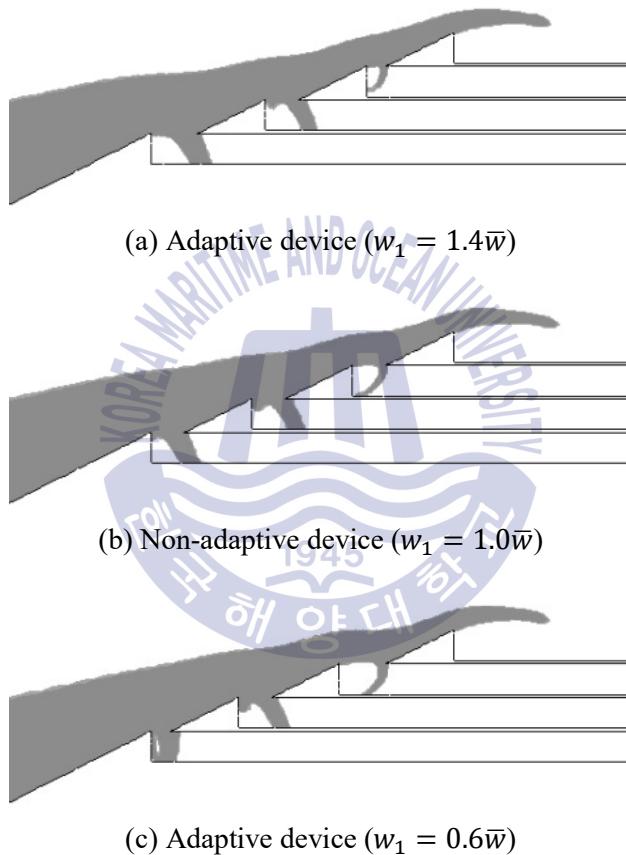
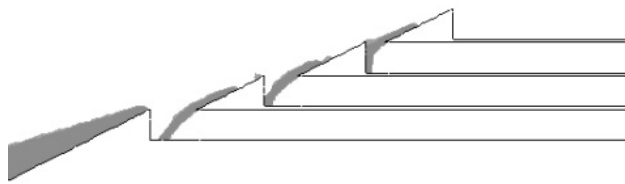
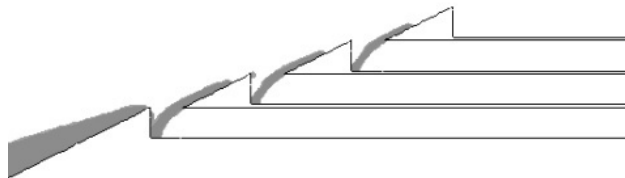


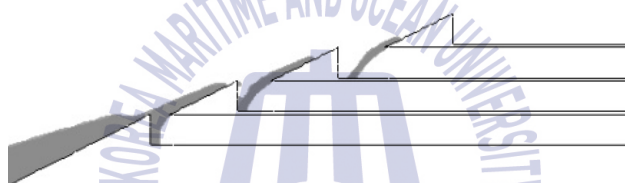
Fig. 4. 27 Run-up process of non- and adaptive devices based on $\bar{w} = 0.5$ m



(a) Adaptive device ($w_1 = 1.4\bar{w}$)



(b) Non-adaptive device ($w_1 = 1.0\bar{w}$)



(c) Adaptive device ($w_1 = 0.6\bar{w}$)

Fig. 4. 28 Fall-down process of non- and adaptive devices based on $\bar{w} = 0.5$ m

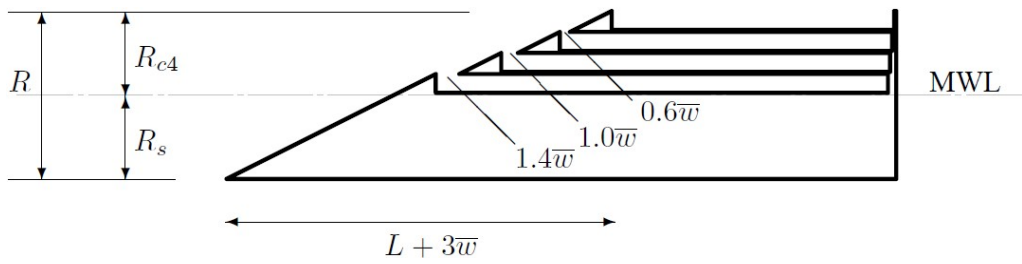
The different layouts design of overtopping wave energy converter are investigated by using a numerical model for two-dimensional flow. The multi-stage device has two design layouts: non-adaptive and adaptive devices. Moreover, the layout of adaptive device has two types: reservoir width varies from large to small and vice versa which are corresponding with negative and positive $\Delta w/\bar{w}$ respectively. The overall hydraulic efficiency of both non-adaptive and adaptive devices are compared. The numerical results show that the overall hydraulic efficiency of non-adaptive device is rather superior compared to that of adaptive devices. In addition, the optimal performance is given by non-adaptive device based on average slot width \bar{w} of 0.4 m. From this result, the loss rate of non-adaptive layout of \bar{w} of 0.4 m is minimum within the range of parametric space considered.

4.4 Effect of overlap ramp of non-adaptive and adaptive devices

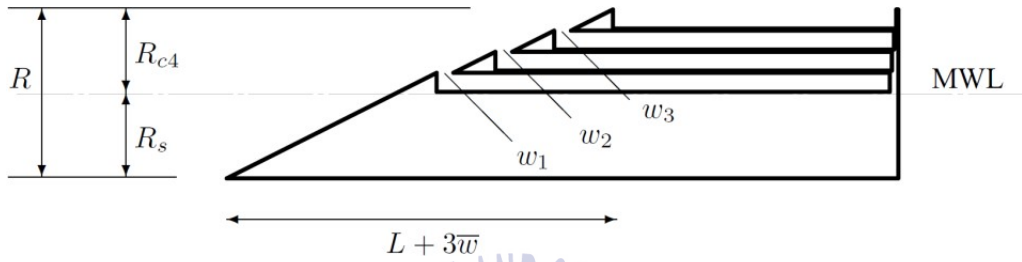
The optimization of the OWEC design concerns particularly the ramp geometry in order to maximize the energy captured by the reservoirs. There are two strategies to achieve the goal: devices with different overlap ramp and devices with different submerged ramp.

The former investigation focuses on the influence of overlap ramp on the hydraulic performance. The base-line model is based on non-adaptive device which is schematically illustrated in Fig. 4.29b. The ramp height R consists of two parts, the submerged depth R_s and freeboard height R_{c4} that both parameters are fixed as 2 m. The slope S of each ramp is defined as the ratio between the ramp height R and horizontal ramp length L which is kept constant as $S = 1/2$ for both freeboard and draught parts. This consequently results in the $3\bar{w}$ extended length of the ramp.

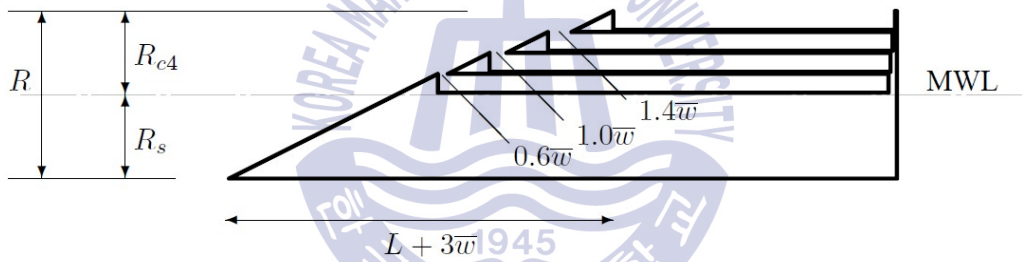
These multi-stage devices have three extra slots which are defined as w_1 (the lowest), w_2 (the middle) and w_3 (the highest). The adaptive layout gives difference in size of the slots as $\Delta w = w_2 - w_1 = w_3 - w_2$, so that the average width of each device is $\bar{w} = w_2$ which is fixed as 0.4 m in the present study. Moreover, the parameter slot width \bar{w} is represented in dimensionless form namely relative slot width as: \bar{w}/R_{c4} of 0.2. The adaptive device has two layouts: reservoir width varies from large to small ($w_1 = 1.4\bar{w}$) and vice versa. The illustration of overlap distance is shown in Fig. 4.30 and is defined by parameter y that is varied within the range of 0.025 to 0.100 m with a 0.025 m increment. This design is applied to both adaptive and non-adaptive devices.



(a) Large to small



(b) Non-adaptive



(c) Small to large

Fig. 4. 29 Layouts of non-overlap ramp multi-stage devices base on the relative slot width of 0.2

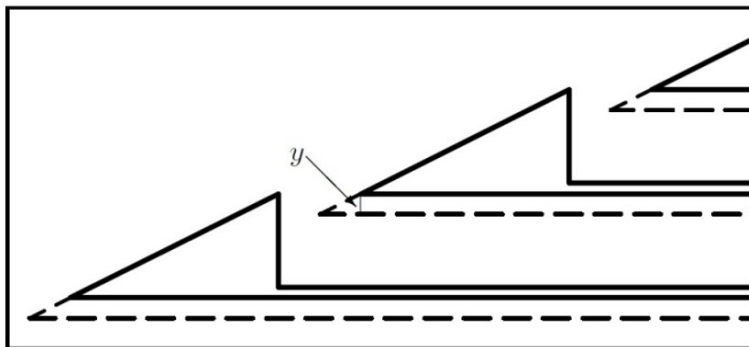


Fig. 4. 30 Example of overlap ramp layout of non-adaptive device.

The slot width of non-adaptive and adaptive devices are summarized in Table 4.7. The distance of slot width is measured horizontally at crest level. Fig. 4.29 shows the layouts of non-overlap ramp multi-stage devices based on the relative slot width of 0.2 which is corresponding to the Table 4.7.

Table 4. 7 Parameters of adaptive slot width

| Device | w_i/\bar{w} | | |
|----------------|---------------|--------|--------|
| | Slot 1 | Slot 2 | Slot 3 |
| Large to small | 1.4 | 1.0 | 0.6 |
| Non-adaptive | 1.0 | 1.0 | 1.0 |
| Small to large | 0.6 | 1.0 | 1.4 |

4.4.1 Combination of overlap ramp and adaptive slot width

The overlap distance y , which is presented in dimensionless form as y/\bar{w} , is shown in the Table 4.8. This overlap design, i.e., extended the ramp of each extra slot, is applied to both adaptive and non-adaptive layouts.

Table 4. 8 Parameter condition of overlap ramp

| | |
|---|-----------------------------|
| Submerged depth, R_s [m] | 2.0 |
| Relative freeboard, R_{c4}/H [-] | 1.0 |
| Relative average slot width, \bar{w}/R_{c4} [-] | 0.2 |
| Overlap distance, y [m] | 0.025, 0.05, 0.075, 0.10 |
| Relative extended ramp, y/\bar{w} [-] | 0.0625, 0.125, 0.1875, 0.25 |

The numerical results are shown in Fig. 4.31 - 33. It can be seen from Fig. 4.31 that the applied overlap distance insignificantly affects the overall hydraulic efficiency whether the device is adaptive or non-adaptive. An example of energy flow for case of $y/\bar{w} = 0.125$ is shown in Fig. 4.32 for both adaptive and non-adaptive devices. A similar trend of energy flow is found for devices with other overlap distances, i.e., $y/\bar{w} = 0.0625, 0.1875, 0.25$ resulting in the overall hydraulic efficiency of about 35 - 39 %.

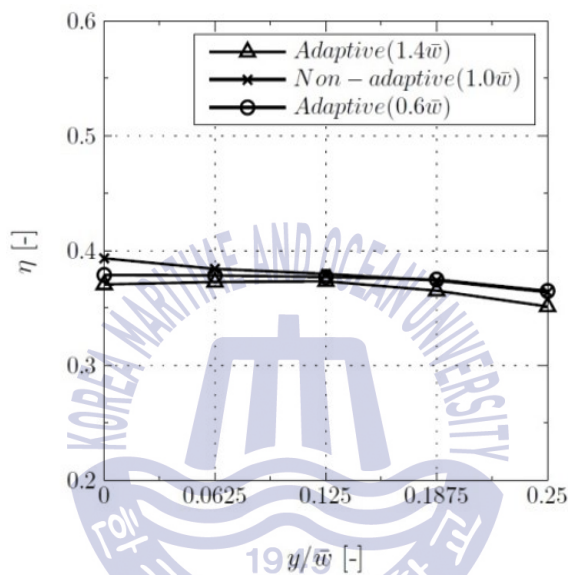


Fig. 4. 31 Effect of overlap ramp applied to multi-stage devices on overall hydraulic efficiency as function of relative extended ramp. The non-overlap ramp is represented by the relative extended ramp $y/\bar{w} = 0$

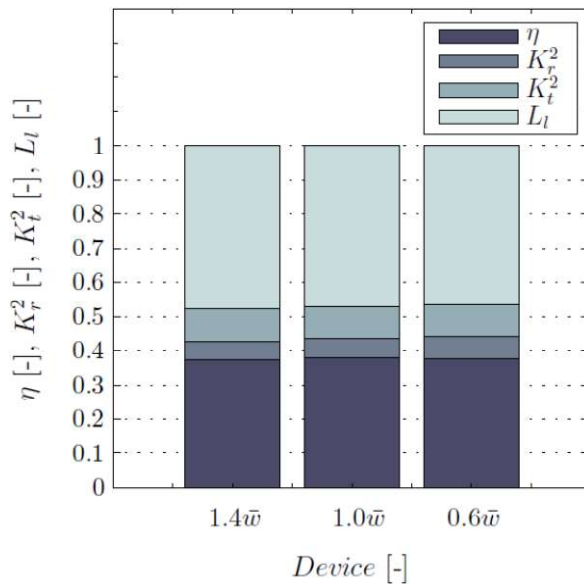
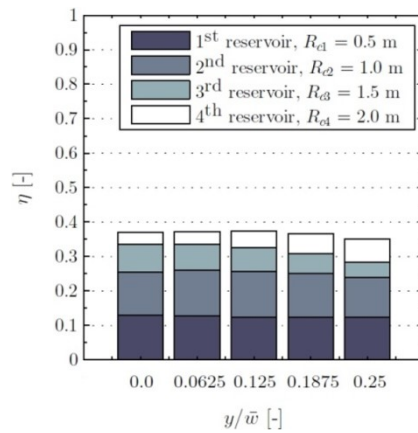
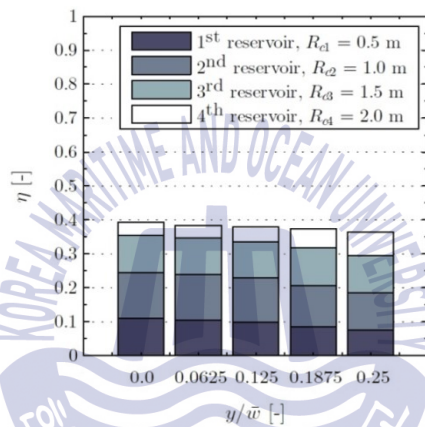


Fig. 4. 32 Comparison of overall hydraulic efficiency, reflection, transmission and loss rates of overlap ramp non-adaptive and adaptive device base on $y/\bar{w} = 0.125$

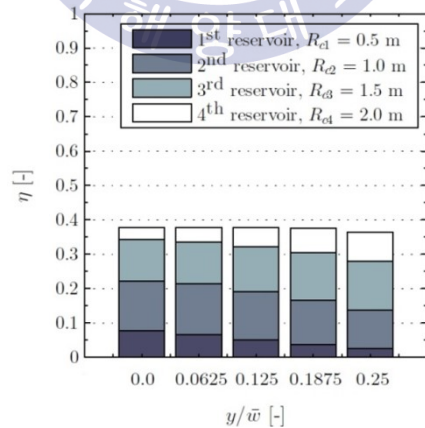
However, the overlap distance has strong influence on the partial hydraulic efficiencies as shown in Fig. 4.33. By increasing the overlap distance, the amount of water collected by lower reservoirs is decreasing while that of the higher reservoirs is increasing. The overlap ramp reduces the gap between two consecutive ramps, as if the slot width is getting smaller and therefore the water can run-up smoothly. The increase in energy captured by lower reservoirs compensates for the decrease of the higher ones giving insignificant change in overall efficiency. This affects the strategy of power extraction process via multi-stage turbines. The water capture mechanism of both run-up and fall-down processes are shown in Fig. 4.34 - 35.



(a) Overlap ramp of adaptive device (w_l is $1.4\bar{w}$)



(b) Overlap ramp of non-adaptive device (w_l is $1.0\bar{w}$)



(c) Overlap ramp of adaptive device (w_l is $0.6\bar{w}$)

Fig. 4. 33 Partial hydraulic efficiencies of each reservoir versus the relative extended ramp

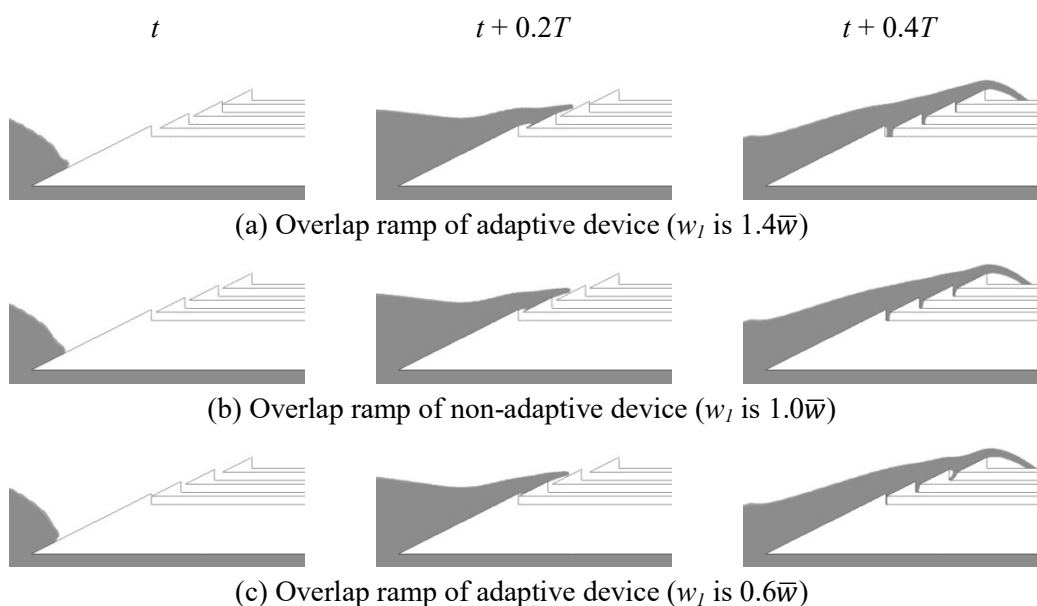


Fig. 4. 34 Water flow run-up processes of overlap ramp multi-stage device based on $y/\bar{w} = 0.25$ at different time

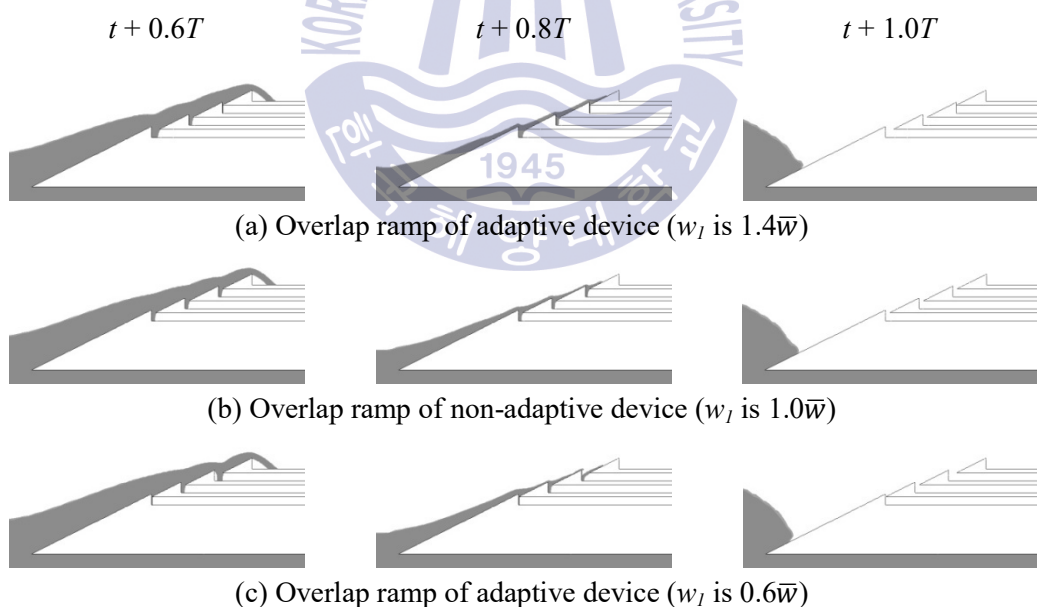


Fig. 4. 35 Water flow fall-down processes of overlap ramp multi-stage device based on $y/\bar{w} = 0.25$ at different time

4.5 Effect of submerged depth on the performance of multi-stage of OWECs

The second investigation concerns the influence of submerged ramp on the performance of land-based OWEC. The parameter R_s is varied within the range 2 to 8 m with a 2 m increment. The schematic illustration of OWEC device installed on breakwater is shown in Fig. 4.36.

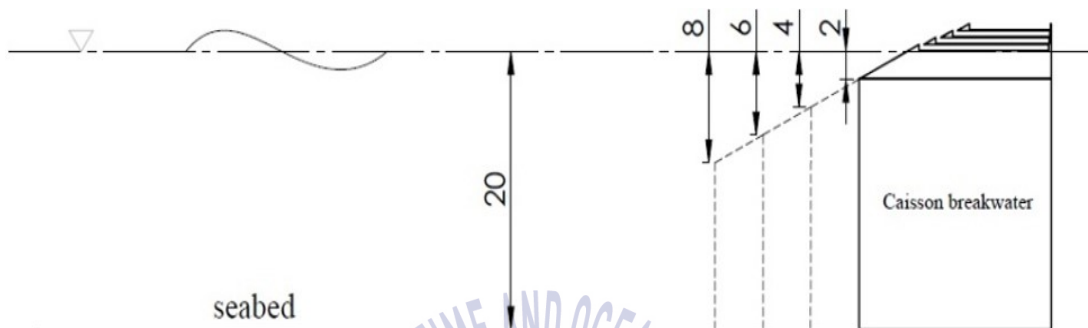


Fig. 4. 36 Schematic of multi-stage device to study the effect of submerged depth on performance

4.5.1 Multi-stage OWEC installed on breakwater

The investigation concerns the influence of submerged ramp on the performance of land-based OWEC. Table 4.9 summarizes the specification of submerged ramp.

Table 4. 9 Parameter of submerged depth study

| | |
|---------------------------------------|------------|
| Relative freeboard, R_{c4}/H [-] | 1.0 |
| Relative slot width, w/R_{c4} [-] | 0.2 |
| Submerged depth, R_s [m] | 2, 4, 6, 8 |
| Relative submerged depth, R_s/H [-] | 1, 2, 3, 4 |

The overall performance of land-based device is considerably superior compared to that of stationary devices with equivalent submerged ramp as shown in Fig. 4.37. For small depth, extending the submerged part of ramp results in relatively great performance enhancement. Further extending the ramp gives gradual increase in efficiency and tends to converge to a certain value. Fig. 4.38a and 4.38b show partial efficiencies of different submerged depth. The overall performance enhancement is achieved by increasing the energy captured by the highest reservoir, while the lower ones are unaffected.

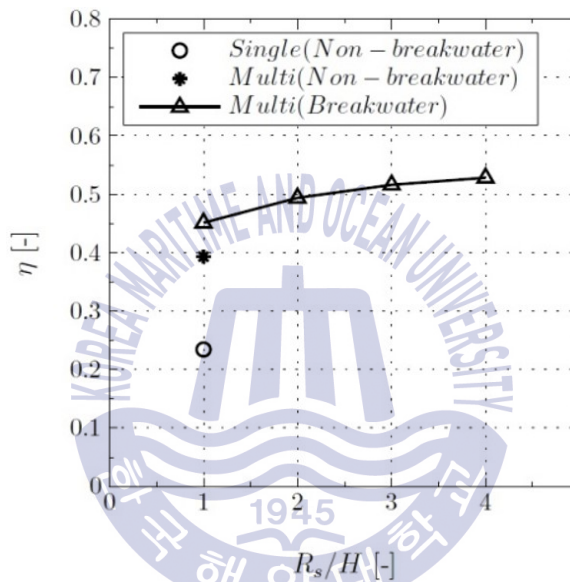
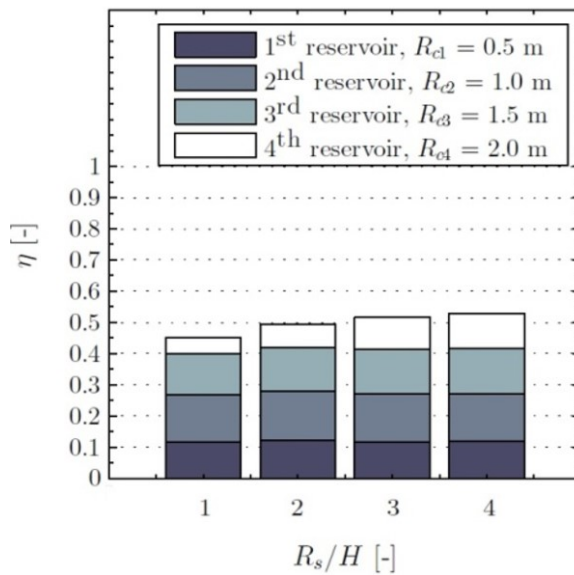
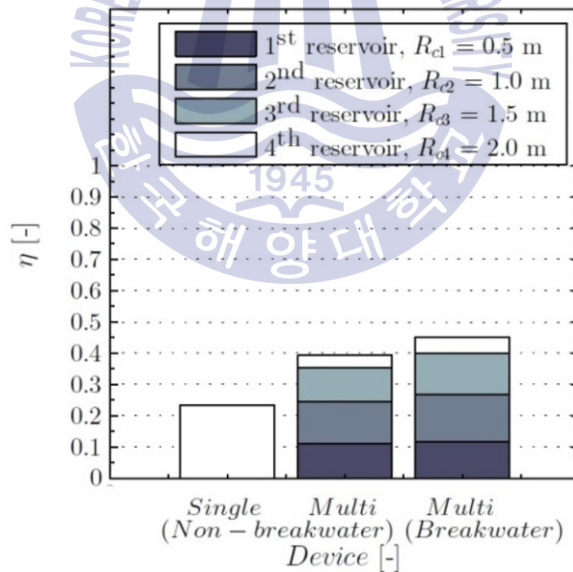


Fig. 4. 37 Overall hydraulic efficiencies of single- and multi-stage device as function of relative submerged depth



(a) Partial hydraulic efficiencies of each reservoir of multi-stage devices are installed on breakwater as function of relative submerged depth



(b) Partial hydraulic efficiencies of each reservoir of single- and multi-stage devices based on relative submerged depth of 1.0

Fig. 4. 38 Effect of submerged depth on overall hydraulic efficiencies of OWEC devices

In case of stationary buoyant devices, a portion of un-captured energy transports with transmission wave. However, a portion of this wave and its energy transforms and run-up, then overtop into reservoirs in case of land-based devices, resulting in greater efficiency as seen in Fig. 4.39a - 4.39b. Increasing the submerged depth is similar to the effect of wave behavior in shoaling water. Wave shoaling is the effect by which surface waves entering shallower water, resulting in change in wave height, and therefore the amount of water in the higher reservoirs is increasing.

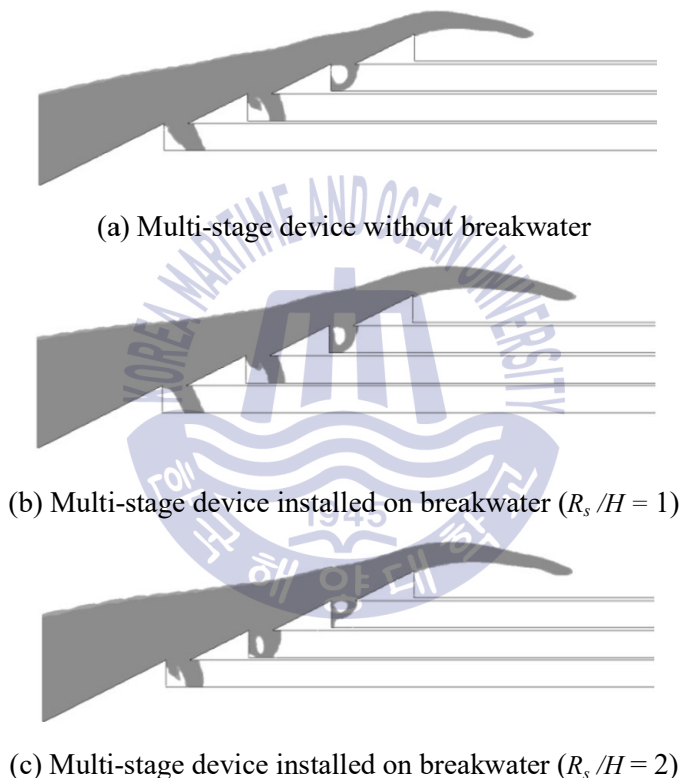


Fig. 4. 39 Water flow into reservoirs of multi-stage device with and without breakwater

The OWEC device installed on breakwater gives significant performance enhancement compared to stationary buoyant device. This is because the breakwater eliminates transmission wave and converts part of it into overtopping flow. As the draft is deepened, the efficiency increases and finally tends to converge to a certain value.

4.6 Effect of span on the performance of multi-stage of OWECs

Three-dimensional device and its effects on the performance of the multi-stage OWEC are investigated and compared to that of two-dimensional device. The baseline model is based on the device with slot width of 0.4 m and the submerged depth of 8 m which is installed on breakwater.

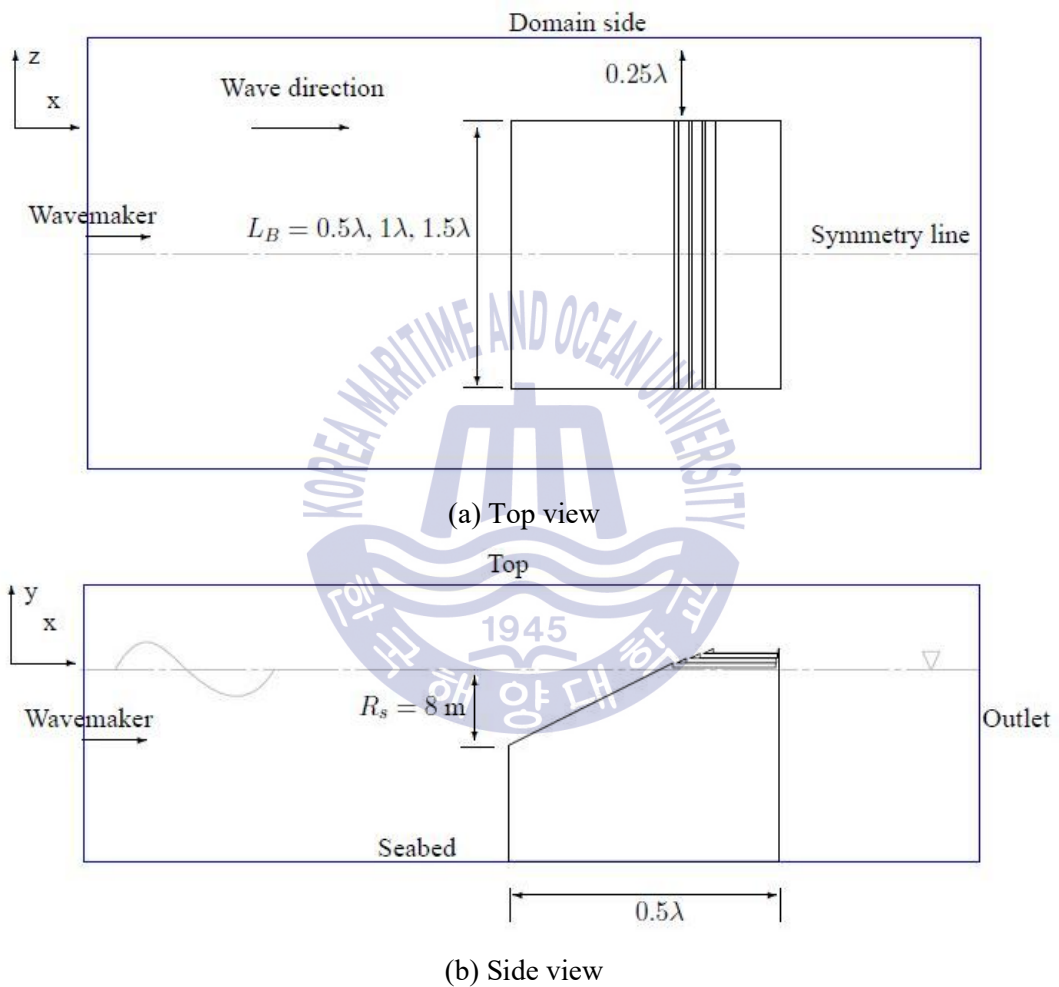


Fig. 4. 40 Schematic of three-dimensional domain to study the effect of span on the performance of multi-stage device

The span length of breakwater is the main parameter to study the effect of three-dimensional geometry on the performance of the wave energy device. The parameter L_B is varied within the range 0.5λ to 1.5λ m with a 0.5λ m increment. The schematic of domain shows in Fig. 4.40.

Grid system of three-dimensional computational domain follows that of two-dimensional, that is, the number of cells per wave height is 20 cells and 100 cells per wavelength is utilized. Adaptive refinement is also applied which gives a dense mesh in the vicinity of free surface and device, as illustrate in Fig. 4.41 and 4.42.

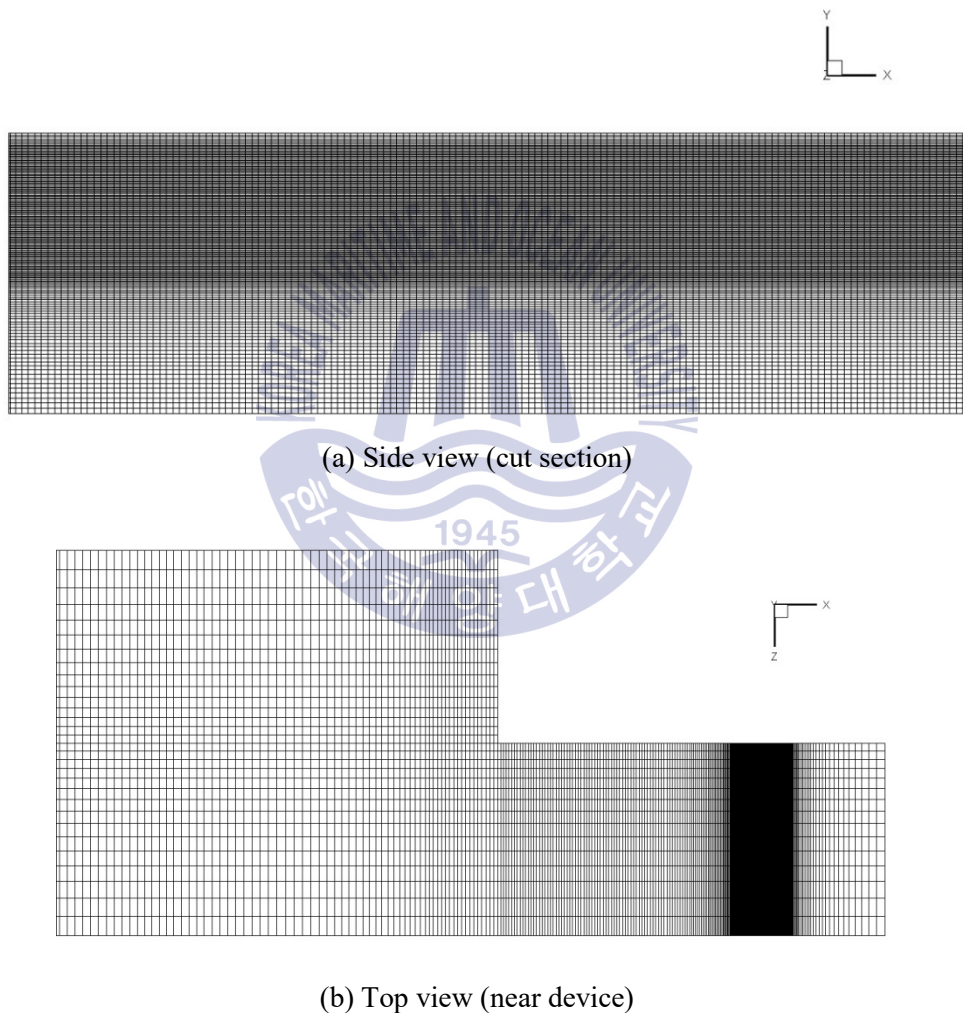


Fig. 4. 41 Mesh of three-dimensional domain

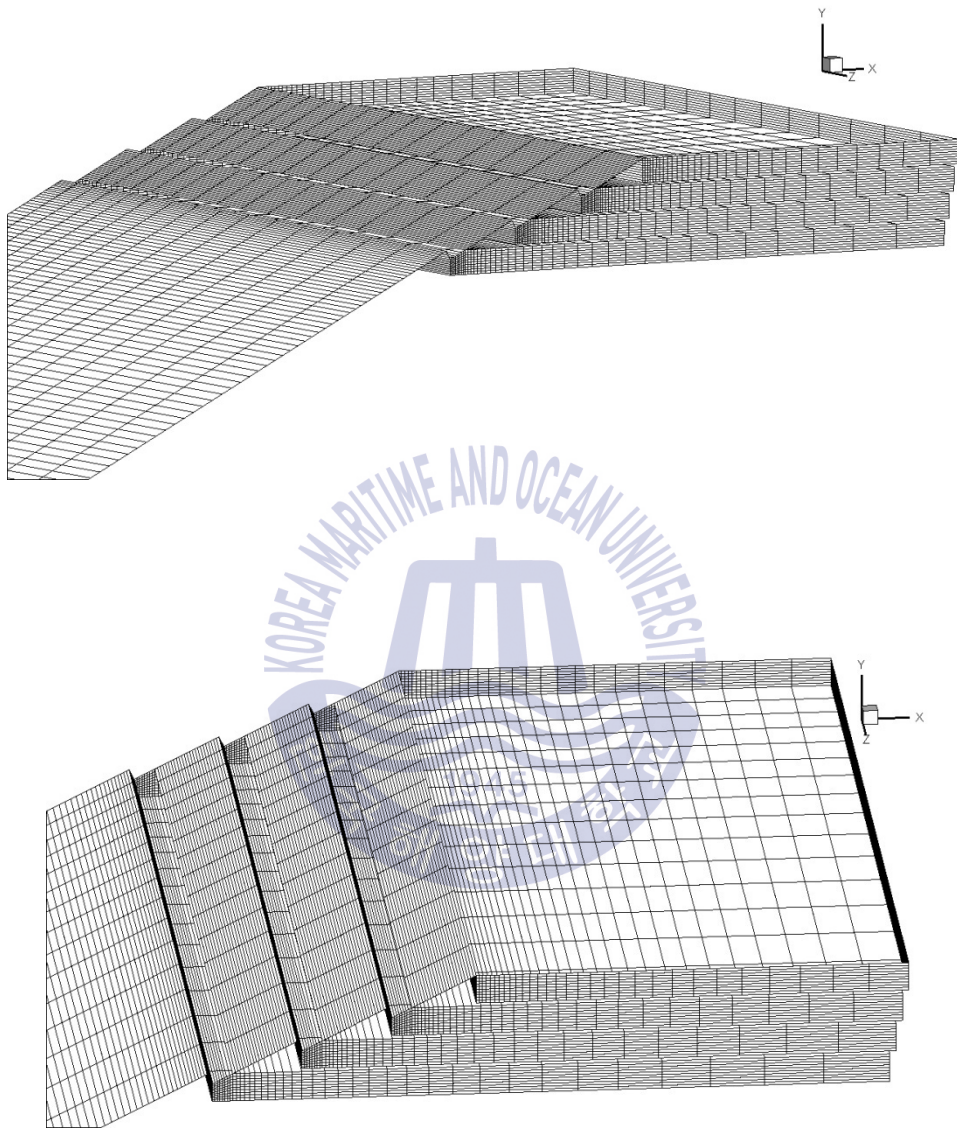


Fig. 4. 42 Surface mesh of multi-stage OWEC device

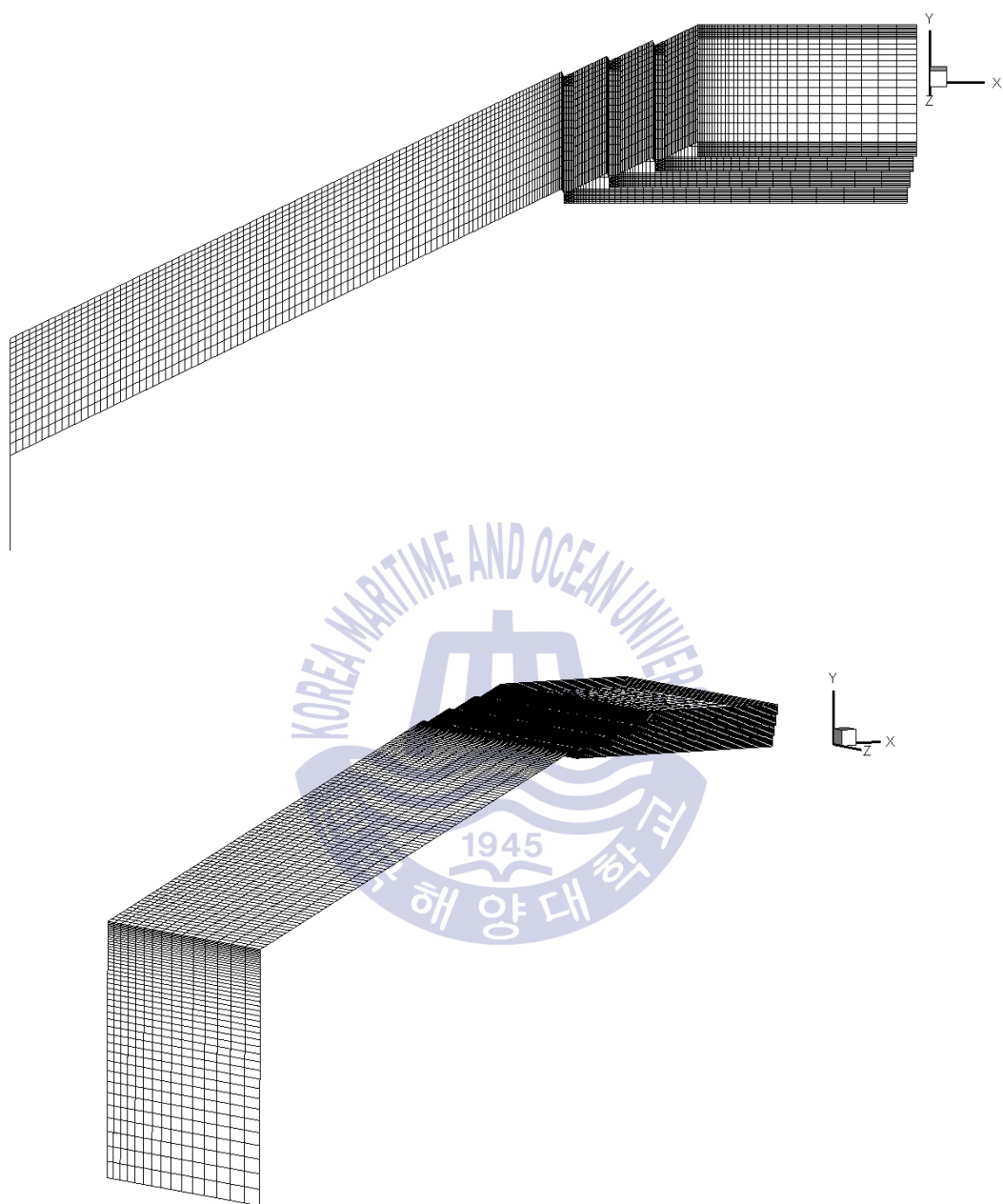


Fig. 4. 42 Surface mesh of multi-stage OWEC device (continue)

In spite of many validations of the two-dimensional model presented in the last section, it would be better to validate the numerical tool again for this three-dimensional study since three-dimensional model can sometimes lead to significantly different results compared to that of two-dimensional model. The generated wave profile is shown in Fig. 4.43 along with calculated wave using linear wave theory. It can be seen that the generated wave using dynamic mesh gives well agreement with the calculated linear wave.

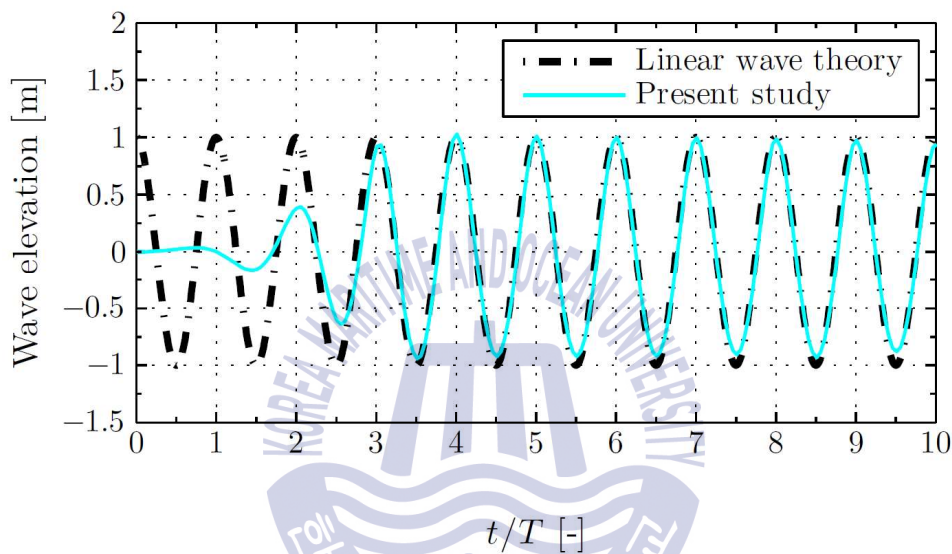


Fig. 4. 43 Numerical wave tank validation in three-dimensional domain.

The generated wave profile is compared with linear wave theory.

(Surface elevation at $x = 1\lambda$)

The overall hydraulic efficiency of three-dimensional device with different span lengths are plotted in Fig 4.44 in comparison with that of two-dimensional device. It can be seen that the three-dimensional effects play an important role in the wave energy capture mechanism as the device with the shortest span gives relatively lowest efficiency, while increasing span length gives greater performance which seemingly tends to converge to that of device with infinite span, i.e., the two-dimensional device. This is analogous to the difference between two- and three-dimensional wings as the wider aspect ratio gives greater lift coefficient, whereas the shorter one results in a lower lift coefficient due

vortices generated at wing tips. The three-dimensional OWEC model has finite span possessing tips, which results in wave falling-down at the tips during the run-up process as seen in Table 4.10. As a result of this, the wave at the tip cannot run-up as high as wave near the centerline. This consequently has noticeable influence on the amount of water being stored by the higher reservoirs, while those of lower ones have relatively smaller effects as presented by the partial hydraulic efficiencies in Fig 4.45. It is suggested to install a guide vane at tips of the device which could prevent or reduce the mentioned three-dimensional effects and hence increase the effective span of the device, similarly to what winglets of aircraft do. Moreover, the graphic of wave elevation in three-dimensional domain is shown in Fig. 4.46.

For this research, a regular wave has been utilized for all simulations. However, the natural ocean waves are irregular waves which are more complicated. In the future, it is suggested to study the performance of the devices operating in irregular wave conditions.

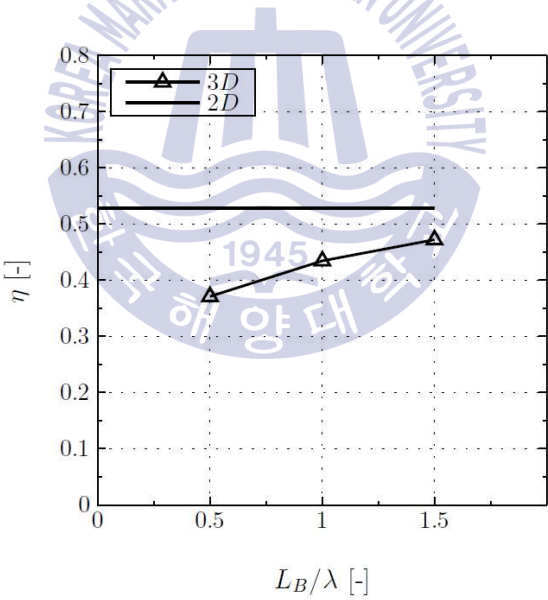


Fig. 4. 44 Overall hydraulic efficiency of multi-stage OWEC in three-dimensional simulation compare with the results of two-dimensional simulation

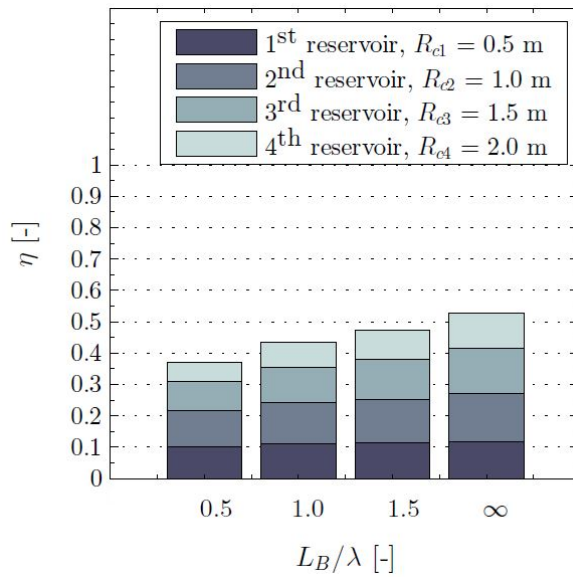
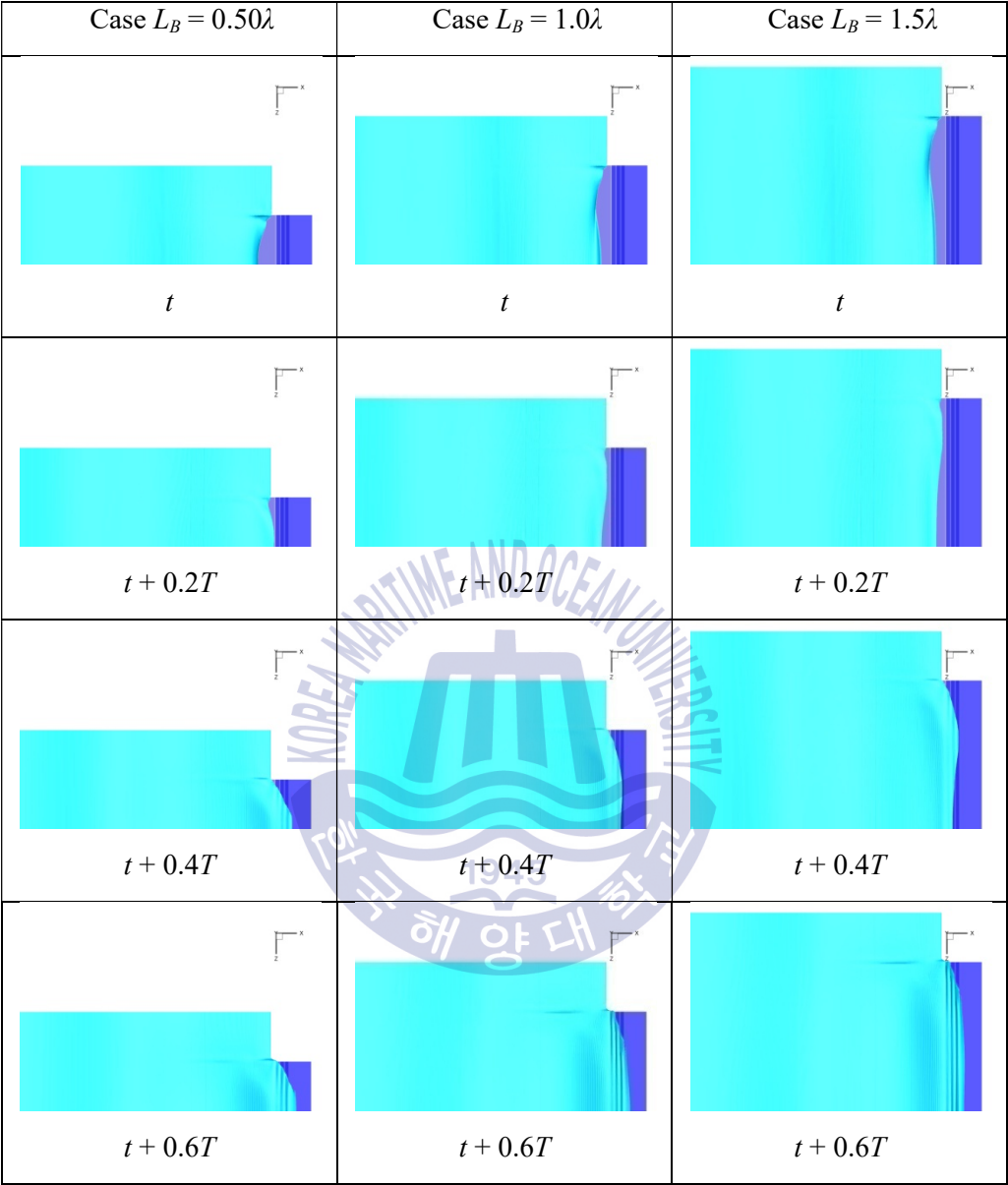


Fig. 4. 45 Partial hydraulic efficiencies of each reservoir of multi-stage devices as function of relative breakwater length. The two-dimensional result is represented by the relative breakwater length $L_B/\lambda = \infty$



Fig. 4. 46 Wave surface elevation in three-dimensional domain

Table 4. 10 Wave elevation of three-dimensional simulation of multi-stage OWEC



4.7 Scenario of overtopping wave energy converter in Thailand

Thailand's energy resources can be divided into different proportions, as shown in Fig. 4.47. It can be seen that most of the energy utilization relies on natural gas while only 5 % comes from alternative energy resource. However, the Thai government continues to encourage and find ways to utilize alternative energy as seen from a 10-year plan to promote the use of alternative energy to 25 % as shown in Fig. 4.48. Considering the proportion of alternative energy derived from marine energy, it is projected to be 2 MW.

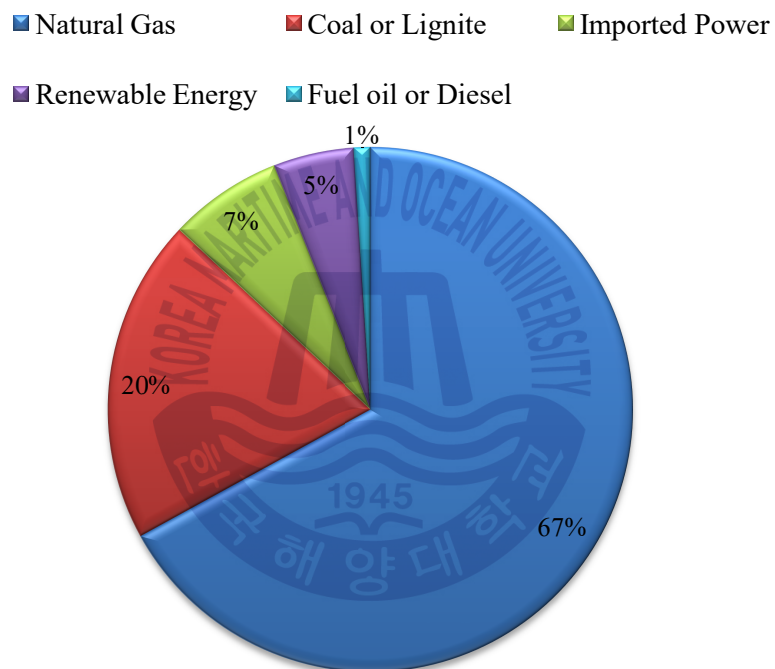


Fig. 4. 47 Energy Sources of Thailand in 2012

Source: Energy Policy and Planning Office, Ministry of Energy (Alternative Energy, 2015)

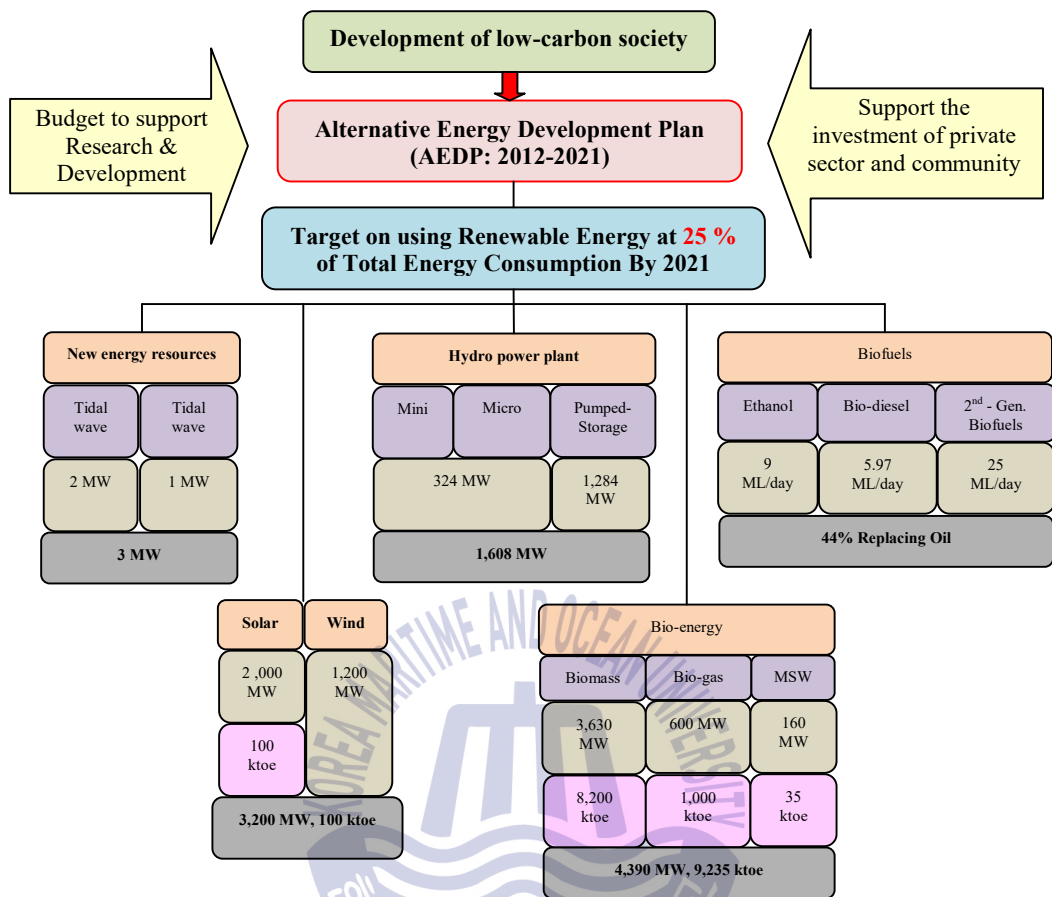
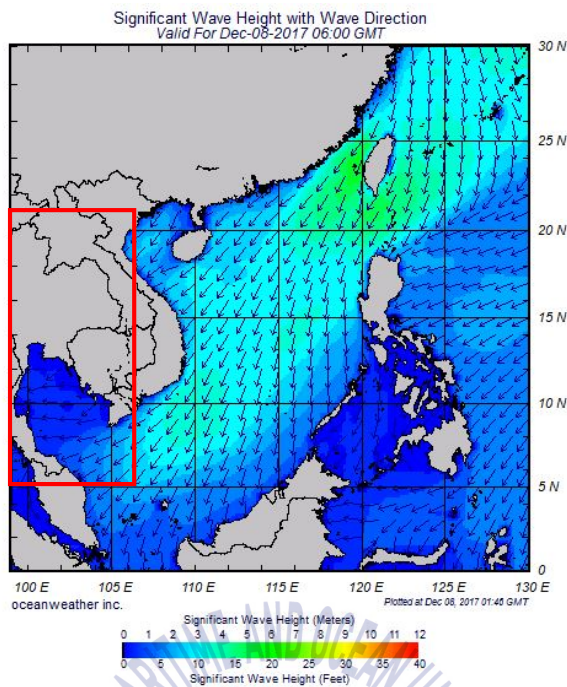


Fig. 4. 48 Ten year alternative energy development plan of Thailand

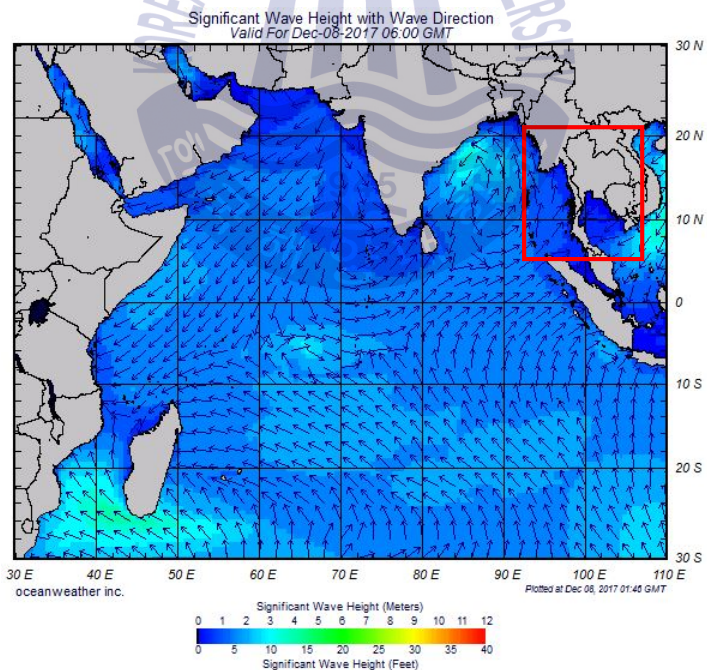
Source: Department of Alternative Energy Development and Efficiency, Ministry of Energy

According to Fig. 2.5 and 2.6, the annual mean wave power in Andaman sea and gulf of Thailand is approximately 2 - 4 kW/m. Although the wave potential in Thailand is relatively low, it is possible to harvest the energy via an efficient device. In this research, we have studied the performance of overtopping wave energy converter. The device will be applied to the sea area in Thailand. As shown in Fig. 4.49, it can be seen that the significant wave height in the southern part of the country is around 1 - 2 m in average, corresponding to the wave height studied in this research. However, some parameters such as wave period and water depth are different from the conditions used in this research. In order to achieve a similar performance to the current research, it may be necessary to adjust the size of the device since matching the dimensionless numbers is a key to achieve validity and similarity.





(a) Significant wave height in Gulf of Thailand



(b) Significant wave height in Andaman Sea

Fig. 4. 49 Significant wave height with wave direction around Thailand
(Ocean weather, 2017)

The overall hydraulic efficiency of the multi-stage seabed structure device can be over 50 %. By taking into account the reservoir efficiency, turbines efficiency, generator efficiency and three-dimensional effects, the overall performance is approximately 33 %.

Areas of interest are Phuket and Nakhon Si Thammarat, as shown in Fig. 4.50. Phuket is located in the south west of Thailand while Nakhon Si Thammarat is located in the south east of Thailand. Since Phuket is an extremely popular tourist destination, it is unsuitable to install any equipment. On the other hand, Nakhon Si Thammarat Province is facing the problem of coastal erosion as seen in Fig. 4.51. If the device is installed at this location, in addition to energy utilization, it can also reduce the severity of coastal erosion. If the target is 100 kW, the length of the device is approximately 150 m, based on the available wave energy potential of 2 kW/m.



Fig. 4. 50 Southern of Thailand map (South Thailand)



(a) Coastal erosion



(b) Breakwater

Fig. 4. 51 Beaches and coastlines in Nakhon Si Thammarat, Thailand
(Department of Marine and Coastal Resources, Thailand, 2007)

Chapter 5 Conclusions and perspectives

A numerical investigation has been performed using two- and three-dimensional RANS simulations in order to study flow physics and performance of wave energy devices used to harvest ocean wave power based on overtopping principle. Firstly, the wave flume has been validated. The airy wave is generated as an incident wave in the present study using dynamic mesh in which the generated wave profile agrees well with the linear wave theory. Moreover, the VOF model used in the present study is validated in comparison with laboratory experimental data and a comparable study. Additionally, it has been shown that the measured overtopping rates from the present study are in satisfactory agreement with the predicted discharges using analytical solutions proposed by a comparable study.

Several geometrical design strategies have been utilized in order to study their effects on the performance of the stationary buoyant overtopping wave energy converter. The hydraulic efficiency based on captured crest energy is the main performance indicator in the present study. The use of multi-stage reservoirs and their corresponding opening with a lower crest height, more precisely a slot, is applied to maximize the efficiency. Two different layouts of multi-stage OWEC: fixed slope and variable slope device have been investigated and compared to the baseline single-stage device. The results show that, for multi-stage devices, the optimal performance based on hydraulic efficiency of multi-stage device exists at an intermediate value of slot width, particularly relative slot width of 0.15 and 0.2 depending on design layouts. This results in a significant enhancement in energy captured and efficiency. The improvement is achieved by increasing the overtopping flow rate into the extra slots during both wave run-up and fall-down processes. However, the overtopping flow rate of the main reservoir is decreased which can be avoided by using a controllable gate or valve which manages to close the extra slots during wave run-up process and automatically open during wave fall-down process.

Moreover, the fixed slope device is studied more in detail via application of adaptive slot width. The numerical results show that the overall hydraulic efficiency of non-adaptive and adaptive slot devices are nearly on par to each other. This can be concluded that the effect of adaptive slot width on performance can be negligible.

Another design strategy, overlap ramp, is investigated which is applied to both non-adaptive and adaptive devices. The numerical results show that the overall hydraulic efficiency of the two layouts are approximately equivalent. The overlap ramp layout slightly affects the overall hydraulic efficiency of OWEC device. However, an increase in overlap distance gives enhancement of overtopping flow rate and hence the hydraulic efficiency of the main reservoir, while those of the lower ones is decreasing. This implies that the control strategy of power take-off unit, i.e., the multi-stage turbines might be affected.

In addition, the effect of submerged depth of multi-stage device installed on breakwater has been studied. It has been shown that the OWEC device installed on breakwater gives significant performance enhancement compared to stationary buoyant device. This is because the breakwater eliminates transmission wave and converts part of it into overtopping energy. For small value of submerged depth, the performance is increasing for increasing the variable. Further increasing the depth, the performance finally tends to converge to a certain value, hence convergence trend of efficiency.

All of above simulations is done on the basis of two-dimensional phenomena. The study of three-dimensional phenomena of overtopping flow has also been studied. As the aspect ratio of the device is widen, the overall hydraulic efficiency seems to converge closely to that of two-dimensional device. In order to increase the effective aspect ratio of the device, it is suggested to install a guide vane at the tips which could avoid the spanwise velocity.

We strongly believe the present study is beneficial for understanding and validating the comparable experiment. A better understanding of overtopping flow mechanism explained in the present study could therefore provide a guideline in the field of OWEC design. Further investigations are recommended in order to study the effects of the suggested control strategies and also the irregular wave conditions. Moreover, the experiment is also recommended in order to validate the simulations.

References

- Airy GB. 1845. On the laws of the tides on the coasts of Ireland, as inferred from an extensive series of observations made in connexion with the Ordnance Survey of Ireland [1844]. Philos. Trans. R. Soc. London, pp. 1– 124
- Alternative Energy, available from (<http://thaiembdc.org/wp-content/uploads/2015/05/Alternative-Energy.pdf>).
- Archimedes Wave Swing, available from (http://www.awsocan.com/media/File/pdf/AWS_feature_The_Engineer_Oct07.pdf).
- Atargis CycWEC, available from ([http:// URL www.atargis.com](http://URL www.atargis.com)).
- Brito, A. and Villate, J.L., 2014. Annual report. Implementing agreement on ocean energy systems-2013. *The Executime Committee of Ocean Energy Systems*.
- Clément, A., McCullen, P., Falcão, A., Fiorentino, A., Gardner, F., Hammarlund, K., Lemonis, G., Lewis, T., Nielsen, K., Petroncini, S. and Pontes, M.T., 2002. Wave energy in Europe: current status and perspectives. *Renewable and sustainable energy reviews*, 6(5), pp.405-431.
- Connell, K.O. and Cashman, A., 2016, March. Development of a numerical wave tank with reduced discretization error. In *Electrical, Electronics, and Optimization Techniques (ICEEOT), International Conference on* (pp. 3008-3012). IEEE.
- Department of Marine and Coastal Resources, Thailand, 2007, available from (<http://www.dmcr.go.th/attachment/download/download.php?WP=q3EZMT1CM5O0hJatrTgjWz04qmWZZz1CM5O0hJatrTDo7o3Q>).

DEXAWAVE, available from ([http:// www.dexawave.com](http://www.dexawave.com)).

Drakoo, available from ([http://www.worldfutureenergysummit.com/Portal/userfiles/ attachments/Development_of_a_Highly_Efficient_and_Cost-effective_Wave_Energy_Convertor_Drakoo-Henry_L_Han.pdf](http://www.worldfutureenergysummit.com/Portal/userfiles/attachments/Development_of_a_Highly_Efficient_and_Cost-effective_Wave_Energy_Convertor_Drakoo-Henry_L_Han.pdf)).

Drakoo device, available from (http://i.ytimg.com/vi/B2V_Hr4tGRA/maxresdefault.jpg).

Drakoo WEC, available from (<http://www.hann-ocean.com/products/drakoo-wave-energy-converter/>).

Drew, B., Plummer, A.R. and Sahinkaya, M.N., 2009. A review of wave energy converter technology.

Du, Q. and Leung, D.Y., 2011. 2D numerical simulation of ocean waves. In *Linköping Electronic Conference Proceedings*. Linköping University Electronic Press. The Journal's web site is located at [http://www. ep. liu. se/ecp/](http://www.ep.liu.se/ecp/).

Energy Industry Challenges, available from ([http://www.i15.p.lodz.pl/strony/EIC/res/ Description_of_technology_wave.html](http://www.i15.p.lodz.pl/strony/EIC/res/Description_of_technology_wave.html)).

Evans, D.V., 1976. A theory for wave-power absorption by oscillating bodies. *Journal of Fluid Mechanics*, 77(1), pp.1-25.

Falnes, J., 1997. Principles for capture of energy from ocean waves. Phase control and optimum oscillation. *Dept. Phys., NTNU Trondheim, Trondheim, Norway, Tech. Rep. N-7034*.

Falnes, J., 2007. A review of wave-energy extraction. *Marine Structures*, 20(4), pp.185-201.

Fernandez, H., Iglesias, G., Carballo, R., Castro, A., Fraguera, J.A., Taveira-Pinto, F. and Sanchez, M., 2012. The new wave energy converter WaveCat: Concept and laboratory tests. *Marine structures*, 29(1), pp.58-70.

Gentova A.A. and Kovalenko S.V. , available from (<http://www.myshared.ru/slide/1039603/>).

Gunn and Stock-Williams, the global wave power resource, 2012, available from (<http://wavepowerlab.weebly.com/blog/the-global-wave-power-resource>).

Hirt, C.W. and Nichols, B.D., 1981. Volume of fluid (VOF) method for the dynamics of free boundaries. *Journal of computational physics*, 39(1), pp.201-225.

Hong, K., Shin, S.H., Hong, S.W. and Ryu, H., 2005, January. Investigation of Seasonal Variation of Wave Energy Density around Jeju Sea based on Long-Term Simulated Wave Data. In *The Fifteenth International Offshore and Polar Engineering Conference*. International Society of Offshore and Polar Engineers.

Hu, X.Z. and Liu, S.J., 2014. Two-dimensional numerical wave tank simulation for deployment of seafloor mining system. *Marine Georesources & Geotechnology*, 32(4), pp.293-306.

IEA-OES, Ocean Energy : Global Technology Development Status, March 2009, available from (http://www.energybc.ca/cache/tidal/annex_1_doc_t0104-1.pdf).

Isaacson, M., 1991. Measurement of regular wave reflection. *Journal of Waterway, Port, Coastal, and Ocean Engineering*, 117(6), pp.553-569.

Jin, J., Liu, Z., Hong, K.Y. and Hyun, B.S., 2012. 3D Numerical investigation on reservoir system for an overtopping wave energy convertor. *Journal of Navigation and Port Research*, 36(2), pp.97-103.

Kofoed, J.P., 2002. *Wave Overtopping of Marine Structures: utilization of wave energy* (Doctoral dissertation, Videnbasen for Aalborg UniversitetVBN, Aalborg UniversitetAalborg University, Det Teknisk-Naturvidenskabelige FakultetThe Faculty of Engineering and Science, Institut for Vand, Jord og MiljøteknikDepartment of Civil Engineering).

Kofoed, J.P., 2005. Model testing of the wave energy converter Seawave Slot-Cone Generator.

Kofoed, J.P., 2006, September. Vertical distribution of wave overtopping for design of multi level overtopping based wave energy converters. In *Coastal Engineering Conference* (Vol. 30, No. 5, p. 4714). ASCE AMERICAN SOCIETY OF CIVIL ENGINEERS.

Kofoed, J.P., Frigaard, P., Friis-Madsen, E. and Sørensen, H.C., 2006. Prototype testing of the wave energy converter wave dragon. *Renewable energy*, 31(2), pp.181-189.

Liu, Z., Hyun, B.S. and Jin, J.Y., 2009a. Computational analysis of parabolic overtopping wave energy convertor. *Journal of the Korean Society for Marine Environment & Energy*, 12(4), pp.273-278.

Liu, Z., Hyun, B.S. and Jin, J.Y., 2009b. 2d computational analysis of overtopping wave energy convertor. *Journal of the Korean Society for Marine Environmental Engineering*, 23(6), pp.1–6.

Liu, Z., Hyun, B.S. and Hong, K.Y., 2008a, January. Practical Calculation of Parabolic Overtopping Wave Energy Converter. In *The Eighth ISOPE Pacific/Asia Offshore Mechanics Symposium*. International Society of Offshore and Polar Engineers.

- Liu, Z., Hyun, B.S. and Jin, J., 2008b, Numerical prediction for overtopping performance of OWEC. *Journal of the Korean Society for Marine Environmental Engineering*, 11(1), pp.35–41.
- Ly, D.K., Aboobacker, V.M., Abundo, S.M.L., Srikanth, N. and Tralich, P., 2014, November. Wave energy resource assessment for Southeast Asia. In *Proceedings of the 5th International Conference on Sustainable Energy and Environment (SEE), Science, Technology and Innovation for Association of Southeast Asian Nations (ASEAN) Green Growth, Bangkok, Thailand* (pp. 19-21).
- Malik, A.Q., 2011. Assessment of the potential of renewables for Brunei Darussalam. *Renewable and Sustainable Energy Reviews*, 15(1), pp.427-437.
- Mei, C.C., 2012. Hydrodynamic principles of wave power extraction. *Phil. Trans. R. Soc. A*, 370(1959), pp.208-234.
- Mirzaei, A., Tangang, F. and Juneng, L., 2014. Wave energy potential along the east coast of Peninsular Malaysia. *Energy*, 68, pp.722-734.
- Margheritini, L., Vicinanza, D. and Frigaard, P., 2009. SSG wave energy converter: Design, reliability and hydraulic performance of an innovative overtopping device. *Renewable Energy*, 34(5), pp.1371-1380.
- Martin, J.C. and Moyce, W.J., 1952. Part IV. An experimental study of the collapse of liquid columns on a rigid horizontal plane. *Philosophical Transactions of the Royal Society of London A: Mathematical, Physical and Engineering Sciences*, 244(882), pp.312-324.
- Minami, M. and Tanaka, H., 2015, July. 3-D Numerical Analysis of Overtopping-type Wave Power Generation Equipment. In *The Twenty-fifth International Ocean and Polar Engineering Conference*. International Society of Offshore and Polar Engineers.

Nam, B.W., Shin, S.H., Hong, K.Y. and Hong, S.W., 2008, January. Numerical simulation of wave flow over the Spiral-Reef overtopping device. In *The Eighth ISOPE Pacific/Asia Offshore Mechanics Symposium*. International Society of Offshore and Polar Engineers.

Ocean Power Technology, available from (<http://www.oceanpowertechnologies>).

Ocean weather, available (<http://www.oceanweather.com/data/index.html>).

OES, 2012, Annual report for 2012 online, Ocean Energy system, available from (www.ocean-energy-systems.org/news/annual-report-for-2012-online/).

OES website, available from (<https://www.ocean-energy-systems.org/ocean-energy-in-the-world/>).

Oh, J.S., 2009. The Study of Overtopping Wave Energy Converter Control and Monitoring System. *Journal of the Korean Society of Marine Engineering*, 33(7), pp.1012-1016.

Omar, Y., Tengku, T. and Mohamad, A., 2006. Prospects for ocean energy in Malaysia. In *Journal of International Conference on Energy and Environment*.

OpenEI, 2014, MarineandHydrokineticTechnologyDatabase, available from ([http://en.openEI.org/wiki/Marine_and_Hydrokinetic_Technology_Data base](http://en.openEI.org/wiki/Marine_and_Hydrokinetic_Technology_Data_base)).

Park, J.Y., Shin, S.H. and Hong, K.Y., 2011. Experimental study for overtopping performance and control system of overtopping wave energy convertor. *Journal of the Korean Society for Marine Environment & Energy*, 14(1), pp.11-18.

Pelamis, available from ([http:// www.pelamiswave.com](http://www.pelamiswave.com)).

Poseidon WEC, available from (<http://www.ecopedia.com/energy/new-york-city-looks-to-floating-energy-generators/>).

Quirapas, M.A.J.R., Lin, H., Abundo, M.L.S., Brahim, S. and Santos, D., 2015. Ocean renewable energy in Southeast Asia: a review. *Renewable and Sustainable Energy Reviews*, 41, pp.799-817.

RenewableUk, available from (<http://www.renewableuk.com>).

Report of KUWave device, Faculty of International Maritime Studies, Kasetsart University Sriracha campus, Thailand, 2013.

Ruol, P., Zanuttigh, B., Martinelli, L., Kofoed, P. and Frigaard, P., 2011. Near-shore floating wave energy converters: Applications for coastal protection. *Coastal Engineering Proceedings*, 1(32), p.61.

Salter's Duck, available from ([http:// www.tinyurl.com/saltersduck.com](http://www.tinyurl.com/saltersduck.com)).

Sanitwong Na Ayutthaya, S. & Iamraksa, P., 2016, The Designing of Drifter Buoy Used as Coastal Ocean Wave Measuring System. Proceeding of The 12th ISOPE Pacific/Asia Offshore Mechanics Symposium.

Shin, S.H. and Hong, K.Y., 2005. Experimental study on wave overtopping rate of wave overtopping control structure for wave energy conversion. *Journal of Ocean Engineering and Technology*, 19(6), pp.8-15.

Shin, S.H. and Hong, K.Y., 2006. An experimental Study of wave overtopping characteristics on the structure for wave overtopping power generating system. *Journal of Navigation and Port Research*, 30(8), pp.649-655.

Siegel, S.G., Jeans, T. and McLaughlin, T.E., 2011. Deep ocean wave energy conversion using a cycloidal turbine. *Applied Ocean Research*, 33(2), pp.110-119.

Siegel, S.G., Fagley, C. and Nowlin, S., 2012. Experimental wave termination in a 2D wave tunnel using a cycloidal wave energy converter. *Applied Ocean Research*, 38, pp.92-99.

Siegel, S.G., 2014. Wave climate scatter performance of a cycloidal wave energy converter. *Applied Ocean Research*, 48, pp.331-343.

SoerensenHC, WeinsteinA. Ocean Energy: Position paper for IPCC, January 2008, available from (<http://123seminaronly.com/Seminar-Reports/037/44753036-Ocean-Energy-IPCC-Final.pdf>).

South Thailand, available from (http://www.thefullwiki.org/South_%28Thailand%29).

Tanaka, H., Inami, T. and Sakurada, T., 2015, July. Characteristics of Volume of Overtopping and Water Supply Quantity for Developing Wave Overtopping Type Wave Power Generation Equipment. In *The Twenty-fifth International Ocean and Polar Engineering Conference*. International Society of Offshore and Polar Engineers.

Tedd, J. and Kofoed, J.P., 2009. Measurements of overtopping flow time series on the Wave Dragon, wave energy converter. *Renewable Energy*, 34(3), pp.711-717.

Thaweewat, N., Phoemsapthawee, S. & Jungrungruentaworn, S., 2013. Asymmetric wave radiation of oscillating wedge buoy. Proceeding of The 27th Conference of the Mechanical Engineering Network of Thailand.

Thaweewat, N., 2017. Asymmetric Buoy Wave Energy Converter. Proceeding of International Conference on Simulation and Modeling.

The European Marine Energy Centre LTD, available from (<http://www.emec.org.uk>).

"United Nations Statistics Division- Standard Country and Area Codes Classifications (M49)". United Nations Statistics Division. 6 May 2015. Retrieved 2010-07-24.

Van der Meer, J.W. and Janssen, P.F.M., 1995. Wave Run-up and Wave Overtopping at Dikes, ASCE book on "Wave Forces on inclined and vertical wall structures", Editor: Z.

Vicinanza, D. and Frigaard, P., 2008. Wave pressure acting on a seawave slot-cone generator. *Coastal Engineering*, 55(6), pp.553-568.

Vicinanza, D., Margheritini, L., Kofoed, J.P. and Buccino, M., 2012. The SSG wave energy converter: Performance, status and recent developments. *Energies*, 5(2), pp.193-226.

Victor, L., Troch, P. and Kofoed, J.P., 2011. On the effects of geometry control on the performance of overtopping wave energy converters. *Energies*, 4(10), pp.1574-1600.

Wave Clapper WEC, available from (<http://www.ecowavepower.com/>).

Wave Dragon, available from ([http:// www.wavedragon.net](http://www.wavedragon.net)).

Acknowledgement

First and foremost this Ph.D. thesis would not have been possible without the financial support from Faculty of International Maritime Studies, Kasetsart University, Thailand.

I would like to reveal my special appreciation and thanks to my advisor Professor Dr. Beom-Soo Hyun, you have been a tremendous mentor for me. I appreciate for taking care of me like I am a daughter. I would like to thank you for encouraging my research and for allowing me to grow as a research scientist. Your advices on both researches as well as on my career have been priceless.

I would also like to thank my committee members, Professor Seung-Jae Lee, Professor Sun-Ho Park, Professor Sung-Wook Lee and Dr. Keyyong Hong for serving as my committee members even at hardship. I also want to thank you for letting my defense be an enjoyable moment, and for your brilliant comments and suggestions, thanks to you.

Special thanks go to my family for all their love and encouragement. Words cannot express how grateful I am to my parents, aunts, uncles and my older sister for all of the sacrifices that you've made on my behalf. Your prayer for me was what sustained me thus far.

My time at Korea Maritime and Ocean University was made enjoyable in large part due to the many friends and groups that became a part of my life. I am grateful for time spent with roommates and friends. I would also like to thank all of my friends for supporting me. Especially, I want to thank my laboratory mate, Mr. Seungkwon Yang who supported me in writing, and incited me to strive towards my goal.

At the end I would like express appreciation to my beloved Nonthipat Thaweewat who spent sleepless nights with and was always my support in the moments when there was no one to answer my queries.

October 26, 2017

Sirirat Jungrungruentaworn

sirirat.sj@gmail.com